



Phosphorus transport in a hotter and drier climate: in-channel release of legacy phosphorus during summer low-flow conditions

Christine L. Dolph¹, Jacques C. Finlay¹, Brent Dalzell^{2,3}, and Gary W. Feyereisen^{2,3,4}

¹Department of Ecology, Evolution and Behavior, University of Minnesota, 140 Gortner, 1479 Gortner Ave, St Paul, MN 55108, USA

²USDA-ARS Soil and Water Management Research Unit, St Paul, MN 55108, USA

³Department of Soil, Water, and Climate, University of Minnesota, 438 Borlaug Hall, 1991 Upper Buford Circle, St Paul, MN 55108, USA

⁴Department of Bioproducts and Biosystems Engineering, University of Minnesota, 1390 Eckles Ave., St Paul, MN 55108, USA

Correspondence: Christine L. Dolph (dolp008@umn.edu)

Received: 7 March 2024 – Discussion started: 3 May 2024

Revised: 2 October 2024 – Accepted: 15 October 2024 – Published: 6 December 2024

Abstract. “Legacy phosphorus” is the historical accumulation of phosphorus (P) in soils and sediments due to past human inputs. River networks represent a potential sink and/or source of legacy P, with many in-channel processes potentially governing the storage and mobilization of P over time. The objective of this study was to evaluate the potential contribution of the in-channel release of legacy P to bioavailable P transport in streams during summer low-flow conditions across a land use gradient in Minnesota, USA. We addressed this objective through the synthesis of (1) water quality and streamflow (Q) data collected for 143 gauged watersheds across the state of Minnesota between 2007–2021 (22 750 total samples); (2) water quality data from 33 additional ditch, stream, and river sites in Minnesota sampled under low-flow conditions in the summer of 2014; and (3) water quality data collected from tile drainage outlets for 10 monitored farm fields between 2011–2021. We used geospatial data and a random forest modeling approach to identify possible drivers of bioavailable P concentrations during summer low flows for gauged watersheds. During low flows in late summer, between one-third to one-half of the gauged watersheds we studied exhibited soluble reactive phosphorus (SRP) concentrations that were above previously identified thresholds for eutrophication of 0.02–0.04 mg L⁻¹. For many of these watersheds, stream SRP concentrations in late summer were above those observed in tile drainage outlets. Elevated SRP concentrations during late-summer low flows

weakened concentration–discharge relationships that would otherwise appear to indicate more strongly mobilizing SRP– Q responses across other seasons and flow conditions. While wastewater discharge likely contributed to elevated P concentrations for watersheds with high densities of treatment plants, many watersheds did not have substantial wastewater impacts. The most important variables for predicting bioavailable P concentrations during late-summer low-flow conditions in a random forest model were land use in riparian areas (particularly crop cover); soil characteristics including soil erodibility, soil permeability, and soil clay content; agricultural intensity (reflected via higher pesticide use, higher phosphorus uptake by crops, and higher fertilizer application rates); watershed precipitation; and stream temperature. These findings suggest that, for stream and river sites heavily impacted by past and current P inputs associated with agriculture and urbanization, biogeochemical processes mediated by climate and geology can result in the release of legacy P from in-channel stores during late-summer low-flow conditions. As summers become hotter and, at times, drier – which are predicted changes in this region – conditions for the release of legacy P stored in stream and river channels will likely become more prolonged and/or more acute, increasing eutrophication risk.

1 Introduction

Phosphorus (P) inputs arising from urbanization and industrial or intensive agriculture have resulted in widespread eutrophication of freshwater and marine environments. Excessive inputs of P along with nitrogen (N) have resulted in costly and sometimes dangerous conditions for human society, including increased prevalence of harmful algal blooms, contamination of drinking-water supplies, decreased recreational opportunities, loss of critical marine fisheries, and negative impacts on biodiversity (Bennett et al., 2001). This problem is particularly acute in the midwestern Corn Belt of the United States, which represents a global hotspot for P fertilization (Haque, 2021).

Most progress in the reduction of P release to the environment has come from the implementation of improved wastewater infrastructure (Keiser and Shapiro, 2019). However, diffuse (nonpoint) sources of P, such as those arising from agricultural and urban landscapes, have yet to be substantially curtailed and remain largely unregulated. In addition to ongoing P inputs to the environment, water quality is also impacted by the existing supply of “legacy P” in the landscape (Goyette et al., 2018). Legacy P is the historical accumulation of P in soils and sediments due to past land use practices, such as agricultural fertilization, the spreading of manure, and wastewater discharge.

Efforts are underway to understand sources of legacy P in the terrestrial environment, including agricultural soils and riparian buffers (e.g., Osterholz et al., 2020). Lentic waterbodies (lakes, impoundments, and wetlands) are well known for their potential to remobilize stored P and become sources instead of sinks for downstream P, especially at high rates of nutrient inputs (e.g., Vilmin et al., 2022). The river network itself represents another potential sink and/or source of legacy P, with many dynamic in-channel processes potentially governing the storage and mobilization of P over time. For example, benthic redox conditions, in-stream primary productivity, microbial respiration, and sediment adsorption–desorption can all modulate whether P is retained in stream sediments, temporarily immobilized as organic P, or released to the water column as bioavailable P (Records et al., 2016).

We previously observed that concentrations of bioavailable P (i.e., soluble reactive phosphorus, SRP) in agriculturally dominated streams and rivers of Minnesota were often elevated during low-flow conditions in late summer (Dolph et al., 2019). However, questions remained about whether the elevated SRP we observed in late summer was sourced predominantly from tile drainage (therefore being indicative of legacy and/or current P sources stored in farm soils), from point sources such as wastewater treatment plants, or possibly from legacy sources in the river network itself. Tile drainage is extensive across the agricultural Midwest (Valayamkunnath et al., 2020) and has been found to contribute substantially to and even dominate soluble-P export in agricultural watersheds (King et al., 2015; Smith et al.,

2015). P concentrations in tile waters have been found to be highest during summer compared to during other seasons (King et al., 2015) and therefore represent a possible driver of elevated SRP in streams and rivers receiving tile drainage at this time of year. Comparatively high SRP concentrations during low flows can also be indicative of the dominance of point discharges; these concentrations are often diluted under wetter conditions (Dupas et al., 2023). Alternatively, however, there is some indication that groundwater and/or in-channel processes may drive the release of bioavailable P in river channels at some times of the year, such as during summer (Schilling et al., 2020; Vissers et al., 2023).

A number of recent papers have examined potential legacy P dynamics in streams and rivers; these studies have typically been deployed at the reach scale (i.e., stream reaches of a few hundred meters or less) or for individual small- to medium-sized watersheds (e.g., Bieroza and Heathwaite, 2015; Casquin et al., 2020; Kreiling et al., 2023; Siebers et al., 2023; Vissers et al., 2023; Dupas et al., 2023; Rode et al., 2023). These in-depth studies are important and highly useful as the microscale dynamics governing P mobility in river channels can be complex. However, few studies have examined the potential contribution of in-channel legacy P at larger regional scales or across a large number of watersheds.

The objective of this analysis was to determine the potential contribution of in-channel legacy P sources to SRP transport under summer low-flow conditions across a relatively broad spatial scale (i.e., the state of Minnesota). We hypothesized that in-stream processes contribute to elevated concentrations of bioavailable P during summer in streams with strong agricultural and/or urban influence in addition to the contribution of tile drainage systems and point source discharges. We addressed this hypothesis through the synthesis of three water quality datasets: (1) water quality and streamflow data collected for 143 gauged watersheds across the state of Minnesota between 2007–2021 (22 750 total samples); (2) water quality data from 33 additional ditch, stream, and river sites in Minnesota sampled under low-flow condition in the summer of 2014; and (3) water quality data collected from tile drainage outlets for 10 monitored farm fields between 2011–2021. We also used geospatial data and a machine learning approach to identify possible drivers of elevated SRP concentrations during summer low flows for gauged streams and rivers.

Watersheds across the state of Minnesota span a land use gradient from being dominated by intensive agriculture typical of the Upper Midwest region to a major metropolitan area to areas of heavy forest and wetland cover with comparatively fewer historic P inputs. This gradient provides a useful contrast that can potentially be applied to identify differential behavior of streams and rivers strongly impacted by legacy P.

2 Methods

2.1 Study area

The study area for this research spans the entire state of Minnesota, USA, encompassing approximately 225 163 km² within the Upper Midwestern region of the United States (Fig. 1). The state includes parts of four major drainage basins: the Upper Mississippi River basin in the central, southern, and southeastern portions of the state; the Red River basin in the northwest; the Great Lakes basin in the northeast; and the Upper Missouri River in the far southwestern corner. Gradients in land use, soils, and precipitation vary from north to south and from east to west (Fig. 1). The majority of the southern and northwestern parts of the state are dominated by industrial row crop agriculture, predominantly corn and soybeans, with a high density of concentrated animal-feeding operations (CAFOs), particularly in the south. By contrast, the northern and northeastern parts of the state are dominated by forest and wetland cover. The state is also home to a major metropolitan area, encompassing the Twin Cities of Minneapolis and St Paul and the seven surrounding counties (population of 3.69 million, 2020 US census), characterized by urban and suburban landscapes. Precipitation varies from being the driest in the northwest (annual average rainfall of ~ 550 mm, 1991–2020) to the wettest in the southeast (annual average rainfall of ~ 950 mm, 1991–2020; Johnson et al., 2022). Mean annual temperatures are higher in the south (annual average temperature of ~ 7 °C, 1991–2020) and lower in the north (annual average temperatures of ~ 2–3 °C, 1991–2020). The entire state is characterized by a cold climate, with average winter temperatures well below freezing and with considerable snowfall historically expected most years. Most soils are formed from glacial and peri-glacial deposits. Soil textures range from sandy soils in the central part of the state to clay loam and silty clay loam soils in the south-central and southwest and to outwash till over karst bedrock in the southeast. Many of the soils in the western part of the state are calcareous with a high pH. Water quality in the state is characterized by widespread impairments in the agriculturally and urban-dominated regions, with the most ubiquitous impairments attributed to turbidity, total phosphorus, fecal coliform, impaired biota, and low dissolved oxygen (MPCA, 2022). Water quality in the northeastern part of the state is comparatively good, with lower levels of nutrient enrichment, although impairments for mercury contamination arising from coal burning and subsequent atmospheric deposition are widespread.

2.2 Overview of study data

For this study, we utilized three independent datasets (Fig. 1):

1. SRP concentration and discharge data (total $n = 22\,750$ flow-matched water chemistry samples) collected for 143 gauged stream and river

watersheds monitored by the state of Minnesota's Watershed Pollutant Load Monitoring Network (<https://public.tableau.com/app/profile/mpca.data.services/viz/WatershedPollutantLoadMonitoringNetworkWPLMNDataviewer/ProgramOverview>, last access: 23 October 2023) between 2007–2021. These data were used to evaluate SRP transport behavior and understand drivers of late-summer SRP.

2. SRP concentration and discharge data available for 10 tiled farm fields across the state, collected between 2011–2021 by the Discovery Farms Minnesota program (<https://discoveryfarmsmn.org/>, last access: 17 March 2023). These data were used to estimate seasonal SRP concentrations for tile outlets as a point of comparison with riverine SRP concentrations.
3. SRP grab samples collected during low-flow conditions in late summer of 2014 for an additional set of ditch, stream, and river sites ($n = 33$; Dolph et al., 2017a (<https://conservancy.umn.edu/handle/11299/189907>, last access: 27 March 2023)). These data were used to provide additional information about SRP concentrations in smaller-order systems that were underrepresented among gauged watersheds.

All data analyses were performed in R (R Core Team, 2023). The study data and R scripts used for data analysis are available at <https://doi.org/10.5281/zenodo.13936951> (Dolph, 2024).

2.3 Water quality data from stream and river gauges

We used paired SRP and daily discharge data from 143 gauged stream and river watersheds (Fig. 1) monitored by Minnesota's Watershed Pollutant Load Monitoring Network (WPLMN; note that the WPLMN also refers to SRP as “dissolved orthophosphate”). The total number of samples across all gauged watersheds was 22 750. Periodic water samples and continuous-flow data were collected by the Minnesota Pollution Control Agency (MPCA) throughout the year at major watershed sites (watershed areas greater than ~ 4000 km²) and during the period of ice-out through 31 October at smaller subwatershed sites (MPCA, 2015). Water quality sampling efforts were conducted approximately bi-weekly, with more intensive sampling focused on snowmelt and storm events, resulting in observations distributed across the range of flows observed at each site (average no. of samples per year = 25 for subwatersheds and 35 for major watersheds; MPCA, 2015). The 143 gauged sites we selected for this study had > 20 water chemistry samples collected across the sampling period (2007–2021). The median number of water quality samples per site across the whole time period was 120 (min = 21, max = 478). To determine detection limits, we inspected the data for repeated minimum concentrations and assigned detection limits equal to those minimum concentrations.

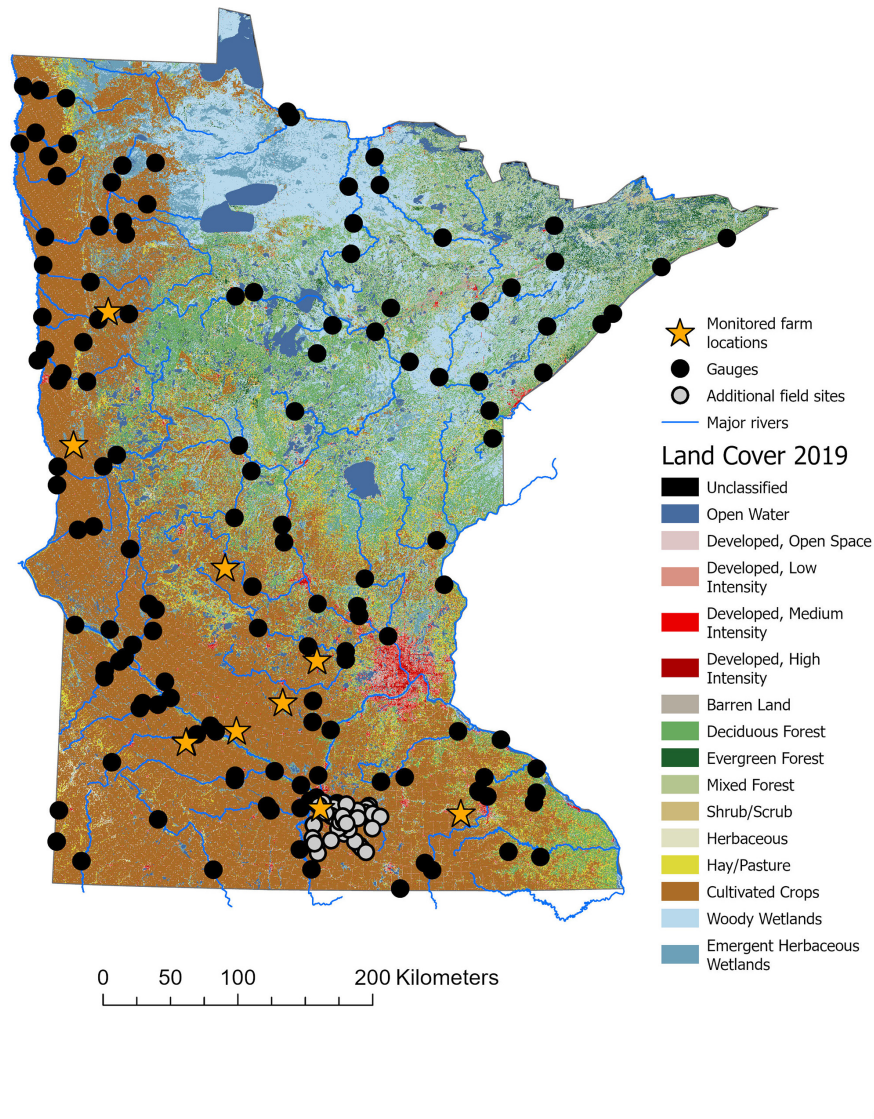


Figure 1. Locations of (1) 143 gauged stream and river watersheds intensively sampled for SRP and flow (total $n = 22\,750$ samples) at the watershed outlet during 2007–2021 (black dots; $n = 143$). Data from these sites were used to evaluate SRP transport behavior and understand drivers of late-summer SRP. (2) Farm fields with tile outlet water quality available (collected between 2011–2021; orange stars; $n = 10$) used to estimate seasonal SRP concentrations for tile outlets as a point of comparison with riverine SRP concentrations. (3) Ditch, stream, and river sites sampled during summer low-flow conditions in 2014 (gray dots; $n = 33$). Data from these sites were used to quantify late-summer SRP concentrations in smaller-order systems. Note that two farm fields (known as RW1N and RW1S) are located in close proximity to each other and so appear to be one location on the map; this location is noted with a white arrow.

Watershed areas for gauged stream and river sites were assembled from multiple sources, including existing watershed delineations ($n = 11$ watersheds) available from USGS (2012) and previously delineated watersheds ($n = 65$ watersheds) from Dolph et al. (2019), or were delineated anew as part of the current study ($n = 68$ watersheds). For newly delineated watersheds, we used gauge locations provided by the Minnesota Department of Natural Resources and the Minnesota Pollution Control Agency (2023) as pour points, and we used existing flow direction and flow accumulation rasters

available from the NHDv2Plus dataset (USEPA, 2019) to delineate watersheds using the Spatial Analyst toolbox in ArcGIS Pro (Esri, 2022). Watersheds were inspected visually and manually corrected for inaccuracies in delineation. Across all gauged sites, watershed area ranged from 20 to 29 145 km² (mean = 1996 km²).

2.4 Farm tile outlets

We used SRP concentration and discharge data from tile outlets draining 10 farm fields across the state, measured

between 2011–2021 (Fig. 1). These tile outlets are monitored by the Discovery Farms Minnesota (DFM) program (<https://discoveryfarmsmn.org/>, last access: 17 March 2023). The DFM program is a farmer-led water quality research and educational program with the goal of collecting water quality information under real-world conditions to support the development of better farm management decisions. During the time of data collection, all monitored farm fields were planted in corn and soybean row crops grown in rotation. Two sites (WR1 and ST1) included dairy operations, and two sites (BE1 and DO1) included swine finishing in addition to row crops. Swine finishing is the final stage of pig farming, where young pigs are fed until they reach market weight.

The drainage areas for monitored farm fields ranged from 10 to 160 acres (mean = 97 acres). Farm field soil textures ranged from poorly drained silty clay loam to well-drained loam. Three of the farms (MC1, RE1, and WR1) each had one surface inlet to the tile drainage system. All other inlets were subsurface. One farm (NO1W) had monitoring data available for two separate fields (NO1W-N and NO1W-S). Water quality and flow data collection is described in detail by MDA (2021). Briefly, tile outlets were monitored continuously for flow (15 min interval) via area velocity sensors installed in the tile drains that measured both stage and velocity. Water quality samples were collected by ISCO 6712 automatic samplers on an equal-flow increment (EFI) composite basis whenever tile outlets were flowing. Water quality samples were composited every 125 mL. Following a runoff event, water quality samples were collected and promptly transported to a state contract lab and measured for dissolved orthophosphorus (i.e., SRP), along with other water quality constituents. From continuous-flow and composited-sample SRP concentrations, we calculated a daily flow-weighted SRP concentration (daily C) as follows: (1) multiply composite concentrations by paired continuous-flow measures to estimate continuous (15 min) loads, (2) sum composite-sample loads into daily loads, and (3) divide daily load by summed daily flow to compute a daily flow-weighted concentration (in mg L^{-1}). Seasonal SRP concentrations were calculated by taking the mean of the daily SRP concentrations for each tile outlet during each season (early winter: November–December; late winter: January–March; spring: April–May; early summer: June–July; late summer: August–September; fall: October).

2.5 Additional field sites

Among gauged stream and river watersheds, small-order systems (especially first- through third-order ditches and streams) are underrepresented relative to their prevalence across the landscape. To get a better understanding of SRP concentrations in smaller-order systems, we also examined late-summer low-flow SRP concentrations collected from 33 agriculturally dominated ditches, streams, and mid-sized rivers in the Le Sueur River basin, Minnesota (Fig. 1).

Data for these sites are part of a larger publicly available field dataset (<https://doi.org/10.13020/D6FH44>, Dolph et al., 2017a) for the region and are described in detail by Dolph et al. (2019). Briefly, SRP concentrations were determined for grab water samples collected from 33 sites during low-flow conditions in August of 2014. Flow conditions at the time of sampling were characterized by flow at the gauged outlet of the major HUC8-scale watershed from which samples were collected (i.e., the Le Sueur River basin) based on daily discharge data available from Minnesota Department of Natural Resources (MNDNR; <https://www.dnr.state.mn.us/waters/csg/index.html>, last access: 25 January 2016). Although flow at watershed outlets is not precisely representative of flow conditions further upstream in the basin, we have shown previously that discharge conditions across study sites scaled reasonably well with drainage area (Dolph et al., 2017b). We sampled on 14, 17, 20, and 26 August 2014, during which time flow conditions at the watershed outlet ranged between the 19–25th percentiles of all daily flows available for this watershed. Sites were categorized as ditches, perennial streams and rivers, or intermittent streams and rivers according to their designation in the NHDPlusv2 (USEPA, 2019).

2.6 Low-flow conditions

Part of our aim in this study was to identify whether in-channel dynamics, such as the in-stream release of legacy P, may affect stream and river SRP concentrations and transport behavior. Thus, we sought to identify low-flow conditions where we assumed that in-channel processes were likely to dominate P dynamics. We identified low-flow conditions as those falling within the lowest 25 % of all daily discharge conditions measured for each watershed during the period of record for that gauge. We defined seasons as follows: early winter (November–December), late winter (January–March), spring (April–May), early summer (June–July), late summer (August–September), and fall (October). We defined these seasons in approximate relation to the agricultural growing seasons in our study region, with spring corresponding to when crops are planted, summer corresponding to when crops grow rapidly, fall corresponding to when dominant crops (corn, soybeans) are harvested, and winter corresponding to when crops are dormant. We divided winter into early winter, which is when snow accumulates and generally does not melt, and late winter, which is associated with snowmelt. We divided summer into early summer, which is when conditions are generally wetter and crops experience rapid growth, and late summer, which is when climate conditions are generally drier and warm-season crops mature rapidly.

We calculated the mean SRP during low-flow conditions for each gauged watershed in each season for gauges that had a minimum of three SRP samples collected during low-flow conditions in that season. Note that not all gauged watersheds had three or more SRP samples collected during low flows in

each season (Table A4 in the Appendix); thus, the number of gauged watersheds with mean low-flow SRP values available for analysis was different during each season (this parallels the availability of low-flow conditions across seasons, with low flows being most common during late summer compared to during other seasons).

We hypothesized that low-flow SRP concentrations could be substantially affected by one or all of the following: tile outlet concentrations, wastewater treatment plant discharges, or riverine legacy P stores. To help discern these influences, we compared low-flow riverine SRP concentrations to tile outlet concentrations. In addition, we evaluated low-flow riverine SRP concentrations for gauged watersheds relative to the wastewater treatment plant density (sites per km²) in the watershed. Wastewater treatment plant density estimates were obtained from the US EPA StreamCat Dataset and were based on wastewater treatment plants listed in the EPA's Facility Registry Services and National Pollutant Discharge Elimination System (Hill et al., 2016). We also evaluated low-flow riverine SRP concentrations relative to the percentage of cropland land use in gauged watersheds to examine the assumption that agricultural land use and the associated past and current P inputs might drive the supply of riverine P. Cropland land use estimates were also obtained from the StreamCat Dataset and were based on the 2019 National Land Cover Database (Dewitz, 2021).

2.7 Influence of late-summer low flows on concentration–discharge relationships

We evaluated the relationship between SRP concentration (C) and discharge (Q) using the power-law relationship in Eq. (1):

$$C = aQ^b, \quad (1)$$

where the curve's coefficient (a) and exponent (b) are representative of the degree, direction, and rate at which SRP is transported as a function of streamflow. Alternatively, this equation can be expressed in log–log scale as Eq. (2):

$$\log(C) = b\log(Q) + \log(a), \quad (2)$$

where b is the slope of the linear log–log relation, and $\log(a)$ is the y intercept. Normalizing Q by the geometric mean of discharge (Q_{GM}) shifts the center of mass of the log-transformed Q data to the y intercept, allowing for comparison of rating curves among different watersheds (Warrick, 2015). We performed linear regression of log-transformed SRP concentrations based on log-transformed normalized discharge using Eq. (3):

$$\log(C) = b\log(Q/Q_{GM}) + \log(a). \quad (3)$$

All regressions were performed in R (R Core Team, 2023). We evaluated the fit of the power-law relationship for all

gauged watersheds using the significance value p , slope b , and R^2 of the linear regression.

The slope b of this relationship describes the per-unit increase in concentration as discharge increases. Concentrating relationships ($b > 0$) imply that higher flows are mobilizing more of a waterborne constituent, particularly through erosion or greater landscape connectivity. Diluting relationships ($b < 0$) suggest that constituents are source-limited or that relatively consistent inputs are diluted by greater discharge (Godsey et al., 2009). When b is near 0, C – Q relationships may be either chemostatic (i.e., relatively constant concentrations across the range of discharge conditions) or chemodynamic (i.e., concentrations are highly variable across the range of discharge conditions but are not linearly related to flow). Chemostatic behavior has been observed for mineral weathering products or for constituents with large legacy sources like nitrate (Godsey et al., 2009; Basu et al., 2010; Musolff et al., 2015), whereas chemodynamic behavior may indicate that biogeochemical processes such as sorption and/or desorption, biotransformation, or oxidation and/or reduction strongly affect nutrient transport behavior (e.g., Wanner et al., 1989). To distinguish between these two behaviors, we evaluated the coefficient of variation of C relative to the coefficient of variation of Q (CV_C/CV_Q). A $CV_C/CV_Q \ll 1$ suggests that concentrations are relatively constant compared to variability in flow, indicating chemostatic behavior. By contrast, a larger CV_C/CV_Q indicates chemodynamic behavior (i.e., comparatively large variations in concentration relative to variation in flow). Thompson et al. (2011) suggested that CV_C/CV_Q values of ≈ 0.3 could be used as a threshold to identify chemostatic vs. chemodynamic behavior.

To determine the influence of low-flow conditions in late summer on the nature of the C – Q relationships for all watersheds, we refit power-law relationships to all watersheds after excluding SRP samples that were collected during late-summer low-flow conditions. We compared regression parameters (p , slope b , and R^2) before and after withholding samples collected during late-summer low-flow conditions to determine if these samples had a widespread effect on C – Q relationships for SRP across gauged watersheds.

2.8 Regression analysis

2.8.1 Random forest models

We used random forest modeling to identify possible predictors of SRP during low-flow conditions in late summer for gauged stream and river watersheds. Random forest regression is a nonparametric ensemble learning method that utilizes predictions from multiple decision trees to improve model accuracy. Each tree is composed of branches (“nodes”) representing yes–no questions where features (i.e., predictive variables) are used to split the dependent variable into two groups that minimize in-group variability and max-

imize between-group variability. We selected a random forest approach because these models require few assumptions about data structure (i.e., data need not conform to assumptions of classical statistics such as linearity, normality, and constant variance), are robust in relation to outliers, and generally perform as well as or better than other data-intensive approaches (Hagenauer et al., 2019). The use of random forest models also allows for the identification of predictors that are important to model accuracy using measures such as condition permutation importance and post hoc partial-dependence plots (see additional details below).

2.8.2 Predictor variables

Predictor variables for random forest (RF) models were assembled from the US EPA StreamCat Dataset (<https://www.epa.gov/national-aquatic-resource-surveys/streamcat-dataset>, last access: 5 February 2024). The StreamCat Dataset contains information for over 600 different environmental metrics linked to individual stream reaches in the NHDv2Plus dataset (Hill et al., 2016). These metrics summarize, at the catchment and watershed scales, diverse geospatial attributes – including aspects of land cover, impervious surfaces and road density, soil type, point source and nutrient inputs, and climatic factors (temperature and precipitation), among others – draining into each reach. Catchments (i.e., local drainage areas) include the immediate land area draining into each individual stream reach in the National Hydrography Dataset (NHD) excluding areas draining to upstream reaches; watersheds include the entire land area draining into each stream reach. The StreamCat Dataset contains land use data for catchments and watersheds summarized from the National Land Cover Database (NLCD) for multiple years. We used only land cover attributes from the 2019 iteration of the NLCD (Dewitz, 2021). To supplement this dataset, we derived estimates of tile density (i.e., area tiled per area watershed) for each gauged watershed using estimates of tiled areas (30 m resolution) from Valayakunnath et al. (2020). Prior to developing a random forest model, we excluded predictors from the StreamCat Dataset that did not contain useful information (i.e., all rows = 0). We also excluded attributes where information was missing (“NA”) for > 20 % sites. Some of the remaining attributes still contained some missing values. Because random forest models cannot handle missing values in predictor variables, we used the `missRanger` package in R (Mayer, 2023) to impute the remaining missing values for the training and testing datasets. In total, we used 253 predictor variables in the model after excluding variables that did not provide useful information (i.e., that were all 0s or had too many missing values), that did not match the timing of our dataset (i.e., land cover data from years other than 2019), or that were not especially relevant (e.g., variables describing forest fire intensity or extent). Prior to random forest modeling, we normalized (i.e., centered and

scaled) numeric attributes to have a mean of 0 and a standard deviation of 1.

2.8.3 Model tuning and selection

We developed the random forest model to predict mean SRP during late-summer low conditions based on data for 127 gauged watersheds. Only 128 of the 143 total gauged watersheds in the study had ≥ 3 SRP samples collected during late-summer low-flow conditions and were therefore used to calculate mean SRP values. Prior to model development, we excluded one additional site from the testing dataset (Buffalo Creek near Glencoe, MN) that had a mean SRP value for late summer that exceeded the range of SRP values in the training dataset (see Fig. A1). To develop the RF model, we used the same general approach to random forest modeling described in detail by Dolph et al. (2023). Data were split randomly into independent model training (70 %, $n = 88$) and model testing (30 %, $n = 39$) datasets. Using the training dataset and the `ranger` package in R (Wright and Ziegler, 2017), we applied 10-fold cross-validation to tune model hyperparameters across a range of possible values. K -fold cross-validation can assist in avoiding model over-fitting and works by partitioning training data into K equal-sized “folds” (in our case, 10). The model is iteratively trained on various combinations of tuning hyperparameters across $K-1$ folds, leaving the remaining fold to evaluate model performance for each combination. The hyperparameters selected for tuning were as follows: `mtry` (i.e., number of variables randomly sampled as candidates at each split) and `min_n` (i.e., the minimum number of data points in a node). The tree hyperparameter (i.e., number of trees) was set to 1000 across all models. We defined a grid of 20 potential combinations of hyperparameters using the `tune_grid()` function from the `tidymodels` collection of packages in R (Kuhn and Wickham, 2020). This approach draws hyperparameter values semi-randomly from the parameter space such that the various combinations cover the whole space of potential values. We selected hyperparameter values using out-of-bag (OOB) RMSE and R^2 for the associated models. Once hyperparameter values were tuned, we reran the random forest model using the `randomForest` package (Liaw and Weiner, 2002) to create a `randomForest` object that was compatible with our selected measure of predictive variable importance (conditional permutation importance; see next paragraph). We evaluated overall model performance using R^2 and RMSE between the predicted and observed SRP values in the independent test dataset (comprising 30 % of the original dataset).

2.8.4 Variable importance

We used conditional permutation importance (CPI) to evaluate the importance of predictors to model performance. CPI aims to capture the dependence between a predictor and the response variable based, conditionally, on the values of all

other predictors. CPI can be used to assess how much each variable contributes to accurately predicting the response variable, given what we know from all other predictive variables. We implemented the CPI approach from the `permimp` package in R (Debeer et al., 2021). In `permimp`, a threshold value, equal to 1 minus the p value for the association between predictor variables, is used to determine whether to include a predictor in the conditioning for the predictor of interest. We used the default value for the threshold parameter in `permimp` (0.95; Debeer et al., 2021).

While the CPI method can rank predictors in terms of their importance to model accuracy, it does not convey information about the nature of the relationship between predictor variables and late-summer SRP concentrations. To visualize these relationships, we created partial-dependence plots (PDPs) using the `partialPlot` function in R (part of the `randomForest` package, Liaw and Weiner, 2002). These plots illustrate the change in predicted SRP concentration when the values of one predictor are changed while all other predictors are kept constant at their original values (Greenwell, 2017). We generated PDPs for the top 15 predictor variables identified as being most important by the measure of CPI.

3 Results

3.1 SRP concentrations at gauged watersheds during low flow

Across gauged watersheds, we expected SRP concentrations under low-flow conditions to differ depending on the extent of historic and current P inputs associated with anthropogenic land use. Most gauged watersheds in our study region (90%, $n = 128$) were substantially impacted by either agricultural or urban land use (defined here as watersheds with $\geq 50\%$ crop cover and/or $\geq 10\%$ high-intensity urban land use). The remaining watersheds ($n = 15$) were characterized as “less impacted”.

Among watersheds with substantial agricultural or urban influences, mean low-flow SRP concentrations were highest in late winter and were lowest in spring and then increased progressively through early summer, late summer, fall, and early winter (Table 1).

However, there was large variation (3–4 orders of magnitude) in low-flow SRP concentrations across sites in any given season (range across all samples = 0.001–3.9 mg L⁻¹). For less impacted sites, seasonal low-flow SRP concentrations were also highest, on average, during late winter, although the absolute concentrations were much lower than for more heavily impacted sites. In contrast to more heavily impacted sites, mean low-flow SRP concentrations at less impacted sites dropped in spring and stayed steady through summer and then dropped slightly again in fall. Less impacted sites showed comparatively low SRP concentrations

and lower variability in low-flow SRP concentrations across sites or seasons (range of 0.001–0.046 mg L⁻¹).

3.2 Influences of wastewater treatment facilities (point sources) on riverine SRP concentrations at low flow

Mean SRP concentrations at low flow for gauged watersheds were significantly related to the density of wastewater treatment plants in the watershed during early winter, late winter, late summer, and fall but not in spring or early summer (Fig. 2). Part of the discrepancy across seasons may have been caused by the fact that few watersheds with a high density of wastewater treatment plants were sampled during low flows in spring and early summer. The relationship between mean low-flow SRP and wastewater treatment plant density was strongest in early winter (though still somewhat weak overall; $R^2 = 0.26$) and comparatively weaker in other seasons (Table A1). These relationships were largely driven by watersheds where the density of wastewater treatment plants was comparatively high (> 0.005 sites km⁻²). When watersheds with a wastewater treatment plant density > 0.005 sites km⁻² were excluded, we observed a persevering very weak significant positive relationship between wastewater treatment plant density and mean low-flow SRP during late summer and late winter ($R^2 = 0.06$ and 0.10, respectively) but not during any other season (see Table A1).

3.3 Riverine SRP at low flows in relation to agricultural land use

We observed consistent and positive relationships between agricultural land use (% cropland) and mean low-flow SRP concentrations across gauged watersheds during all seasons, with the strongest relationships occurring during late summer and late winter (Fig. 3; Table A2). When we examined only sites without wastewater treatment plant influence, these relationships appeared to be even stronger, as evidenced by increased R^2 values (Fig. 4; Table A2). The strongest correlations were evident in late summer and early winter (R^2 of 0.69 and 0.86, respectively; Fig. 4). However, it should be noted that the sample size for early winter was small ($n = 5$), which may have inflated the R^2 value for this season.

3.4 SRP concentrations at tile outlets

Across tile outlets for 10 conventionally farmed fields (corn–soybean rotation), the mean SRP concentration of tile drainage was highest in late winter (mean SRP = 0.131 mg L⁻¹) and was lowest in early and late summer and early winter (mean SRP = 0.03 mg L⁻¹; Table 2). Two sites (WR1 and ST1) included dairy operations, and two sites (BE1 and DO1) included swine finishing in addition to row crops. The two dairy-influenced farm fields (WR1 and ST1) had notably higher tile SRP concentrations across all seasons relative to other sites. Three sites (MC1 RE1, and WR1) had one surface inlet to the tile system (all

Table 1. Mean, minimum, and maximum low-flow SRP concentrations (mg L^{-1}) for more heavily impacted gauged watersheds ($\geq 50\%$ crop cover and/or $\geq 10\%$ high-intensity urban land use) and less impacted gauged watersheds ($< 50\%$ crop cover and/or $< 10\%$ high-intensity urban land use) across seasons.

Degree of anthropogenic disturbance	Season	Mean SRP	Min SRP	Max SRP
More impacted	Late winter	0.129	0.002	3.550
	Spring	0.030	0.001	0.384
	Early summer	0.039	0.001	0.526
	Late summer	0.055	0.001	1.350
	Fall	0.069	0.002	1.595
	Early winter	0.117	0.002	3.900
Less impacted	Late winter	0.008	0.002	0.019
	Spring	0.007	0.002	0.031
	Early summer	0.006	0.001	0.028
	Late summer	0.005	0.001	0.046
	Fall	0.004	0.002	0.008
	Early winter	0.008	0.002	0.030

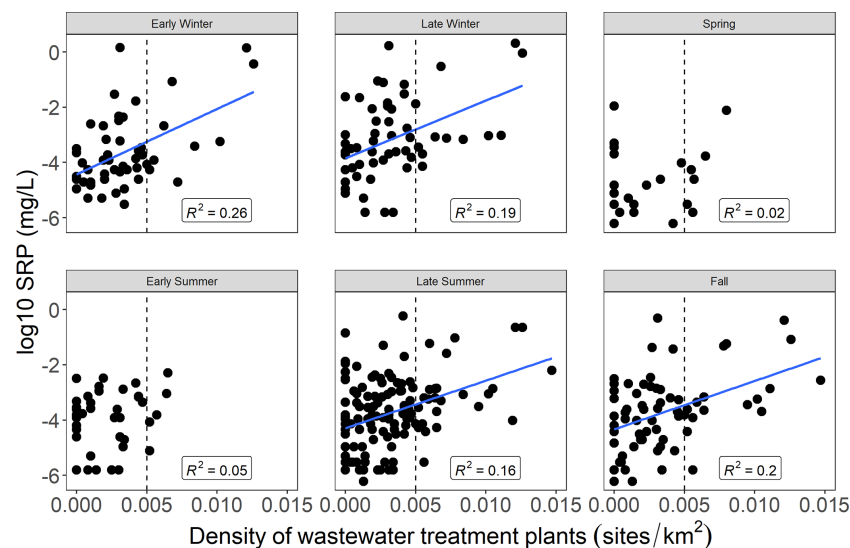


Figure 2. Relationship of SRP concentrations at low flows (log scale) in gauged watersheds to the density of wastewater treatment plants (sites km^{-2}) in the watershed by season. Blue lines indicate statistically significant linear regressions ($p < 0.05$). Linear regression statistics are shown in Table A1. The dashed line indicates a wastewater treatment plant density of $0.005 \text{ sites km}^{-2}$. Note that not all gauged watersheds had sufficient samples collected during low flows in each season to generate mean values; thus, the number of gauged watersheds with low-flow mean SRP values available was different during each season.

other inlets were subsurface). These sites appeared to have higher mean SRP concentrations in late winter (coinciding with snowmelt) and early summer (in the case of WR1), but of the surface inlet sites, only WR1 (the dairy farm site) had higher mean SRP concentrations in late summer.

3.5 Riverine SRP at low flows compared to tile concentrations

We evaluated SRP during low-flow conditions for each gauged watershed in each season (Table A3) and compared these riverine SRP values to SRP concentrations in moni-

tored tile outlets. Note that not all gauged watersheds had sufficient samples collected during low flows in each season to generate mean values (Table A4); thus, the number of gauged watersheds with available mean low-flow SRP values was different during each season. Comparisons for late winter, spring, and late summer are shown in Fig. 5 (only a subset of seasons are shown for improved clarity in data visualization; similar figures for early winter, early summer, and fall are shown in Fig. A2).

In early winter, 36% of gauged watersheds ($n = 18/50$ sites for which low-flow data were available) exhibited SRP concentrations at low flows that were higher than mean tile

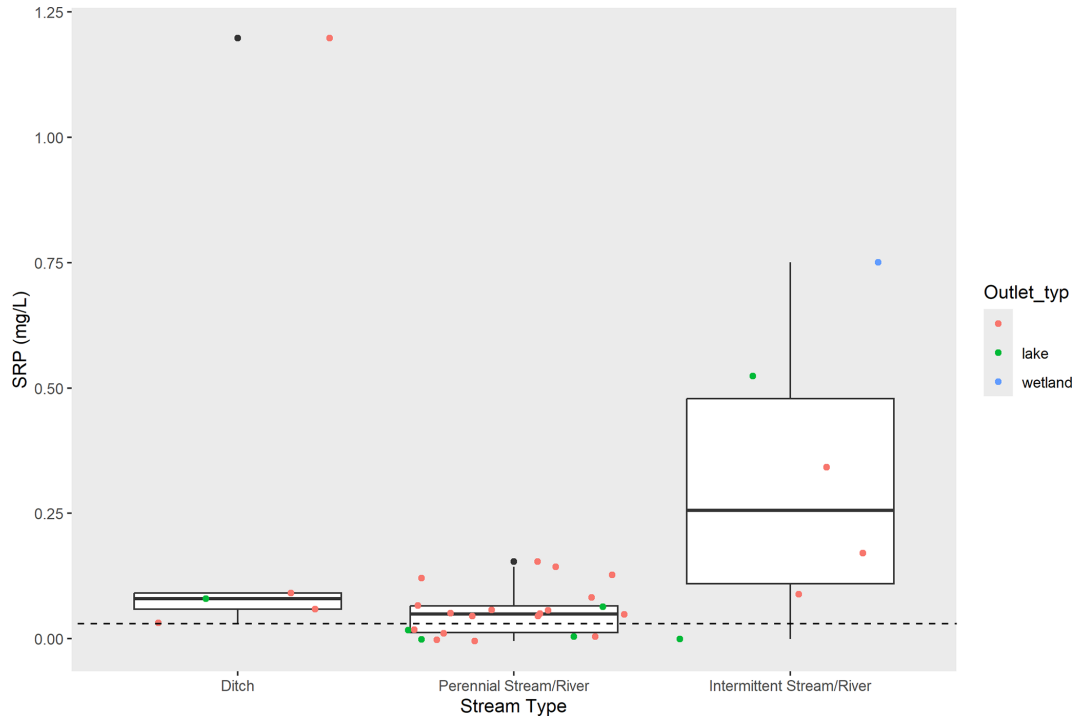


Figure 3. Mean low-flow SRP concentrations across gauges (log scale) in relation to percentage crop cover by season. Color scale indicates density of wastewater treatment plants in the watershed. Relationships in all seasons were significant and positive. Linear regression statistics are shown in Table A2.

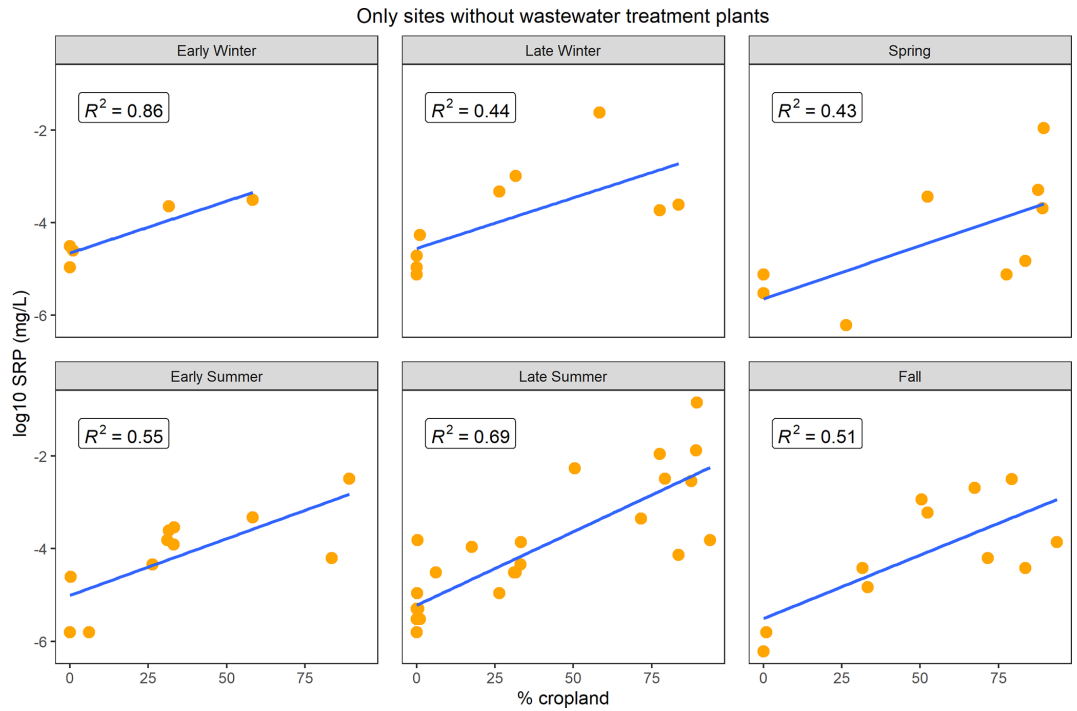


Figure 4. Mean low-flow SRP concentrations across gauges (log scale) in relation to percentage crop cover by season for sites with *no wastewater treatment plant influence*. Relationships in all seasons were significant and positive. Linear regression statistics are shown in Table A2.

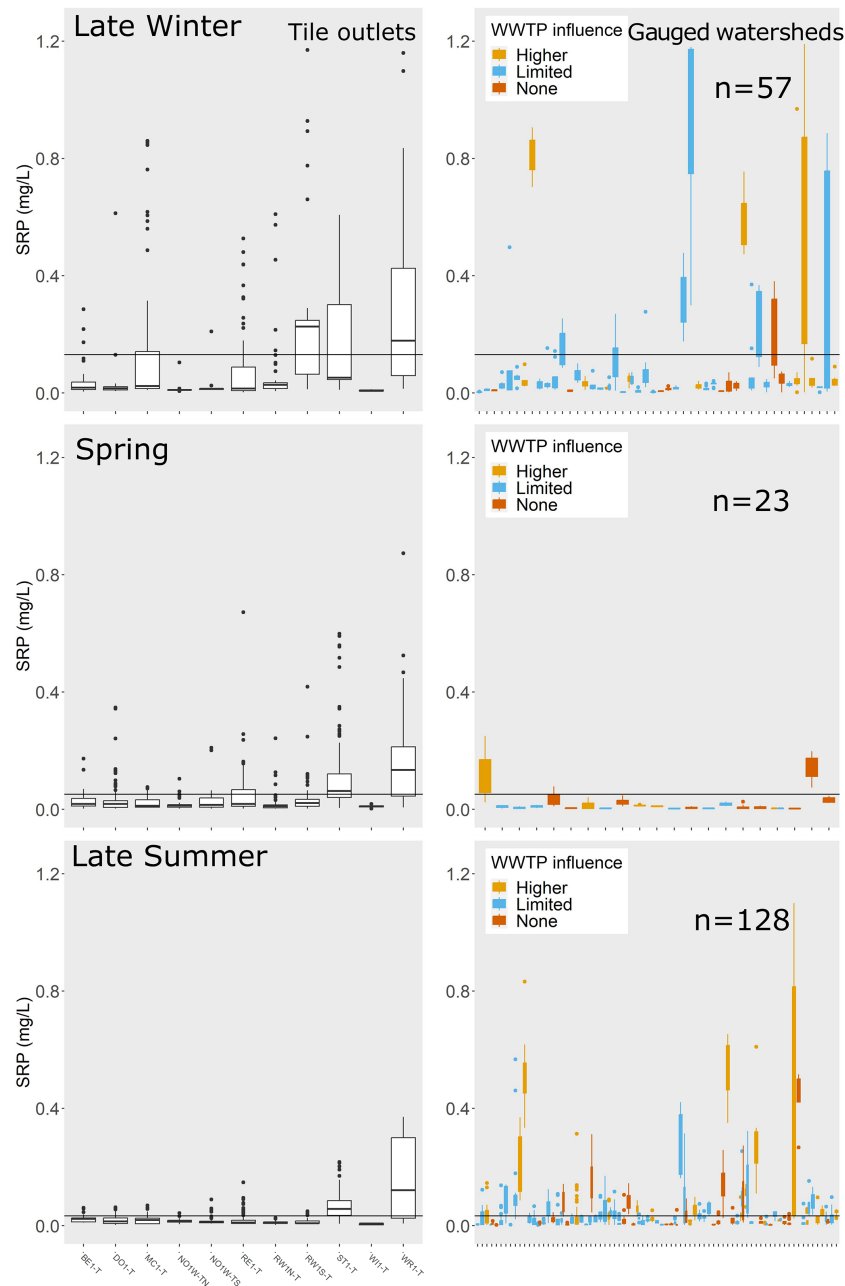


Figure 5. SRP concentrations (mg L^{-1}) for tile outlets and during low-flow conditions for gauged watersheds by season. Only a subset of seasons are shown for improved clarity in data visualization; similar figures for the remaining seasons are shown in Fig. A2. The horizontal line in each plot is the mean SRP concentration among tile outlets for that season. For gauged watersheds, the color of the boxplots indicates the degree of influence from wastewater treatment plants: light orange indicates wastewater treatment plant density > 0.005 sites km^{-2} , blue indicates wastewater treatment plant density < 0.005 sites km^{-2} but greater than zero, and red indicates no wastewater treatment plant sites in watershed. The number of gauges for which low-flow data were available in each season is printed on the plot. To improve data visibility, the y axis for SRP was limited to a maximum of 1.25 mg L^{-1} , which eliminated a small number of outliers from the plots for tile outlets ($n = 34$ out of 11 079 records) and gauged watersheds ($n = 16$ out of 2696 low-flow records).

Table 2. Mean flow-weighted daily SRP concentrations (mg L^{-1}) from farm tile outlets by season. Tile outlet data were collected from 10 farms between 2011–2021. Note that one farm field (NOW1) had two tile outlets (NOW1-N and NOW1-S) that drained different areas of the same field.

Site	Early winter	Late winter	Spring	Early summer	Late summer	Fall	Annual mean
BE1 ^c	0.064	0.053	0.031	0.017	0.023	0.132	0.036
DO1 ^c	0.012	0.029	0.036	0.015	0.018	0.010	0.023
MC1 ^b	0.019	0.139	0.023	0.012	0.022	0.024	0.037
NO1W-N	0.008	0.011	0.018	0.015	0.016	0.008	0.014
NO1W-S	0.017	0.025	0.024	0.012	0.018	0.015	0.018
RE1 ^b	0.014	0.070	0.045	0.075	0.022	0.043	0.049
RW1N	0.023	0.231	0.025	0.014	0.011	0.033	0.061
RW1S	0.011	0.278	0.059	0.019	0.017	0.045	0.069
ST1 ^a	0.053	0.164	0.091	0.062	0.073	0.048	0.084
W11	0.011	0.008	0.009	0.008	0.005	0.010	0.008
WR1 ^{a,b}	0.055	0.307	0.156	0.119	0.157	0.105	0.151
All sites	0.029	0.131	0.051	0.036	0.033	0.035	0.052

Early winter: November–December. Late winter: January–March. Spring: April–May. Early summer: June–July. Late summer: August–September. Fall: October. ^a Farms included dairy operations. ^b Farms included a surface inlet to the tile drainage system. ^c Farms included swine finishing.

SRP concentration. Six of these watersheds were characterized by a comparatively high wastewater treatment plant density (defined as > 0.005 sites km^{-2}). In late winter, when tile SRP concentrations were highest, 23 % of gauged watersheds ($n = 13/57$) exhibited SRP concentrations at low flows that were higher than the mean tile concentrations. A minority of these sites ($n = 3/13$) had considerable wastewater treatment plant influence (wastewater treatment plant density > 0.005 sites km^{-2}). In spring, SRP concentrations during low-flow conditions were uniformly low across nearly all gauged watersheds. SRP samples collected during low-flow conditions were fairly uncommon, with only 23 watersheds having ≥ 3 SRP samples collected during spring low flows. Of these, two sites (9 %) had SRP concentrations at low flows that were higher than the mean tile concentrations. In early summer (June–July), 28 % of sites ($n = 11/40$) had SRP concentrations at low flow that were higher than the mean tile concentrations. Two of these sites had considerable wastewater treatment influence. In late summer (August–September), 39 % of gauged watersheds ($n = 50/128$) had SRP concentrations at low flow that were higher than the mean tile concentrations, and 16 of these sites had considerable wastewater treatment influence. In fall (October), 35 % of gauged watersheds ($n = 24/68$) had SRP concentrations at low flow that were higher than the mean tile concentrations; eight of these sites had comparatively higher wastewater treatment plant density.

3.6 Low-flow SRP concentrations from additional field sites

Among gauged stream and river sites, small-order systems (especially first- through third-order ditches and streams) were underrepresented relative to their prevalence across the

landscape. These smaller-order systems are also less likely to have substantial point source discharges. To get a better understanding of SRP conditions in smaller-order systems, we examined SRP concentrations collected from 33 agriculturally dominated ditches, streams, and mid-sized rivers in southern Minnesota during low-flow conditions in August 2014 (Dolph et al., 2017). During this sampling event, SRP concentrations at most sites were higher than mean SRP concentrations from farm tile outlets (Fig. 6). Mean SRP concentrations in late summer were highest in ditches and intermittent streams (0.19 mg L^{-1} and 0.30 mg L^{-1} , respectively).

3.7 C–Q relationships at stream and river gauges

When C–Q relationships were evaluated using all flow data for each gauge, the majority of gauged watersheds (72 %, $n = 103$) showed mobilizing behavior for SRP in relation to streamflow (i.e., significant positive slopes for the C–Q power-law relationship and $\text{CV}_C/\text{CV}_Q > 0.3$; Fig. A3). Mobilizing behavior for bioavailable P ranged from very weak ($R^2 = 0.01$) to comparatively strong ($R^2 = 0.68$). Watersheds with positive SRP–Q relationships were located predominantly in the agriculturally dominated regions of the state (the southern and western parts of the state corresponding to the southern part of the Upper Mississippi River basin, the Minnesota River basin, the Driftless Area in the southeast, and the Red River basin; Fig. 7). Chemodynamic behavior (non-significant slopes for the C–Q power-law relationship and $\text{CV}_C/\text{CV}_Q > 0.3$) was observed for 24 % ($n = 34$) of sites, most of which are located in the central and northeastern parts of the state dominated by forest and wetland cover (Fig. 7). A small number of sites ($n = 4$, 3 %) showed diluting behavior for SRP, as defined by significant negative slopes for the C–Q power-law relationship

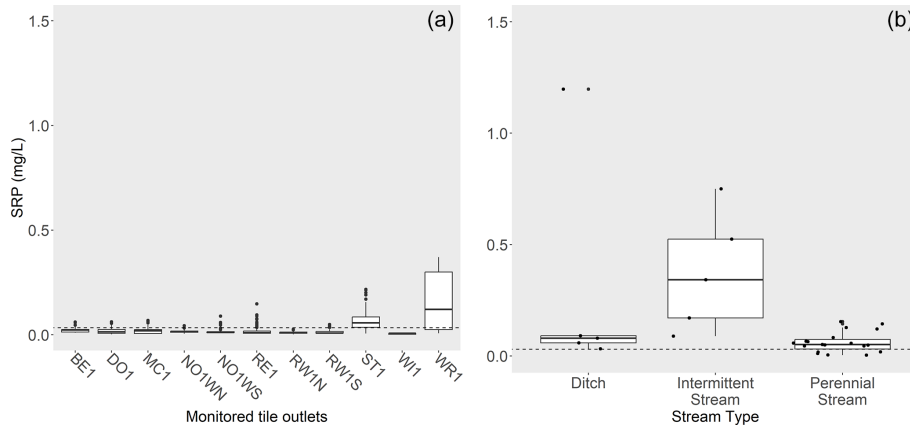


Figure 6. SRP concentrations (mg L^{-1}) among tile outlets (a) compared to sampled ditches ($n = 5$), intermittent streams and rivers ($n = 6$), and perennial streams or rivers ($n = 22$) and (b) during late-summer low-flow conditions. Dashed line shows mean SRP concentration for tile outlets in late summer.

and $\text{CV}_C/\text{CV}_Q > 0.3$. Two of these sites showed considerable wastewater treatment plant influences (wastewater treatment plant density > 0.005 sites km^{-2} Table A3). Three sites (2 %) showed chemostatic behavior for SRP transport, as defined by a $\text{CV}_C/\text{CV}_Q \leq 0.3$.

When low-flow samples from late summer were removed, 54 % of gauged watersheds ($n = 78$) exhibited an increase in the slope of the mobilizing relationship between SRP and Q (Fig. 7; Table A5). For these sites, slopes of the C – Q relationships increased by 23 %, on average, after late-summer low-flow samples were excluded (the range, in percentage slope increase, was 0.1%–273 %). In other words, mobilizing behavior for SRP was stronger when these late-summer low-flow conditions were excluded. Examples of this phenomenon for four different gauged watersheds are shown in Fig. 8, where the slope of the C – Q relationship is steeper when late-summer low-flow samples were excluded and comparatively flatter when they are included. Watersheds where late-summer low flows modulated (flattened) the slope of the C – Q relationship for SRP were again located predominantly in the agriculturally dominated regions of the state (Fig. 7).

3.8 Regression analysis to identify drivers of elevated SRP concentrations in late summer

The final selected hyperparameters for the random forest model based on model tuning with 10-fold cross-validation for this dataset were $\text{mtry} = 7$, $\text{trees} = 1000$, and $\text{min}_n = 6$. The evaluation of the predicted vs. actual late-summer SRP for the independent test dataset indicated a model RMSE of 0.10 and an R^2 of 0.41 (Fig. A4). On average, the random forest model underestimated actual mean SRP concentrations during late-summer low flows compared to actual measured values among test sites (mean of estimated – true values = -0.005). However, this negative bias was driven by

poor predictive model performance for three sites with exceptionally high mean SRP concentrations of 0.293, 0.525, and 0.526 mg L^{-1} (Fig. A4). For the remaining test sites (all with mean SRP $< 0.2 \text{ mg L}^{-1}$), the predictive bias (mean of estimate – true values = 0.02) was actually positive. For most sites, in other words, the random forest model overestimated mean late-summer SRP concentrations compared to measured values.

The top 15 predictors of model performance are shown in Fig. 9. Importance values for all predictors are shown in Table A6. Partial-dependence plots for these top predictors (Fig. 10) showed that higher SRP during late-summer low-flow conditions was associated with higher cropland land use in riparian areas, various soil characteristics (higher soil erodibility, lower soil permeability, higher soil clay content), greater agricultural intensity (higher pesticide use, higher phosphorus uptake by crops, higher fertilizer application rates), more urban land use in riparian areas, lower woody wetlands and mixed forest in riparian areas, lower grassland land use in watersheds, lower surplus precipitation in the watershed (precipitation minus evaporation), and higher stream temperatures. Table 3 summarizes possible mechanisms linking these attributes to riverine SRP concentrations.

4 Discussion

In this study we observed that between one-third to one-half of the gauged watersheds in Minnesota exhibited SRP concentrations during late-summer low flows that were above previously identified thresholds for eutrophication of 0.02 – 0.04 mg L^{-1} for freshwater environments (Zeng et al., 2016; Poikane et al., 2021) (34 % were above a threshold of 0.04 mg L^{-1} , and 53 % of watersheds were above 0.02 mg L^{-1}). One avenue for future research is to investigate how the timing and duration of elevated summer SRP

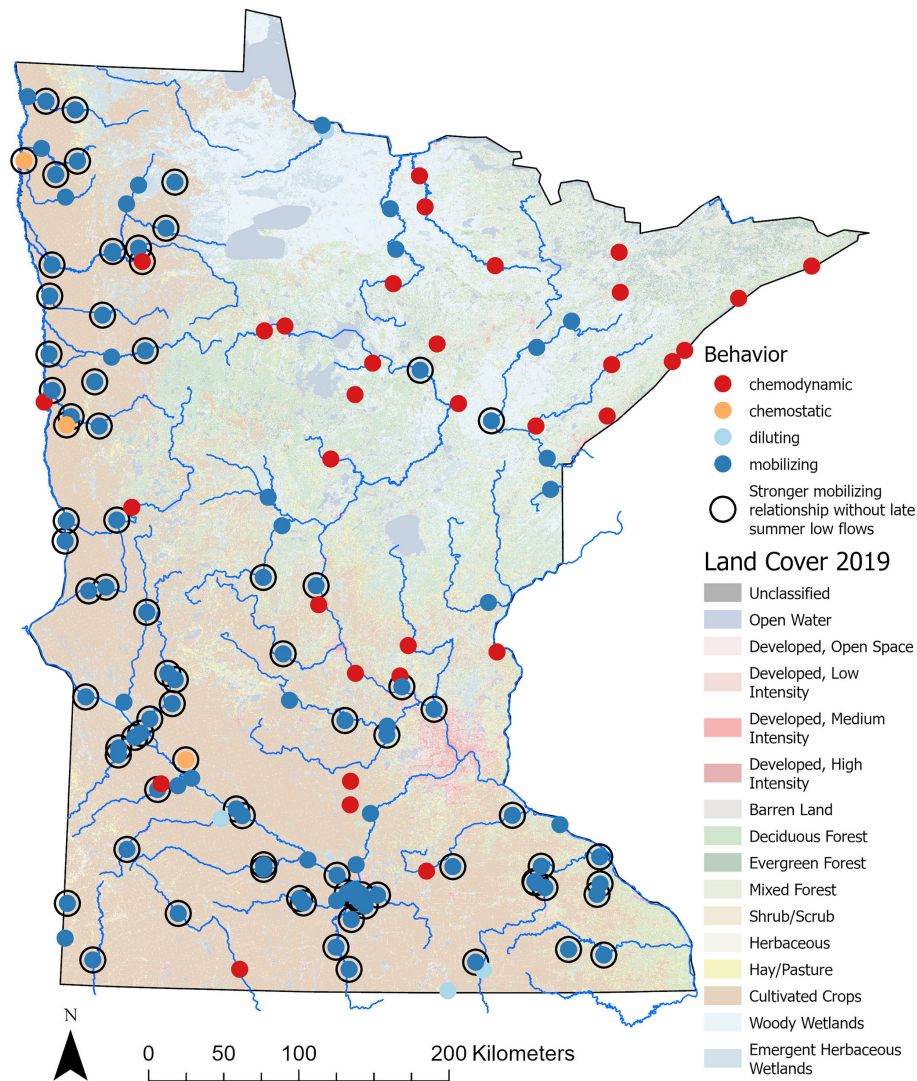


Figure 7. Transport behavior of SRP in relation to flow (Q) for gauged watersheds ($n = 143$). Dots indicate gauge locations. The color of the dots indicates transport behavior diagnosed by slope b of the C – Q power-law relationship and CV_C/CV_Q . Mobilizing behavior is indicated by dark-blue dots ($n = 103$), chemodynamic behavior is indicated by red dots ($n = 34$), diluting behavior is indicated by light-blue dots ($n = 4$), and chemostatic behavior is indicated by orange dots ($n = 3$). Sites with a stronger mobilizing relationship (i.e., an increase in slope b) when late-summer low flows are excluded are shown as open circles ($n = 78$). Land cover is based on the 2019 National Land Cover Database.

concentrations affect local and downstream eutrophication outcomes. On the one hand, the large majority of annual P export by load is likely to occur under high-flow conditions in late winter and spring (Dolph et al., 2019; Schilling et al., 2020). However, the release of highly bioavailable P during hot, dry summer periods when conditions are optimal for algal growth in lakes and rivers may also drive increased eutrophication risk, resulting in outcomes such as increased occurrence of harmful algal blooms (Paerl and Huisman, 2008). As climate change is expected to result in increased prolonged periods of drought and heat during summer in the Upper Midwest (Wilson et al., 2023), the effects of elevated

bioavailable P at low flows could be extended for longer parts of the season.

We also observed that, for more than half of the gauged watersheds we studied (54 %), elevated SRP concentrations during low flows in late summer dampened C – Q relationships which would have otherwise appeared to be more strongly mobilizing across other seasons and flow conditions. Strongly mobilizing relationships are indicative of landscape connectivity as a key driver for SRP export (Musolff et al., 2015), with flow accumulation and riparian areas identified as critical source areas for SRP (Casquin et al., 2020; Dupas et al., 2023). Thus, for many of the sites we studied, connectivity appears to be important to SRP export during

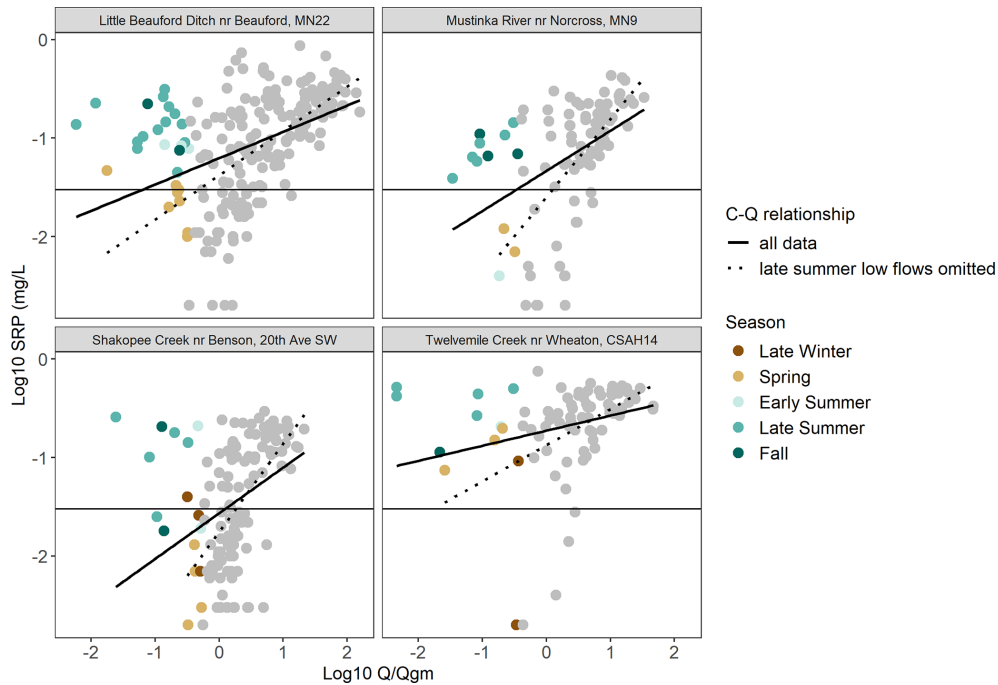


Figure 8. Example watersheds where low flows in late summer modulate the slope of the $C-Q$ relationship for SRP. Low-flow samples are shown as colored points, where the color indicates the season in which they were collected. All other samples are shown in gray. When all data are included, the slope of the overall $C-Q$ relationship is reduced (solid line) compared to slopes for analyses with late-summer low-flow samples omitted (dashed line), indicating stronger mobilizing behavior.

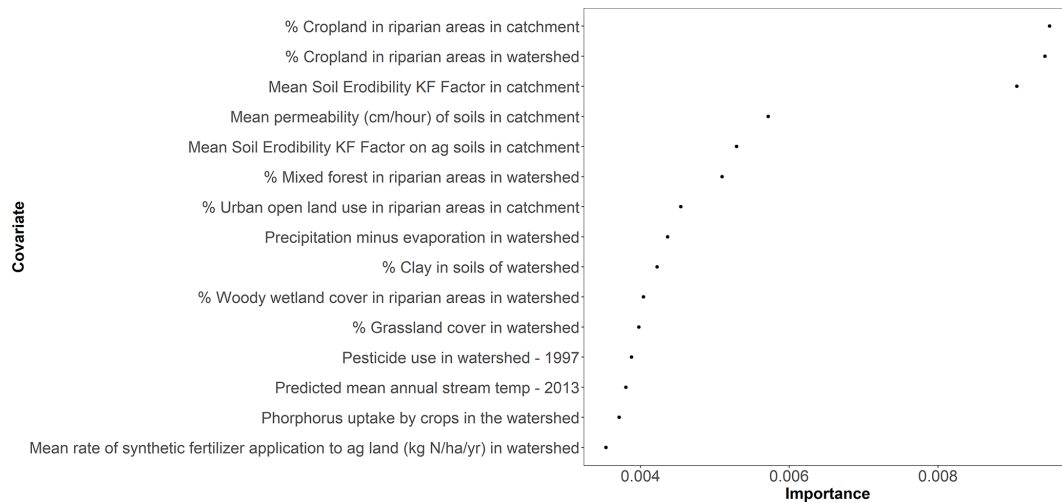


Figure 9. Conditional permutation importance (CPI) values for the top 15 predictors in the random forest model for late-summer SRP during low flows and in stream and river gauges. CPI is a measure that can be used to assess how much each variable “adds” to accurately predicting the response variable, given what we know from all other covariates. Importance values for all attributes are given in Table A6.

winter, spring, and early summer and under moderate- to high-flow conditions at all times of year. During late-summer low flows, by contrast, other in-channel dynamics may cause riverine $C-Q$ patterns to deviate from linear relationships (Meybeck and Moatar, 2012). Below, we discuss possible mechanisms that may contribute to comparatively high SRP

concentrations during late-summer low-flow conditions in the streams and rivers of our study region.

4.1 Drivers of SRP during late-summer low flows

Overall, our analysis shows that landscape drivers that govern diffuse P inputs and legacy P supply in the river net-

Table 3. Possible mechanisms linking random forest model predictor variables to late-summer SRP concentrations during low-flow conditions for the top 15 attributes identified as being most important to the performance of the random forest model. All attributes are from the US EPA StreamCat Dataset.

Attribute	Relationship	General mechanism category	Potential specific mechanism(s) linked to elevated late-summer SRP
Percentage of local NHD catchment classified as crop land use (NLCD 2019) within a 100 m buffer of NHD streams	Increasing SRP with increasing crop cover grown in proximity to river network	Direct inputs and/or legacy P supply	Indicator of current and historic P inputs from agricultural land use, especially in local riparian areas
Percentage of watershed classified as crop land use (NLCD 2019) within a 100 m buffer of NHD streams	Increasing SRP with increasing crop cover grown in proximity to river network	Direct inputs and/or legacy P supply	Indicator of current and historic P inputs from agricultural land use, especially in local and up-stream riparian areas
Mean soil erodibility factor (KFFACT, via STATSGO) within local NHD catchment – represents a relative index of susceptibility of bare, cultivated soil to particle detachment and transport by rainfall	Increasing SRP with increasing soil erodibility	Direct inputs and/or legacy P supply	Inputs of soil-associated P into river networks, either current or historic
Mean permeability (cm h^{-1}) of soils (STATSGO) within local NHD catchment	Higher SRP at very low soil permeability	Mediates biogeochemical processes in near-channel environment	Low permeability impedes oxygen exchange to the hyporheic zone, facilitating redox-mediated P release
Percentage of watershed classified as mixed-forest land cover (NLCD 2019) within a 100 m buffer of NHD streams	Higher SRP with low mixed-forest cover in riparian areas	Direct inputs and/or legacy P supply and/or mediates biogeochemical processes	Fewer current or historic inputs of P into river networks with forested riparian areas; potential for forested riparian areas to trap P; shading of river channel alters stream productivity or stream metabolism
Percentage of local NHD catchment classified as developed, open-space land use (NLCD 2019) within a 100 m buffer of NHD streams	Higher SRP with higher open urban land use in riparian buffer	Direct inputs and/or legacy P supply and/or mediates biogeochemical processes	Indicator of urban land use and associated P inputs; could also mediate biogeochemical processes by altering stream temperature or flow conditions (i.e., higher stream temperatures in urban areas, stormwater infrastructure contributing to low-flow conditions during dry periods)
Precipitation (mm) minus potential evaporation within watershed	Higher SRP at low and high ends of precipitation range	Mediates biogeochemical processes in near-channel environment	Dry conditions contribute to higher stream temperatures and lower discharge, influencing biologically mediated P release
Mean percentage of clay content of soils within watershed	Higher SRP with greater clay content in soils	Mediates biogeochemical processes in near-channel environment	Fe-containing clay sediments can adsorb P and release it via redox reactions
Percentage of watershed classified as woody-wetland land cover (NLCD 2019) within a 100 m buffer of NHD streams	Higher SRP with low woody-wetland cover in riparian buffers	Mediates biogeochemical processes in near-channel environment	Woody wetlands acting as sinks for SRP
Percentage of local catchment classified as grassland or herbaceous land cover (NLCD 2019)	Higher SRP at low grassland cover	Direct inputs and/or legacy P supply	Fewer historic and ongoing P inputs into grasslands vs. agricultural or urban land
Mean pesticide use (kg km^{-2}) in 1997 within watershed	Increasing SRP with increasing pesticide use	Direct inputs and/or legacy P supply	Indicator of agricultural intensity and degree of historic and/or current P inputs
Predicted mean annual stream temperature for 2013	Higher SRP with higher stream temperatures	Mediates biogeochemical processes in near-channel environment; proxy for direct inputs and/or legacy P supply	Indicator of temperature-mediated biological activity or of land use differences across climate gradients associated with P inputs (e.g., more agriculture and associated legacy P supplies in warmer climates)
Phosphorus uptake by crops in the watershed	Increasing SRP with increasing P uptake	Direct inputs and/or legacy P supply	Indicator of agricultural intensity and degree of historic and/or current P inputs
Mean rate of synthetic nitrogen fertilizer application to agricultural land ($\text{in kg N ha}^{-1} \text{ yr}^{-1}$) within the watershed	Increasing SRP with increasing fertilizer inputs	Direct inputs and/or legacy P supply	Indicator of agricultural intensity and degree of historic and/or current P inputs

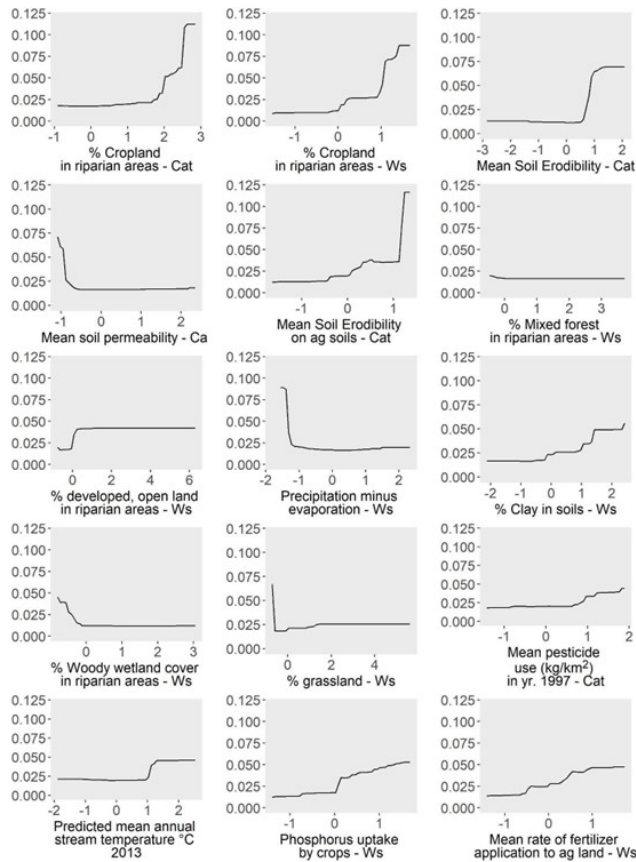


Figure 10. Partial dependence (y axis indicates the change in predicted SRP value) for each of the 15 most important predictors of model performance. Partial dependence shows the change in the response variable (late-summer low-flow SRP) when each predictor of interest is varied while all other predictors stay constant. “Ws” refers to predictors summarized at the watershed scale, and “Ca” refers to predictors summarized at the catchment scale. All predictor variables are from the US EPA StreamCat Dataset (Hill et al., 2016).

work, as well as wastewater inputs and biogeochemical processes, are associated with high late-summer SRP concentrations during low flows at many anthropogenically dominated sites. Crop cover was strongly and directly related to SRP concentrations during low-flow conditions in all seasons, and crop cover in riparian areas at the local catchment and watershed scales was one of the top two most important variables with regard to the performance of the random forest model used to predict late-summer low-flow SRP concentrations. Other top variables with regard to model performance included aspects of agricultural intensity at the watershed or catchment scale (pesticide use, phosphorus uptake by crops, and fertilizer application), as well as urban land use in riparian areas. The importance of these variables points to historic and ongoing inputs of P arising from intensive and/or industrial agricultural and urban land uses that have resulted in the accumulation of legacy P in riverine channels, which can

potentially be released under environmental conditions such as warm temperatures, low oxygen, and variable moisture. Conversely, greater mixed forest or woody-wetland land use in riparian areas was associated with lower SRP concentrations during late-summer low flows, perhaps because these environments may act as sinks for bioavailable P (Ury et al., 2023). Overall, it is notable that land use in riparian areas showed up as one of the top variables of importance with regard to model performance, suggesting that near-channel environments (and, therefore, potentially, near-channel management practices) may be important in regulating elevated SRP during late-summer low flows. Lastly, both geologic and climatic variables (soil erodibility, soil permeability, clay content of soils, mean annual stream temperatures, and precipitation minus evaporation) were also identified as important in the random forest model in terms of predicting late-summer low-flow SRP, suggesting that environmental factors which mediate biogeochemical processes are also likely to play an important role in driving late-summer riverine SRP concentrations.

Interestingly, SRP concentrations during late-summer low-flow conditions in anthropogenically dominated watersheds often exceeded tile SRP concentrations. Although tile drainage is known to represent a key input of P to river networks (Smith et al., 2015), it may be that in-channel dynamics beyond tile concentrations drive variability in SRP concentration during summer low flows. However, it is also important to note that the two tile outlets draining farms with dairy operations exhibited much higher SRP concentrations during late summer (and at all times of the year) compared to tile outlets draining fields characterized only by corn and soybean row crops. Thus, the prevalence of CAFOs and other animal agriculture operations is likely to strongly influence the contribution of tile drainage to riverine SRP concentrations. Three sites also had a surface inlet to their tile drainage system. These tile systems had comparatively high SRP during winter, spring, or early summer (depending on the site), which can likely be explained by the additional loss of sediment and nutrients to surface inlets during snowmelt on frozen and thawing soils (Feyereisen et al., 2015). However, the two surface-inlet-influenced sites without dairy operations exhibited SRP concentrations during late summer similar to those of other impacted non-dairy sites.

Wastewater treatment plant density did not rank among the most important predictors in our random forest model performance, and a substantial portion of sites (38 %) exhibited elevated SRP concentrations (above 0.02 mg L^{-1}) during late-summer low-flow conditions despite having limited or no wastewater treatment plant influence in their watersheds. However, the influence of wastewater on summer low-flow SRP was evident in the elevated SRP concentrations at sites with strong wastewater influence throughout most seasons (apart from spring, when low-flow SRP concentrations were nearly universally low, presumably due to rapid in-stream uptake or abiotic immobilization).

4.2 Biogeochemical processes and riverine SRP

Previous studies have identified a number of biogeochemical processes that can affect riverine concentrations of SRP at low flows. These processes include (1) the concentration of legacy P entering the stream via groundwater and/or streambed pore water, (2) the redox-driven release of P from stream sediments, and (3) the release of P resulting from mineralization of organic matter.

During low-flow conditions, groundwater and/or pore water can become proportionately dominant components of flow, with stores of legacy P in these sources contributing more strongly to overall riverine SRP. These groundwater sources can include tile drainage (Schilling et al., 2020; Rode et al., 2023) but can also include streambed pore water entering from the hyporheic zone via upwelling flow paths with P concentrations that are distinct and potentially higher than that of tile drainage (Vissers et al., 2023). Upwelling of P-rich pore water can be patchy and is likely to be controlled by hyper-local spatial and temporal conditions operating at the reach scale, such as the availability and extent of reducing vs. oxic conditions (e.g., Vissers et al., 2023).

SRP can also be released into river channels from stream sediments. Stream sediments often have the potential to buffer stream SRP concentrations by adsorbing P (Simpson et al., 2021). However, this buffering capacity will depend on sediment and stream characteristics, including sorption affinity; stream pH; exchangeable P concentration; sediment particle sizes; and seasonal variations in temperature, light, discharge, redox, primary productivity, stream respiration, and sediment inputs (Simpson et al., 2021). Seasonal release of SRP is commonly thought to occur via the reduction of Fe-, Mn-, or Al-oxyhydroxide-containing sediments under anoxic conditions, releasing PO_4^{3-} . These anoxic conditions typically arise when flow velocities are low, when water and sediment temperatures increase, and when oxygen becomes depleted due to increased microbial activity. For example, Smolders et al. (2017) showed that high summer concentrations of bioavailable P for rivers in Belgium were likely to be explained by internal loading from legacy P that was released from sediments when dissolved oxygen concentrations were low and when P:Fe molar ratios in sediment were large.

Lastly, Jarvie et al. (2020) showed that, in a wetland-pond system, microbial respiration and the resulting mineralization of organic matter can also represent a source of bioavailable P under low-flow conditions in summer and fall. They found that SRP release was potentially related to drier and hotter conditions that could facilitate both higher rates of biomass accumulation and its subsequent breakdown via microbial processes. Presumably, this dynamic could also be at play for slow-moving ditches and streams in parts of our study region where water is sometimes nearly stagnant in summer. Under low-flow conditions and warm temperatures, ditches and streams may operate in ways that are similar to wetlands or other lentic waterbodies. The stream

network is also populated with in-channel and riparian wetlands that may further affect ambient SRP concentrations. Felton et al. (2023) found elevated dissolved P concentrations along a longitudinal stream gradient where the channel intersected wetlands and concluded that locally elevated SRP could reflect P release from the decomposition of organic matter in wetland environments; however, in that study, elevated P concentrations did not persist downstream and were assumed to be rapidly assimilated or adsorbed to sediments.

Our findings provide some insight into the relative importance of these potential in-channel processes in determining seasonally elevated SRP concentrations at low flow. The importance of climate and geologic variables in the random forest model we used to predict late-summer low-flow SRP suggests that characteristics of stream sediments and/or climate-mediated biotic activity may play an important role in elevated SRP concentrations in late summer. Partial-dependence plots indicated that increased SRP during late-summer low flows was associated with the drier conditions (lower precipitation minus evaporation in gauged watersheds) and warmer conditions (higher predicted mean stream temperatures)¹. This finding could be consistent with the important role of biologically mediated processes, such as microbial respiration, that are affected by temperature and stream discharge. Microbial activity is important in both the decomposition of organic matter (i.e., mineralization) and the reduction of redoximorphic sediments (i.e., sediments containing Fe, Al, Mn), both of which can result in the release of SRP. The predicted mean stream temperature values used in this study were derived from Hill et al. (2013) and were themselves influenced by air temperature, soil permeability, agricultural and urban land use, stream slope, reservoirs, and watershed area. The positive relationship between stream temperature and late-summer SRP at low flow needs further investigation but could also be related to the greater influence of groundwater or to climate gradients that correspond to variations in biological activity or in land use and associated P inputs.

Soil erodibility was also identified as one of the most important variables with regard to random forest model performance, with partial-dependence plots showing higher SRP during late-summer low flows corresponding with greater soil erodibility in the local catchment. Eroded soils have long been understood to be a primary vector by which P enters river networks (Berhe et al., 2018). Recently, this understanding has been expanded to include eroded stream bank sediments as an additional driver of downstream P transport (Margenot et al., 2023). Sediment-associated P may be temporarily stored in river channels, with desorption of P oc-

¹Note that stream temperature data in the US EPA StreamCat Dataset are derived from Hill et al. (2013) and take into account natural factors and certain aspects of anthropogenic influence (i.e., reservoirs, urban land use, and agricultural land use) but do not account for wastewater effluence.

curing under certain environmental conditions, as described above.

Partial-dependence plots showed that late-summer low-flow SRP concentrations were highest where the soil permeability of soils in local catchments was low. This finding is also consistent with the release of P from stream sediments. Low soil permeability is characteristic of fine sediments (Ren and Santamarina, 2018). If broader watershed soil types are indicative of in-stream sediment, very low permeability of fine-grained stream sediments could impede oxygen exchange to the hyporheic zone, potentially creating anoxic conditions to facilitate redox-mediated P release (Mendoza-Lera and Detry, 2017).

Partial-dependence plots also indicated that increased SRP during late-summer low-flow conditions was associated with increased clay content of soils in gauged watersheds. Clay particles are small in size, providing greater P adsorption potential (Simpson et al., 2021). Clay sediments also typically contain iron (Fe) that can bind P and can therefore provide a substrate for microbially mediated redox reactions (Pentřáková et al., 2013). Our findings are consistent with a mechanism whereby clay sediments bind considerable P under some conditions and then release it via redox reactions during late summer when oxic conditions are low due to microbial decomposition of organic matter.

Environmental conditions in large parts of our study region are consistent with those previously reported to foster situational SRP release from sediments. Previous studies have observed the release of SRP from stream sediments when SRP-to-Fe ratios in sediments are high and when dissolved oxygen concentrations are low (Inamdar et al., 2020; van Dael et al., 2020; Diamond et al., 2023). These conditions are characteristic of slow-moving lowland streams with large legacy P stores arising from current and historic P inputs and may be especially common in headwater streams (Diamond et al., 2023). Such conditions are widespread across our study region. Ditches, streams, and rivers in the flat to gently rolling landscapes of southern and northwestern Minnesota are characterized by relatively low gradients, high current and historic P loading from agriculture and urban land use (Boardman et al., 2019), and high rates of in-stream primary productivity (Dolph et al., 2017b). During late summer, these conditions are likely to result in high rates of microbial respiration, anoxic streambed environments, and P release.

Overall, our findings agree with previous studies that have identified the importance of biogeochemical processes in seasonally modulating nutrient concentrations during low flows in lowland lotic systems (e.g., Smolders et al., 2017) and, in many ways, are parallel to findings for eutrophic lakes (Søndergaard et al., 2001). Further study is needed to parse the importance of pore water, stream sediment dynamics, and mineralization to the elevated SRP concentrations we observed at various stream and river sites during late-summer low-flow conditions.

4.2.1 Limitations and future study

A major limitation of this study is that we did not have direct information about legacy P supply in stream and river channels. Efforts to quantify the P content of stream sediments and the potential of stream sediments to adsorb and/or desorb SRP in different geographic, seasonal, and hydrologic contexts could provide additional valuable information about the extent to which the in-channel release of legacy P is affecting downstream water quality.

It is also important to note that the performance of the random forest model we used to predict late-summer SRP concentrations was middling ($R^2 = 0.41$). We speculate that improved model performance will depend on reach-scale variables that may strongly determine SRP dynamics, such as channel morphology, the characteristics and volume of bed sediment, and stream productivity and respiration. Future research could aim to incorporate both reach-scale and broader-scale variables into a more precise understanding of in-channel SRP dynamics. For example, the sampling platform described by Felton et al. (2023) presents the intriguing possibility of monitoring stream conditions intensively along longitudinal gradients and could be refined to include measures of dissolved oxygen, CO₂ (as a proxy for respiration), temperature, and sorption capacity and/or to identify P inputs associated with tile and point discharges or certain aspects of channel morphology.

5 Conclusions

In this study, we observed widespread elevation of SRP concentrations during late-summer low-flow conditions among anthropogenically dominated ditches, streams, and rivers in Minnesota. These elevated SRP concentrations altered $C-Q$ transport behavior for more than half (54 %) of the gauged watersheds we studied, weakening what was otherwise more strongly mobilizing behavior during higher-flow conditions and other times of year.

While wastewater discharge likely contributed to elevated SRP concentration during low flows for some sites, most sites exhibiting elevated SRP concentrations during late-summer low-flow conditions did not have substantial wastewater treatment impacts. Moreover, elevated SRP concentrations during low flows at these sites typically exceeded tile drainage SRP concentrations from corn- and soy-planted farm fields during late summer. We found that late-summer low-flow SRP concentrations were related to land use, soil characteristics, measures of agricultural intensity, and climate. Taken together, these findings suggest that climate and geologically mediated biogeochemical processes likely result in the release of in-channel stores of legacy P during late-summer low-flow conditions in a substantial number of stream and river sites that have been heavily impacted by past and current P inputs associated with industrial and/or inten-

sive agriculture and urbanization. As summers become hotter and drier – predicted climate changes in our region – conditions for the release of legacy P stored in stream and river channels will likely become more prolonged and/or more acute, contributing to the increased occurrence of adverse events such as harmful algal blooms. Further study is needed to determine the duration, fate, and dominant mechanisms associated with the riverine release of bioavailable P during late summer and other times of the year.

Our findings suggest that efforts to reduce the impacts of bioavailable P on freshwater will need to address both (1) the mobilization of dissolved P from the landscape during high-flow conditions and (2) the in-channel environments that result in the release of accumulated legacy P from streams and rivers during summer low flows when freshwater systems are especially vulnerable to eutrophication outcomes. With regards to management, the association of land use in riparian areas with SRP during late-summer low flows suggests that practices targeting near-channel and riparian environments may be important in regulating elevated SRP. In Minnesota, state law implemented in 2015 has already mandated vegetative 50 ft (15 m) riparian buffers along the state's waterbodies to protect water quality (Riparian Protection and Water Quality Practices Act, 2015, <https://www.revisor.mn.gov/statutes/cite/103F.48>, last access: 23 February 2024). Our findings suggest that, perhaps, specific vegetative conditions within these riparian buffers – for example, whether mixed forests or woody wetlands are present – could additionally enhance legacy P retention and mitigate release. Further study is needed to examine the way these habitat types interact with legacy P over time and under different conditions.

Controlling ongoing P inputs will also be instrumental to reducing riverine P loading. For example, in Minnesota, additional phosphorus regulations added to National Pollutant Discharge Elimination System (NPDES) permits since the year 2000 have resulted in substantial reductions in P loading arising from wastewater facilities (<https://www.pca.state.mn.us/business-with-us/phosphorus-in-wastewater>, last access: 7 March 2024). Policies and management approaches to substantially reduce the inputs of fertilizer, manure, and wastewater, as well their losses via surface, tile, and other groundwater pathways, remain critical to achieving societal water quality goals.

Appendix A

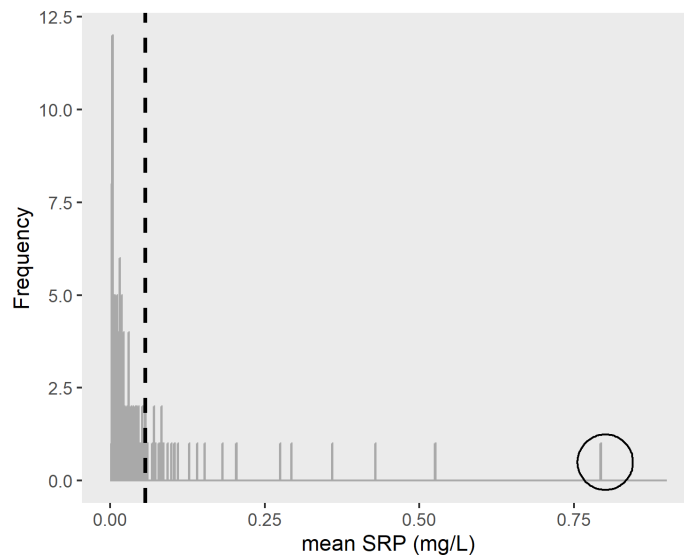


Figure A1. Distribution of mean SRP concentrations (mg L^{-1}) during late-summer low-flow conditions for 128 gauged watersheds with more than three SRP samples collected during late-summer low flows. Note that one outlier (circled value) was excluded prior to model development. The dashed line indicates the mean of all mean SRP values.

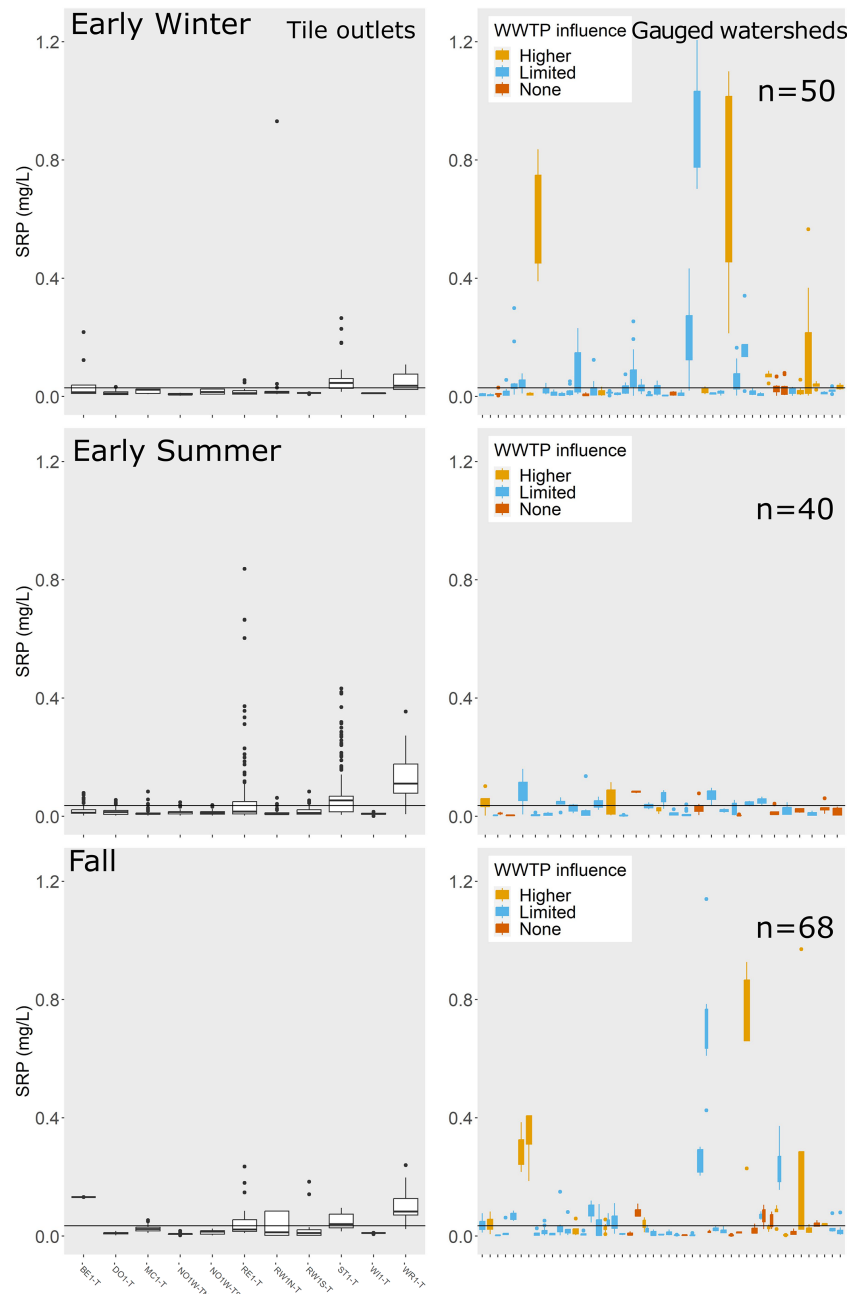


Figure A2. SRP concentrations (mg L^{-1}) for tile outlets and during low-flow conditions for gauged watersheds for early winter, early summer, and fall. See main text for similar plots for other seasons. The horizontal line in each plot is the mean SRP concentration among tile outlets for that season. The number of gauges for which low-flow data were available in each season is printed on the plot. For gauged watersheds, the color of the boxplots indicates the degree of influence from wastewater treatment plants: orange indicates wastewater treatment plant density > 0.005 sites km^{-2} , blue indicates wastewater treatment plant density < 0.005 sites km^{-2} but greater than zero, and red indicates no wastewater treatment plant sites in the watershed. To improve data visibility, the y axis for SRP was limited to a maximum of 1.25 mg L^{-1} , which eliminated a small number of outliers from the plots for tile outlets ($n = 34$ out of 11 079 low-flow records) and gauged watersheds ($n = 16$ out of 2696 low-flow records).

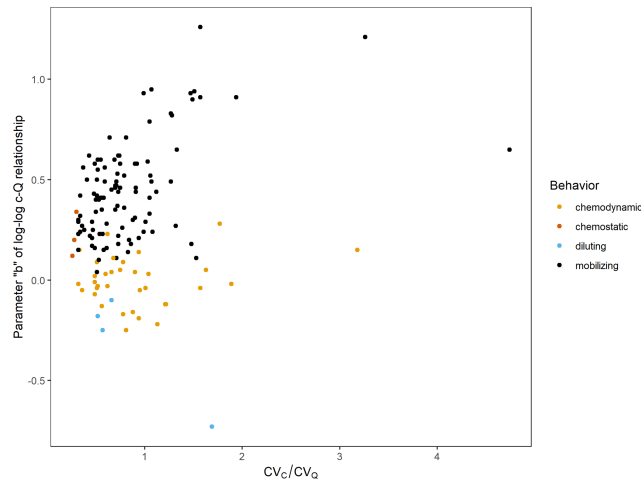


Figure A3. Parameter b (slope) of the event-scale log–log C – Q relationship for soluble reactive phosphorus (SRP, mg L^{-1}) in relation to CV_C/CV_Q for 143 gauged watersheds. Color indicates export behavior based on criteria defined for b and CV_C/CV_Q . Chemostatic: $CV_C/CV_Q \leq 0.3$ (sensu Thompson et al., 2011); chemodynamic: $CV_C/CV_Q > 0.3$ and no significant b ($p > 0.05$); diluting: significant $b < 0$; mobilizing: significant $b > 0$.

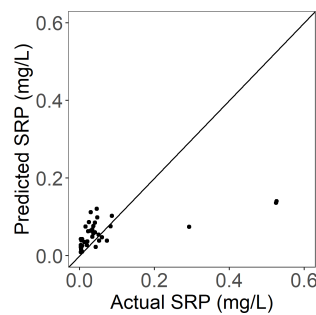


Figure A4. Actual vs. predicted late-summer SRP concentrations (mg L^{-1}) for gauged streams and rivers in the independent test dataset (i.e., not used to build the model). $R^2 = 0.41$, $\text{RMSE} = 0.010$, $p < 0.0001$. Solid line shows 1-to-1 relationship.

Table A1. Linear regression statistics for mean SRP (log scale) during low-flow conditions in relation to the density of wastewater treatment plants (sites km^{-2}) across gauged watersheds by season. Linear regressions were calculated for all sites and were recalculated where sites with a density of wastewater treatment plants $> 0.005 \text{ sites km}^{-2}$ were excluded. Note that “WWTP” refers to wastewater treatment plant throughout.

Season	Slope	T statistic	p	R^2	n	WWTP influence
Early winter	102.77	4.06	< 0.001	0.26	50	all watersheds
Early winter	87.12	1.61	0.12	0.06	40	gauges with WWTP $> 0.005 \text{ sites km}^{-2}$ excluded
Late Winter	90.57	3.62	< 0.001	0.19	57	all watersheds
Late winter	121.36	2.14	0.04	0.1	45	gauges with WWTP $> 0.005 \text{ sites km}^{-2}$ excluded
Spring	29.47	0.7	0.49	0.02	23	all watersheds
Spring	−55.71	−0.7	0.5	0.03	17	gauges with WWTP $> 0.005 \text{ sites km}^{-2}$ excluded
Early summer	51.93	1.4	0.17	0.05	40	all watersheds
Early summer	47.84	0.91	0.37	0.02	35	gauges with WWTP $> 0.005 \text{ sites km}^{-2}$ excluded
Late summer	74.76	4.84	< 0.001	0.16	128	all watersheds
Late summer	80.66	2.44	0.02	0.06	102	gauges with WWTP $> 0.005 \text{ sites km}^{-2}$ excluded
Fall	76.03	4.07	< 0.001	0.2	68	all watersheds
Fall	95.19	1.85	0.07	0.07	51	gauges with WWTP $> 0.005 \text{ sites km}^{-2}$ excluded

Table A2. Linear regression statistics for mean SRP (log scale) during low-flow conditions in relation to percentage crop cover across gauged watersheds by season. Linear regressions were calculated for all sites and were recalculated for sites with no wastewater treatment plant influence in their watersheds.

Season	Slope	<i>T</i> statistic	<i>p</i>	<i>R</i> ²	<i>n</i>	WWTP influence
Early winter	0.01	5.09	< 0.001	0.35	50	all watersheds
Early winter	0.01	4.25	0.02	0.86	5	no WWTP present in watershed
Late winter	0.02	7.65	< 0.001	0.52	57	all watersheds
Late winter	0.01	2.5	0.04	0.44	10	no WWTP present in watershed
Spring	0.01	3.75	< 0.001	0.4	23	all watersheds
Spring	0.01	2.27	0.06	0.43	9	no WWTP present in watershed
Early summer	0.01	3.56	< 0.001	0.25	40	all watersheds
Early summer	0.01	3.32	0.01	0.55	11	no WWTP present in watershed
Late summer	0.01	10.66	< 0.001	0.47	128	all watersheds
Late summer	0.01	7.39	< 0.001	0.69	26	no WWTP present in watershed
Fall	0.01	5.63	< 0.001	0.32	68	all watersheds
Fall	0.01	3.09	0.01	0.51	11	no WWTP present in watershed

Table A3. Mean SRP during low-flow conditions (flow conditions \leq lowest 25th percentile of flows on record) for each gauged watershed during each season. Note that means were only calculated where gauged watersheds had \geq three low-flow samples collected during a season. NA indicates that fewer than three low-flow samples were collected during that season. “WS area” refers to the watershed land area draining into each gauge (in km²). “WWTP density” is wastewater treatment plant density for each watershed (in sites km⁻²).

Site name	WS area (km ²)	Human impact	WWTP density	Spring	Early summer	Late summer	Fall	Early winter	Late winter
Brule River near Hovland, MN61	544.30	Less impacted	0	NA	NA	NA	NA	NA	NA
Poplar River near Lutsen, 0.2 mi US of MN61	293.29	Less impacted	0.003	NA	NA	0.003	0.003	0.004	0.003
Baptism River near Beaver Bay, MN61	358.44	Less impacted	0.003	NA	NA	0.004	NA	0.006	0.003
Beaver River near Beaver Bay, 1.2 mi us of MN61	318.73	Impacted	0.003	NA	NA	0.003	NA	NA	NA
Big Sucker Creek near Palmers, CR258	93.48	Less impacted	0	NA	0.003	0.003	NA	0.011	0.009
St Louis River at Floodwood, CSAH8	4978.62	Impacted	0.004	0.002	NA	0.011	NA	NA	NA
St Louis River near Forbes, US53	1793.51	Impacted	0.006	0.003	NA	0.004	0.003	NA	NA
Second Creek near Aurora, 0.6 mi us of CSAH110	56.66	Impacted	0	NA	NA	0.004	0.002	NA	0.006
St Louis River at Scanlon, MN	8893.21	Impacted	0.003	NA	0.009	0.004	NA	0.007	NA
Cloquet River near Brimson, CSAH44	330.99	Less impacted	0	NA	NA	0.004	NA	NA	NA
Cloquet River near Burnett, CR694	2032.29	Less impacted	0.001	0.005	0.005	0.003	NA	0.008	NA
Nemadji River near Pleasant Valley, MN23	324.41	Impacted	0	NA	NA	0.005	NA	NA	NA
Mississippi River near Bemidji, CSAH11	958.60	Impacted	0.001	NA	0.028	0.03	NA	NA	NA
Mississippi River near Bemidji, MN	1627.93	Impacted	0.002	NA	0.003	0.003	NA	NA	NA
Leech Lake River near Ball Club, CR139	3464.53	Impacted	0.001	0.004	0.003	0.004	NA	NA	NA
Boy River nr Boy River, CSAH53	750.13	Less impacted	0.001	NA	NA	0.002	NA	NA	NA
Prairie River near Taconite, MN	79.80	Impacted	0	0.006	NA	0.005	NA	NA	0.006
Mississippi River at Grand Rapids, MN	8483.32	Impacted	0.001	0.003	0.003	0.005	0.007	NA	0.003

Table A3. Continued.

Site name	WS area (km ²)	Human impact	WWTP density	Spring	Early summer	Late summer	Fall	Early winter	Late winter
Swan River near Jacobson, CR438	758.11	Impacted	0.012	NA	NA	0.018	NA	NA	NA
Swan River near Sobieski, MN238	462.60	Impacted	0.002	NA	NA	0.021	NA	NA	NA
Pine River near Jenkins, CSAH15	743.11	Impacted	0	NA	NA	NA	NA	NA	NA
Leaf River near Staples, CSAH29	2232.34	Impacted	0.003	NA	NA	0.022	NA	0.013	0.025
Long Prairie River at Philbrook, 313th Ave	2346.60	Impacted	0.005	NA	0.035	0.023	NA	0.024	0.022
Long Prairie River at Long Prairie, MN	1271.78	Impacted	0.005	0.014	NA	NA	NA	NA	0.016
Two Rivers near Bowlus, 40th St	386.26	Impacted	0.008	NA	NA	NA	NA	NA	NA
Sauk River near St Martin, CR12	2887.54	Impacted	0.005	0.018	NA	0.059	NA	NA	NA
Clearwater River near Clearwater, CR145	436.24	Impacted	0.002	0.008	NA	0.003	NA	NA	NA
Elk River near Big Lake, MN	1373.83	Impacted	0.003	NA	0.027	NA	NA	NA	NA
St Francis River near Big Lake, 164th St	530.84	Impacted	0	NA	0.02	0.013	NA	NA	NA
Middle Fork Crow River near Manannah, CSAH30	702.11	Impacted	0.006	0.01	0.022	0.012	NA	NA	NA
North Fork Crow River near Cokato, CSAH4	2638.30	Impacted	0.004	NA	0.07	0.031	NA	NA	NA
North Fork Crow River near Rockford, Farmington Ave	3444.89	Impacted	0.005	NA	NA	0.02	0.021	0.031	0.045
South Fork Crow River at Delano, Bridge Ave	3295.67	Impacted	0.004	NA	NA	0.182	0.239	0.168	0.218
Buffalo Creek near Glencoe, CSAH1	969.28	Impacted	0.004	NA	NA	0.793	NA	NA	NA
West Branch Rum River near Princeton, CR102	482.91	Impacted	0.006	NA	NA	NA	NA	NA	NA
Rum River at Anoka, headwater side of dam	4113.49	Impacted	0.004	NA	0.043	NA	NA	0.01	0.015
Minnesota River near Lac qui Parle, MN	10 546.93	Impacted	0.003	NA	NA	0.085	0.055	0.094	0.126
Yellow Bank River near Odessa, CSAH40	1191.21	Impacted	0.004	NA	NA	0.03	NA	0.021	0.31
Pomme de Terre River at Appleton, MN	2227.38	Impacted	0.002	NA	NA	NA	NA	0.024	0.082
Pomme de Terre River near Hoffman, CR76	1026.90	Impacted	0.002	NA	NA	0.013	0.01	NA	NA
Lac qui Parle River near Lac qui Parle, CSAH31	2487.56	Impacted	0.004	NA	0.042	0.019	NA	0.028	0.063
Lac qui Parle River near Providence, CSAH23	983.91	Impacted	0.004	NA	NA	0.023	NA	NA	NA
West Branch Lac qui Parle River at Dawson, Diagonal St	1220.43	Impacted	0.002	NA	NA	0.083	NA	NA	NA
Hawk Creek near Maynard, MN23	1226.46	Impacted	0.003	NA	0.056	0.051	0.034	NA	NA
Hawk Creek near Granite Falls, CR52	1321.42	Impacted	0.003	NA	0.003	0.01	0.013	0.083	0.158

Table A3. Continued.

Site name	WS area (km ²)	Human impact	WWTP density	Spring	Early summer	Late summer	Fall	Early winter	Late winter
Beaver Creek near Beaver Falls, CSAH2	495.39	Impacted	0.004	NA	NA	0.053	0.041	NA	NA
Yellow Medicine River near Granite Falls, MN	1716.39	Impacted	0.002	NA	NA	0.034	0.012	0.02	0.35
Yellow Medicine River near Hanley Falls, CR18	1171.62	Impacted	0.001	NA	NA	0.019	0.027	NA	NA
Spring Creek near Hanley Falls, 480th St	332.81	Impacted	0.006	NA	NA	0.293	NA	NA	NA
Chippewa River near Clontarf, CSAH22	1731.39	Impacted	0.004	NA	NA	0.016	0.009	NA	NA
Shakopee Creek near Benson, 20th Ave SW	786.32	Impacted	0	0.006	NA	0.141	NA	NA	0.024
Chippewa River near Milan, MN40	4626.36	Impacted	0.002	NA	NA	0.022	0.009	0.02	0.027
East Branch Chippewa River near Benson, CR78	1305.27	Impacted	0.001	NA	0.043	0.048	0.019	NA	NA
Redwood River near Redwood Falls, MN	1619.96	Impacted	0.003	NA	NA	0.099	0.731	1.175	1.247
Redwood River at Russell, CR15	599.04	Impacted	0	NA	NA	0.035	0.015	NA	NA
Minnesota River at Morton, MN	23 008.88	Impacted	0.003	NA	NA	0.046	0.058	0.098	0.141
Minnesota River at Judson, CSAH42	28 865.06	Impacted	0.003	NA	0.01	0.027	0.028	0.04	0.08
Seven Mile Creek near St Peter, 0.6 mi us of US169	94.16	Impacted	0	0.008	0.015	0.016	0.012	NA	0.027
Cottonwood River near New Ulm, MN68	3374.02	Impacted	0.003	0.01	0.007	0.007	0.007	0.016	0.048
Sleepy Eye Creek near Cobden, CR8	706.81	Impacted	0	NA	NA	0.022	0.021	NA	NA
Cottonwood River near Leavenworth, CR8	2281.68	Impacted	0.004	NA	NA	0.013	NA	NA	NA
Blue Earth River near Winnebago, CSAH12	3592.84	Impacted	0.004	NA	NA	0.027	0.025	NA	NA
East Branch Blue Earth River at Blue Earth, CSAH16	764.22	Impacted	0.003	NA	NA	0.071	0.062	NA	NA
Blue Earth River near Rapidan, MN	6274.80	Impacted	0.004	NA	NA	0.015	0.006	0.015	0.028
South Fork Watonwan River near Madelia, CSAH13	515.74	Impacted	0.004	NA	NA	0.052	NA	NA	NA
Watonwan River near La Salle, CSAH3	875.15	Impacted	0.005	NA	NA	0.073	NA	NA	NA
Watonwan River near Garden City, CSAH13	2205.66	Impacted	0.005	NA	NA	0.016	0.022	0.017	0.152
Maple River near Sterling Center, CR18	801.21	Impacted	0.004	NA	NA	0.071	NA	NA	NA
Big Cobb River near Beauford, CSAH16	787.09	Impacted	0.006	NA	0.048	0.041	0.042	NA	NA
Maple River near Rapidan, CR35	877.79	Impacted	0.005	NA	NA	0.02	0.038	NA	NA
Little Beauford Ditch near Beauford, MN22	22.03	Impacted	0	0.025	0.083	0.153	NA	NA	NA
Le Sueur River near Rapidan, CR8	1156.71	Impacted	0.005	0.004	0.017	0.029	0.027	NA	NA

Table A3. Continued.

Site name	WS area (km ²)	Human impact	WWTP density	Spring	Early summer	Late summer	Fall	Early winter	Late winter
Le Sueur River near Rapidan, MN	2873.06	Impacted	0.005	NA	0.006	0.014	0.012	0.014	0.032
Le Sueur River at St Clair, CSAH28	919.12	Impacted	0.006	0.023	0.101	0.058	NA	NA	NA
High Island Creek near Arlington, CR9	428.96	Impacted	0	0.037	NA	0.079	NA	NA	NA
High Island Creek near Henderson, CSAH6	624.30	Impacted	0.002	NA	NA	0.019	NA	NA	NA
Snake River near Pine City, MN	2563.68	Impacted	0.003	NA	0.02	0.012	NA	0.014	0.02
Sunrise River at Sunrise, CR88	870.50	Impacted	0.005	NA	NA	0.037	NA	NA	NA
Wells Creek near Frontenac, US61	176.12	Impacted	0	0.032	NA	NA	0.04	NA	NA
Cannon River at Welch, MN	3477.94	Impacted	0.007	NA	NA	0.204	NA	0.009	0.044
Cannon River at Morristown, CSAH16	627.90	Impacted	0.008	0.121	NA	NA	0.29	NA	NA
Straight River near Faribault, MN	1129.24	Impacted	0.006	NA	NA	NA	NA	0.069	NA
Whitewater River near Beaver, CSAH30	689.62	Impacted	0.01	NA	NA	0.047	0.039	0.039	0.048
North Fork Whitewater River at Elba, Whitewater Dr	269.37	Impacted	0.011	NA	NA	NA	0.057	NA	0.049
North Fork Zumbro River near Mazeppa, CSAH7	621.81	Impacted	0.006	NA	NA	0.057	0.026	NA	0.046
Zumbro River at Kellogg, US61	3677.89	Impacted	0.008	NA	NA	0.046	NA	0.033	0.042
South Fork Zumbro River near Oronoco, CR121	885.55	Impacted	0.015	NA	NA	0.11	0.077	NA	NA
South Branch Middle Fork Zumbro River near Oronoco, 5th St	569.86	Impacted	0.011	NA	NA	0.057	0.025	NA	NA
Middle Fork Zumbro River near Oronoco, 5th St	534.52	Impacted	0.006	NA	NA	0.041	0.02	NA	NA
South Branch Root River at Lanesboro, Rochelle Ave N	738.36	Impacted	0.01	NA	NA	0.03	0.032	NA	NA
Middle Branch Root River near Fillmore, CSAH5	506.94	Impacted	0.006	NA	NA	0.039	0.035	NA	NA
Cedar River near Austin, MN	1030.86	Impacted	0.013	NA	NA	0.525	0.338	0.65	0.954
Turtle Creek at Austin, 43rd St	382.45	Impacted	0.008	NA	NA	0.359	0.268	NA	NA
Shell Rock River near Gordonsville, CSAH1	496.65	Impacted	0.012	NA	NA	0.526	0.68	1.159	1.368
West Fork Des Moines River near Avoca, CSAH6	1233.33	Impacted	0.006	NA	NA	0.014	NA	NA	NA
West Fork Des Moines River at Jackson, River St	3216.99	Impacted	0.007	NA	NA	0.037	NA	0.342	0.592
Bois de Sioux River near Doran, MN	4713.44	Impacted	0.002	NA	0.084	0.086	NA	0.069	0.128
Mustinka River near Norcross, MN9	486.58	Impacted	0	NA	NA	0.083	0.082	NA	NA

Table A3. Continued.

Site name	WS area (km ²)	Human impact	WWTP density	Spring	Early summer	Late summer	Fall	Early winter	Late winter
Twelve Mile Creek near Wheaton, CSAH14	1006.00	Impacted	0	0.141	NA	0.429	NA	NA	NA
Pelican River near Fergus Falls, MN210	1294.46	Impacted	0.003	NA	0.02	0.019	0.006	NA	NA
Otter Tail River near Elizabeth, MN	2974.42	Impacted	0.001	NA	NA	0.003	0.002	NA	0.005
Otter Tail River at Breckenridge, CSAH16	5116.19	Impacted	0.002	NA	NA	0.016	0.011	0.005	0.01
Red River of the North near Kragnes, CSAH26	28 555.84	Impacted	0.003	NA	NA	0.275	0.254	0.217	0.332
Buffalo River near Georgetown, CR108	2820.97	Impacted	0.002	NA	NA	0.093	0.067	0.042	0.052
Buffalo River near Glyndon, CSAH19	998.93	Impacted	0.004	NA	NA	0.068	NA	NA	NA
South Branch Buffalo River near Glyndon, 28th Ave S	1314.84	Impacted	0.001	NA	NA	0.128	NA	NA	NA
Buffalo River near Hawley, MN	837.03	Impacted	0.001	NA	NA	0.06	NA	NA	NA
Wild Rice River near Mahnomen, CSAH25	1473.79	Impacted	0	NA	NA	0.019	NA	NA	NA
Wild Rice River at Twin Valley, MN	2405.45	Impacted	0.001	NA	NA	0.007	NA	NA	NA
Wild Rice River at Hendrum, MN	4091.49	Impacted	0.002	NA	NA	0.03	0.031	0.012	0.018
S Br. Wild Rice River at CR27 near Felton, MN	499.54	Impacted	0.006	NA	NA	0.055	NA	NA	NA
Sand Hill River near Fertile, 450th St. SW	620.95	Impacted	0.002	NA	0.052	0.029	0.018	NA	NA
Sand Hill River at Climax, MN, US-75	1209.33	Impacted	0.001	NA	NA	0.034	0.024	0.014	0.031
Red Lake River at High Landing near Goodridge, MN	5963.65	Impacted	0	NA	0.003	0.011	NA	NA	NA
Red Lake River at Red Lake Falls, CR13	9413.51	Impacted	0	0.003	0.023	0.004	0.004	NA	NA
Red Lake River at Fisher, MN	14 466.12	Impacted	0.001	NA	0.034	0.013	NA	0.009	0.017
Thief River near Thief River Falls, MN	2515.45	Impacted	0	NA	0.027	0.011	0.012	0.026	0.05
Thief River downstream of CSAH 7, 6 mi E of Holt	1658.23	Impacted	0	0.002	0.013	0.007	NA	NA	0.036
Mud River near Grygla, MN89	481.28	Impacted	0	NA	0.029	0.021	0.008	NA	NA
Clearwater River at Plummer, MN	1454.55	Impacted	0.002	NA	NA	0.043	0.027	NA	NA
Lost River near Brooks, CR119	772.13	Impacted	0.003	NA	NA	0.042	0.085	NA	NA
Clearwater River at Red Lake Falls, MN	3474.65	Impacted	0.002	NA	NA	0.009	0.009	0.01	0.04
Snake River near Big Woods, MN220	2006.98	Impacted	0.001	NA	NA	NA	0.068	0.074	0.191
Middle River at Argyle, MN	643.64	Impacted	0.002	NA	0.062	0.043	0.048	NA	NA
Snake River above Warren, MN	491.56	Impacted	0	NA	NA	NA	0.068	NA	NA

Table A3. Continued.

Site name	WS area (km ²)	Human impact	WWTP density	Spring	Early summer	Late summer	Fall	Early winter	Late winter
Tamarac River near Florian, CSAH1	464.17	Impacted	0	NA	0.022	0.011	NA	NA	NA
Tamarac River near Stephen, CSAH22	909.20	Impacted	0	NA	0.036	NA	NA	0.03	0.198
Two Rivers near Hallock, CSAH16	2660.25	Impacted	0	NA	NA	0.016	NA	0.018	0.03
South Branch Two Rivers at Hallock, MN175	1669.83	Impacted	0.001	NA	NA	0.052	NA	NA	NA
South Branch Two Rivers at Lake Bronson, MN	1380.24	Impacted	0	NA	NA	0.104	0.053	NA	NA
Kawishiwi River near Winton, CSAH18	3415.83	Less impacted	0	0.004	NA	0.004	NA	0.007	0.007
Stony River near Babbitt, Tomahawk Rd	550.10	Less impacted	0	NA	NA	0.003	NA	NA	NA
Little Fork River near Linden Grove, TH73	736.54	Impacted	0.003	NA	NA	0.02	0.018	NA	NA
Little Fork River at Little Fork, MN	4382.42	Less impacted	0	NA	NA	0.004	0.004	0.009	0.015
Little Fork River near Little Fork, MN65	3492.09	Less impacted	0.001	NA	NA	0.007	0.005	NA	NA
Big Fork River near Big Fork, MN6	1567.06	Less impacted	0	NA	0.01	0.007	NA	NA	NA
Big Fork River at Big Falls, MN	3888.36	Less impacted	0.001	NA	0.003	0.004	0.003	0.005	0.011
Big Fork River near Craigville, MN6	2555.10	Less impacted	0.001	NA	NA	0.004	NA	NA	NA
East Fork Rapid River near Clementson, CSAH18	709.40	Less impacted	0	NA	NA	0.022	NA	NA	NA
Rapid River at Clementson, MN11	2486.55	Impacted	0	NA	NA	0.004	0.003	0.01	0.014
Split Rock Creek near Jasper, 201st St	822.62	Impacted	0.004	NA	NA	0.011	NA	0.014	0.027
Pipestone Creek near Pipestone, CSAH13	308.55	Impacted	0.006	NA	NA	0.025	NA	NA	NA
Rock River at Luverne, CR4	1084.55	Impacted	0.005	NA	NA	0.016	NA	0.02	0.025

Table A4. Number of SRP samples collected during low-flow conditions in each season for each gauged watershed. Note that mean SRP values (Table S3) were only calculated in seasons where fewer than three samples had been collected during low-flow conditions for that gauged watershed.

Site name	Early winter	Late winter	Spring	Early summer	Late summer	Fall
Baptism River near Beaver Bay, MN61	4	5	NA	2	9	NA
Beaver Creek near Beaver Falls, CSAH2	NA	1	1	1	6	5
Beaver River near Beaver Bay, 1.2 mi us of MN61	NA	NA	NA	2	4	1
Big Cobb River near Beauford, CSAH16	NA	2	2	4	18	4
Big Fork River at Big Falls, MN	6	10	1	4	14	3
Big Fork River near Big Fork, MN6	NA	NA	NA	4	14	NA
Big Fork River near Craigville, MN6	NA	NA	NA	2	10	1
Big Sucker Creek near Palmers, CR258	6	4	NA	3	4	NA
Blue Earth River near Rapidan, MN	11	7	2	2	19	3
Blue Earth River near Winnebago, CSAH12	NA	1	NA	NA	8	3
Bois de Sioux River near Doran, MN	10	5	2	6	12	2
Boy River near Boy River, CSAH53	NA	NA	1	2	5	2
Brule River near Hovland, MN61	NA	NA	NA	NA	1	2
Buffalo Creek near Glencoe, CSAH1	NA	1	2	1	3	1

Table A4. Continued.

Site name	Early winter	Late winter	Spring	Early summer	Late summer	Fall
Buffalo River near Georgetown, CR108	8	7	NA	NA	11	4
Buffalo River near Glyndon, CSAH19	NA	NA	NA	NA	3	2
Buffalo River near Hawley, MN	NA	2	1	NA	4	2
Cannon River at Morristown, CSAH16	NA	1	3	NA	2	3
Cannon River at Welch, MN	8	5	1	NA	6	1
Cedar River near Austin, MN	10	4	NA	1	9	4
Chippewa River near Clontarf, CSAH22	NA	2	1	2	5	4
Chippewa River near Milan, MN40	11	8	NA	NA	9	4
Clearwater River at Plummer, MN	NA	NA	2	NA	5	6
Clearwater River at Red Lake Falls, MN	14	9	2	1	16	9
Clearwater River near Clearwater, CR145	NA	2	3	1	3	1
Cloquet River near Brimson, CSAH44	NA	NA	1	1	7	NA
Cloquet River near Burnett, CR694	3	2	4	4	13	2
Cottonwood River near Leavenworth, CR8	NA	NA	2	1	6	2
Cottonwood River near New Ulm, MN68	14	8	3	3	14	6
East Branch Blue Earth River at Blue Earth, CSAH16	NA	1	NA	1	8	3
East Branch Chippewa River near Benson, CR78	NA	NA	NA	6	6	3
East Fork Rapid River near Clementson, CSAH18	NA	NA	1	2	8	NA
Elk River near Big Lake, MN	NA	1	2	5	2	1
Hawk Creek near Granite Falls, CR52	13	7	1	3	12	5
Hawk Creek near Maynard, MN23	NA	1	2	3	5	4
High Island Creek near Arlington, CR9	NA	1	4	1	5	1
High Island Creek near Henderson, CSAH6	NA	1	2	1	8	1
Kawishiwi River near Winton, CSAH18	3	6	3	1	5	1
Lac qui Parle River near Lac qui Parle, CSAH31	9	4	2	3	5	2
Lac qui Parle River near Providence, CSAH23	NA	NA	NA	NA	3	2
Le Sueur River at St Clair, CSAH28	NA	1	3	4	14	2
Le Sueur River near Rapidan, CR8	NA	2	3	6	17	4
Le Sueur River near Rapidan, MN	16	7	1	3	19	4
Leaf River near Staples, CSAH29	7	9	NA	1	7	NA
Leech Lake River near Ball Club, CR139	1	2	3	5	8	1
Little Beauford Ditch near Beauford, MN22	NA	NA	8	3	14	2
Little Fork River at Little Fork, MN	7	9	NA	1	11	4
Little Fork River near Linden Grove, TH73	NA	NA	NA	NA	4	3
Little Fork River near Little Fork, MN65	NA	NA	NA	1	8	6
Long Prairie River at Long Prairie, MN	NA	3	4	1	1	2
Long Prairie River at Philbrook, 313th Ave	14	11	1	3	5	2
Lost River near Brooks, CR119	NA	NA	NA	NA	12	3
Maple River near Rapidan, CR35	NA	NA	NA	2	11	3
Maple River near Sterling Center, CR18	NA	1	NA	2	15	2
Middle branch of Root River near Fillmore, CSAH5	NA	NA	NA	NA	8	5
Middle Fork Crow River near Manannah, CSAH30	NA	1	3	3	3	2
Middle Fork Zumbro River near Oronoco, 5th St	NA	1	NA	NA	8	5
Middle River at Argyle, MN	NA	NA	NA	3	3	4
Minnesota River at Judson, CSAH42	12	6	NA	4	14	5
Minnesota River at Morton, MN	12	5	NA	1	7	8
Minnesota River near Lac qui Parle, MN	5	5	NA	2	3	4
Mississippi River at Grand Rapids, MN	2	5	8	8	13	4
Mississippi River near Bemidji, CSAH11	NA	NA	NA	3	3	1
Mississippi River near Bemidji, MN	NA	NA	1	3	4	1
Mud River near Grygla, MN89	NA	NA	NA	8	15	3
Mustinka River near Norcross, MN9	NA	NA	2	1	6	3
Nemadji River near Pleasant Valley, MN23	NA	NA	NA	1	6	1
North Fork Crow River near Cokato, CSAH4	NA	1	2	3	3	1
North Fork Crow River near Rockford, Farmington Ave	5	7	NA	2	4	3

Table A4. Continued.

Site name	Early winter	Late winter	Spring	Early summer	Late summer	Fall
North Fork Whitewater River at Elba, Whitewater Dr	NA	3	2	1	2	3
North Fork Zumbro River near Mazeppa, CSAH7	NA	3	2	NA	4	4
Otter Tail River at Breckenridge, CSAH16	10	7	NA	1	11	8
Otter Tail River near Elizabeth, MN	NA	7	1	1	7	3
Pelican River near Fergus Falls, MN210	NA	NA	2	4	5	3
Pine River near Jenkins, CSAH15	NA	NA	NA	1	2	NA
Pipestone Creek near Pipestone, CSAH13	NA	1	1	1	7	NA
Pomme de Terre River at Appleton, MN	9	7	NA	1	2	2
Pomme de Terre River near Hoffman, CR76	NA	NA	NA	2	7	3
Poplar River near Lutsen, 0.2 mi US of MN61	3	7	1	1	7	4
Prairie River near Taconite, MN	NA	3	3	NA	6	2
Rapid River at Clementson, MN11	8	11	1	2	13	3
Red Lake River at Fisher, MN	13	8	NA	4	17	2
Red Lake River at High Landing near Goodridge, MN	NA	NA	2	4	6	2
Red Lake River at Red Lake Falls, CR13	NA	NA	3	4	8	5
Red River of the North near Kragnes, CSAH26	14	8	NA	NA	7	4
Redwood River at Russell, CR15	NA	1	2	NA	7	4
Redwood River near Redwood Falls, MN	12	7	2	1	11	6
Rock River at Luverne, CR4	7	6	1	1	4	2
Rum River at Anoka, headwater side of dam	10	14	1	6	1	NA
S Br. Wild Rice River at CR27 near Felton, MN	NA	NA	NA	NA	4	1
Sand Hill River at Climax, MN, US-75	10	11	2	1	9	3
Sand Hill River near Fertile, 450th St. SW	NA	NA	NA	3	10	4
Sauk River near St Martin, CR12	NA	NA	3	2	4	1
Second Creek near Aurora, 0.6 mi us of CSAH110	NA	3	2	1	9	4
Seven Mile Creek near St Peter, 0.6 mi us of US169	NA	3	9	8	22	5
Shakopee Creek near Benson, 20th Ave SW	NA	3	4	2	5	2
Shell Rock River near Gordonsville, CSAH1	9	6	NA	NA	3	5
Sleepy Eye Creek near Cobden, CR8	NA	NA	1	NA	8	3
Snake River above Warren, MN	NA	NA	2	1	1	3
Snake River near Big Woods, MN220	13	3	NA	1	2	3
Snake River near Pine City, MN	4	8	NA	5	7	NA
South Branch Buffalo River near Glyndon, 28th Ave S	NA	NA	NA	1	7	2
South Branch Middle Fork Zumbro River near Oronoco, 5th St.	NA	1	NA	NA	3	5
South Branch Root River at Lanesboro, Rochelle Ave N	NA	2	NA	1	7	4
South Branch Two Rivers at Hallock, MN175	NA	1	NA	1	4	2
South Branch Two Rivers at Lake Bronson, MN	NA	1	NA	2	3	4
South Fork Crow River at Delano, Bridge Ave	5	7	1	NA	6	4
South Fork Watonwan River near Madelia, CSAH13	NA	1	NA	NA	6	1
South Fork Zumbro River near Oronoco, CR121	NA	1	NA	NA	6	5
Split Rock Creek near Jasper, 201st St.	6	7	NA	NA	6	2
Spring Creek near Hanley Falls, 480th St.	NA	1	2	1	7	2
St Francis River near Big Lake, 164th St.	NA	1	NA	6	5	1
St Louis River at Floodwood, CSAH8	NA	NA	3	2	5	1
St Louis River at Scanlon, MN	3	1	1	4	11	2
St Louis River near Forbes, US53	NA	NA	3	1	9	5
Stony River near Babbitt, Tomahawk Rd	NA	1	2	1	6	1
Straight River near Faribault, MN	5	2	NA	NA	2	NA
Sunrise River at Sunrise, CR88	2	2	NA	NA	4	NA
Swan River near Jacobson, CR438	NA	NA	2	2	4	1
Swan River near Sobieski, MN238	NA	NA	NA	NA	3	2
Tamarac River near Florian, CSAH1	NA	NA	1	4	10	2
Tamarac River near Stephen, CSAH22	11	6	NA	3	2	NA
Thief River downstream of CSAH 7, 6 mi E of Holt	NA	3	4	5	6	1
Thief River near Thief River Falls, MN	12	12	1	3	11	3

Table A4. Continued.

Site name	Early winter	Late winter	Spring	Early summer	Late summer	Fall
Turtle Creek at Austin, 43rd St.	NA	NA	NA	1	9	4
Twelve Mile Creek near Wheaton, CSAH14	NA	2	3	1	5	1
Two Rivers near Bowlus, 40th St.	NA	NA	NA	2	NA	NA
Two Rivers near Hallock, CSAH16	11	9	NA	2	9	2
Watowwan River near Garden City, CSAH13	11	8	1	1	15	3
Watowwan River near La Salle, CSAH3	NA	1	1	NA	6	2
Wells Creek near Frontenac, US61	NA	NA	4	1	2	3
West Branch Lac qui Parle River at Dawson, Diagonal St.	NA	NA	NA	NA	4	2
West Branch Rum River near Princeton, CR102	NA	NA	NA	NA	NA	1
West Fork Des Moines River at Jackson, River St.	8	8	1	NA	5	2
West Fork Des Moines River near Avoca, CSAH6	NA	NA	1	1	5	1
Whitewater River near Beaver, CSAH30	7	5	2	1	5	3
Wild Rice River at Hendrum, MN	8	11	2	1	14	5
Wild Rice River at Twin Valley, MN	NA	1	NA	NA	4	1
Wild Rice River near Mahnomon, CSAH25	NA	NA	NA	NA	5	NA
Yellow Bank River near Odessa, CSAH40	6	5	NA	NA	4	2
Yellow Medicine River near Granite Falls, MN	7	5	2	NA	8	7
Yellow Medicine River near Hanley Falls, CR18	NA	1	2	NA	7	5
Zumbro River at Kellogg, US61	7	6	NA	NA	9	2
Total number of sites with fewer than three samples collected during low flows	50	57	23	40	128	68

Table A5. Linear regression statistics for the log–log relationship between SRP concentrations (mg L^{-1}) and normalized flow (Q/Q_{GM}). The regressions were run twice. The first regressions (denoted with (1) in the table) included all samples collected for a given site. The second set of regressions (denoted with (2) in the table) excluded samples collected during late-summer low flows. “Percentage change in slope” indicates the change in slope between the first and second regression for each site. CV_C/CV_Q is reported using all samples collected for each site. Statistics in bold indicate statistically significant ($p < 0.05$) relationships.

Site name	Behavior	CV_C/CV_Q	Slope(1)	$p(1)$	$R^2(1)$	$n(1)$	Slope(2)	$p(2)$	$R^2(2)$	$n(2)$	Percentage slope change
Baptism River near Beaver Bay, MN61	chemodynamic	0.66	0.04	0.21	0.01	184	0.05	0.14	0.01	175	30.8
Beaver Creek near Beaver Falls, CSAH2	mobilizing	0.34	0.42	< 0.01	0.36	113	0.45	< 0.01	0.37	107	7.7
Beaver River near Beaver Bay, 1.2 mi us of MN61	chemodynamic	0.51	0.09	0.20	0.04	48	0.07	0.42	0.02	44	–24.03
Big Cobb River near Beauford, CSAH16	mobilizing	0.56	0.35	< 0.01	0.20	243	0.47	< 0.01	0.20	225	32.66
Big Fork River at Big Falls, MN	mobilizing	0.61	0.16	< 0.01	0.06	264	0.12	0.01	0.03	250	–26.35
Big Fork River near Big Fork, MN6	chemodynamic	1.01	–0.04	0.62	0.00	116	–0.01	0.91	0.00	102	–70.13
Big Fork River near Craigville, MN6	mobilizing	0.73	0.22	< 0.01	0.07	112	0.15	0.10	0.03	102	–32.38
Big Sucker Creek near Palmers, CR258	chemodynamic	0.6	0.03	0.40	0.00	162	0.01	0.71	0.00	158	–54.47
Blue Earth River near Rapidan, MN	mobilizing	0.74	0.62	< 0.01	0.45	437	0.64	< 0.01	0.41	418	1.69
Blue Earth River near Winnebago, CSAH12	mobilizing	0.71	0.47	< 0.01	0.27	139	0.50	< 0.01	0.22	131	6.3
Bois de Sioux River near Doran, MN	mobilizing	0.32	0.23	< 0.01	0.26	426	0.24	< 0.01	0.25	414	2.88
Boy River near Boy River, CSAH53	chemodynamic	1.77	0.28	0.09	0.06	49	0.29	0.14	0.05	44	0.7
Brule River near Hovland, MN61	chemodynamic	0.94	0.14	0.17	0.10	21	0.14	0.20	0.09	20	2.09
Buffalo Creek near Glencoe, CSAH1	chemodynamic	0.95	–0.05	0.56	0.00	71	0.09	0.39	0.01	68	–260.73
Buffalo River near Georgetown, CR108	mobilizing	0.32	0.30	< 0.01	0.25	438	0.32	< 0.01	0.26	427	7.98
Buffalo River near Glyndon, CSAH19	mobilizing	0.50	0.40	< 0.01	0.28	73	0.46	< 0.01	0.32	70	15.25
Buffalo River near Hawley, MN	mobilizing	0.53	0.40	< 0.01	0.27	97	0.43	< 0.01	0.28	93	6.76
Cannon River at Morristown, CSAH16	chemodynamic	0.81	–0.25	0.07	0.06	58	–0.20	0.18	0.03	56	–20.19
Cannon River at Welch, MN	mobilizing	1.07	0.49	< 0.01	0.09	119	0.68	< 0.01	0.17	113	37.33
Cedar River near Austin, MN	diluting	0.57	–0.25	< 0.01	0.19	265	–0.22	< 0.01	0.14	256	–12.34
Chippewa River near Clontarf, CSAH22	mobilizing	1.51	0.94	< 0.01	0.28	123	1.03	< 0.01	0.29	118	10.1
Chippewa River near Milan, MN40	mobilizing	1.33	0.65	< 0.01	0.29	304	0.68	< 0.01	0.28	295	4.66
Clearwater River at Plummer, MN	mobilizing	0.73	0.44	< 0.01	0.15	99	0.55	< 0.01	0.19	94	24.76
Clearwater River at Red Lake Falls, MN	mobilizing	0.55	0.41	< 0.01	0.18	396	0.37	< 0.01	0.14	380	–10.15
Clearwater River near Clearwater, CR145	chemodynamic	1.22	–0.12	0.44	0.01	59	–0.28	0.10	0.05	56	137.88
Cloquet River near Brimson, CSAH44	chemodynamic	0.62	–0.03	0.75	0.00	80	–0.13	0.29	0.02	73	325.35
Cloquet River near Burnett, CR694	chemodynamic	1.04	0.03	0.59	0.00	142	–0.02	0.77	0.00	129	–165.87
Cottonwood River near Leavenworth, CR8	mobilizing	0.91	0.46	< 0.01	0.35	136	0.47	< 0.01	0.27	130	1.75

Table A5. Continued.

Site name	Behavior	CV_C/CV_Q	Slope(1)	$p(1)$	$R^2(1)$	$n(1)$	Slope(2)	$p(2)$	$R^2(2)$	$n(2)$	Percentage slope slope change
Cottonwood River near New Ulm, MN68	mobilizing	0.73	0.62	< 0.01	0.49	389	0.60	< 0.01	0.44	375	-3.08
East Branch Blue Earth River at Blue Earth, CSAH16	mobilizing	0.84	0.20	< 0.01	0.06	140	0.29	< 0.01	0.08	132	41.42
East Branch Chippewa River near Benson, CR78	mobilizing	0.91	0.44	< 0.01	0.13	119	0.69	< 0.01	0.24	113	57.36
East Fork Rapid River near Clementson, CSAH18	diluting	0.52	-0.18	< 0.01	0.18	93	-0.14	0.01	0.07	85	-24.78
Elk River near Big Lake, MN	mobilizing	1.12	0.44	0.02	0.09	63	0.50	0.01	0.11	61	11.55
Hawk Creek near Granite Falls, CR52	mobilizing	0.51	0.50	< 0.01	0.37	375	0.44	< 0.01	0.31	363	-11.18
Hawk Creek near Maynard, MN23	chemostatic	0.3	0.34	< 0.01	0.30	120	0.34	< 0.01	0.29	115	2.35
High Island Creek near Arlington, CR9	chemodynamic	0.78	0.09	0.12	0.02	100	0.14	0.07	0.03	95	54.04
High Island Creek near Henderson, CSAH6	mobilizing	0.79	0.36	< 0.01	0.20	96	0.33	< 0.01	0.11	88	-10.11
Kawishiwi River near Winton, CSAH18	chemodynamic	1.21	-0.12	0.08	0.02	143	-0.16	0.02	0.04	138	34.45
Lac qui Parle River near Lac qui Parle, CSAH31	mobilizing	0.71	0.49	< 0.01	0.33	186	0.49	< 0.01	0.31	181	0.31
Lac qui Parle River near Providence, CSAH23	mobilizing	0.49	0.58	< 0.01	0.40	72	0.70	< 0.01	0.44	69	20.68
Le Sueur River at St Clair, CSAH28	mobilizing	0.34	0.32	< 0.01	0.21	179	0.38	< 0.01	0.20	165	21.25
Le Sueur River near Rapidan, CR8	mobilizing	0.43	0.62	< 0.01	0.50	269	0.67	< 0.01	0.45	252	7.11
Le Sueur River near Rapidan, MN	mobilizing	0.59	0.56	< 0.01	0.46	478	0.55	< 0.01	0.42	459	-0.76
Leaf River near Staples, CSAH29	mobilizing	0.54	0.23	< 0.01	0.15	181	0.23	< 0.01	0.14	174	-0.59
Leech Lake River near Ball Club, CR139	chemodynamic	1.63	0.05	0.68	0.00	77	0.05	0.76	0.00	69	-13.76
Little Beauford Ditch near Beauford, MN22	mobilizing	0.36	0.27	< 0.01	0.18	198	0.42	< 0.01	0.32	184	57.82
Little Fork River at Little Fork, MN	chemodynamic	0.49	0.02	0.62	0.00	251	-0.04	0.27	0.01	240	-336.91
Little Fork River near Linden Grove, TH73	chemodynamic	0.36	-0.05	0.35	0.02	50	-0.02	0.79	0.00	46	-65.46
Little Fork River near Little Fork, MN65	chemodynamic	0.49	-0.01	0.88	0.00	113	-0.05	0.36	0.01	105	598.71
Long Prairie River at Long Prairie, MN	mobilizing	1.05	0.41	< 0.01	0.14	60	0.44	< 0.01	0.16	59	7.12
Long Prairie River at Philbrook, 313th Ave	mobilizing	0.71	0.11	0.02	0.02	279	0.10	0.04	0.02	274	-5.65
Lost River near Brooks, CR119	chemodynamic	0.68	0.11	0.24	0.02	79	0.42	< 0.01	0.15	67	273.75
Maple River near Rapidan, CR35	mobilizing	0.37	0.56	< 0.01	0.50	216	0.62	< 0.01	0.49	205	11.2
Maple River near Sterling Center, CR18	mobilizing	0.34	0.24	< 0.01	0.22	269	0.33	< 0.01	0.26	254	36.51
Middle Branch Root River near Fillmore, CSAH5	mobilizing	0.72	0.53	< 0.01	0.32	121	0.60	< 0.01	0.33	113	12.67
Middle Fork Crow River near Manannah, CSAH30	mobilizing	1.57	0.91	< 0.01	0.28	70	0.83	< 0.01	0.25	67	-8.82
Middle Fork Zumbro River near Oronoco, 5th St.	mobilizing	0.75	0.58	< 0.01	0.50	127	0.62	< 0.01	0.51	119	6.60
Middle River at Argyle, MN	mobilizing	0.49	0.16	< 0.01	0.11	99	0.17	< 0.01	0.10	96	3.79
Minnesota River at Judson, CSAH42	mobilizing	0.79	0.52	< 0.01	0.21	433	0.53	< 0.01	0.19	419	1.36
Minnesota River at Morton, MN	mobilizing	0.77	0.26	< 0.01	0.06	299	0.28	< 0.01	0.07	292	9.18
Minnesota River near Lac qui Parle, MN	mobilizing	0.9	0.31	0.01	0.05	165	0.35	< 0.01	0.06	162	12.09
Mississippi River at Grand Rapids, MN	mobilizing	1.32	0.27	< 0.01	0.06	184	0.42	< 0.01	0.11	171	56.08
Mississippi River near Bemidji, CSAH11	chemodynamic	1.13	-0.22	0.18	0.04	44	-0.19	0.32	0.03	41	-16.08
Mississippi River near Bemidji, MN	chemodynamic	1.89	-0.02	0.92	0.00	42	-0.12	0.66	0.01	38	449.62
Mud River near Grygla, MN89	mobilizing	1.01	0.29	< 0.01	0.17	157	0.40	< 0.01	0.23	142	40.11
Mustinka River near Norcross, MN9	mobilizing	0.58	0.41	< 0.01	0.20	91	0.62	< 0.01	0.30	85	51.09
Nemadji River near Pleasant Valley, MN23	mobilizing	0.88	0.30	< 0.01	0.31	68	0.28	< 0.01	0.26	62	-7.72
North Fork Crow River near Kokato, CSAH4	mobilizing	1.49	0.90	< 0.01	0.19	74	1.02	< 0.01	0.21	71	14.2
North Fork Crow River near Rockford, Farmington Ave	mobilizing	1.05	0.33	< 0.01	0.07	206	0.32	< 0.01	0.06	202	-4.36
North Fork Whitewater River at Elba, Whitewater Dr	mobilizing	0.99	0.93	< 0.01	0.68	82	0.94	< 0.01	0.68	80	1.08
North Fork Zumbro River near Mazeppa, CSAH7	mobilizing	0.90	0.58	< 0.01	0.40	99	0.60	< 0.01	0.39	95	2.88
Otter Tail River at Breckenridge, CSAH16	mobilizing	3.26	1.21	< 0.01	0.22	231	1.35	< 0.01	0.24	220	11.46
Otter Tail River near Elizabeth, MN	chemodynamic	3.18	0.15	0.32	0.01	70	0.21	0.23	0.02	63	41.57
Pelican River near Fergus Falls, MN210	mobilizing	1.27	0.49	0.01	0.09	77	0.60	< 0.01	0.11	72	23.70
Pine River near Jenkins, CSAH15	chemodynamic	0.62	0.23	0.21	0.08	22	0.36	0.10	0.15	20	60.81
Pipestone Creek near Pipestone, CSAH13	mobilizing	0.55	0.60	< 0.01	0.55	73	0.71	< 0.01	0.56	66	18.10
Pomme de Terre River at Appleton, MN	mobilizing	1.07	0.95	< 0.01	0.33	166	0.94	< 0.01	0.33	164	-0.47
Pomme de Terre River near Hoffman, CR76	mobilizing	1.94	0.91	< 0.01	0.25	110	1.25	< 0.01	0.32	103	38.26
Poplar River near Lutsen, 0.2 mi US of MN61	chemodynamic	0.75	0.05	0.20	0.01	167	0.04	0.42	0.00	160	-29.4
Prairie River near Taconite, MN	chemodynamic	0.56	-0.13	0.08	0.05	59	-0.18	0.05	0.08	53	33.85
Rapid River at Clementson, MN11	mobilizing	0.51	0.04	0.05	0.01	309	0.01	0.66	0.00	296	-74.51
Red Lake River at Fisher, MN	mobilizing	0.81	0.71	< 0.01	0.34	383	0.77	< 0.01	0.35	366	7.81
Red Lake River at High Landing near Goodridge, MN	mobilizing	4.74	0.65	0.01	0.11	59	0.90	< 0.01	0.17	53	37.65
Red Lake River at Red Lake Falls, CR13	mobilizing	1.47	0.93	< 0.01	0.42	121	1.00	< 0.01	0.39	113	6.80
Red River of the North near Kragnes, CSAH26	chemodynamic	0.32	-0.02	0.46	0.00	376	0.00	0.89	0.00	369	-80.69
Redwood River at Russell, CR15	mobilizing	0.61	0.28	< 0.01	0.12	104	0.34	< 0.01	0.13	97	21.16
Redwood River near Redwood Falls, MN	diluting	0.66	-0.10	< 0.01	0.02	327	-0.20	< 0.01	0.10	316	96.5
Rock River at Luverne, CR4	mobilizing	0.64	0.71	< 0.01	0.52	194	0.71	< 0.01	0.51	190	0.10
Rum River at Anoka, headwater side of dam	mobilizing	0.72	0.37	< 0.01	0.14	171	0.38	< 0.01	0.14	170	1.48
S Br. Wild Rice River at CR27 near Felton, MN	mobilizing	0.32	0.29	< 0.01	0.29	48	0.30	< 0.01	0.26	44	2.91
Sand Hill River at Climax, MN, US-75	mobilizing	0.41	0.50	< 0.01	0.43	331	0.51	< 0.01	0.43	322	2.12
Sand Hill River near Fertile, 450th St. SW	mobilizing	0.70	0.47	< 0.01	0.23	104	0.52	< 0.01	0.23	94	9.61
Sauk River near St Martin, CR12	mobilizing	1.27	0.83	< 0.01	0.30	60	1.01	< 0.01	0.37	56	21.66
Second Creek near Aurora, 0.6 mi us of CSAH110	mobilizing	1.48	0.18	0.04	0.04	108	0.20	0.06	0.04	99	8.43
Seven Mile Creek near St Peter, 0.6 mi us of US169	mobilizing	0.56	0.41	< 0.01	0.39	326	0.40	< 0.01	0.33	304	-2.53
Shakopee Creek near Benson, 20th Ave SW	mobilizing	0.75	0.46	< 0.01	0.13	135	0.76	< 0.01	0.28	130	64.74
Shell Rock River near Gordonsville, CSAH1	diluting	1.69	-0.73	< 0.01	0.29	192	-0.73	< 0.01	0.28	189	-0.47
Sleepy Eye Creek near Cobden, CR8	mobilizing	0.51	0.42	< 0.01	0.44	118	0.43	< 0.01	0.40	110	3.6

Table A5. Continued.

Site name	Behavior	CV _c /CV _Q	Slope(1)	p(1)	R ² (1)	n(1)	Slope(2)	p(2)	R ² (2)	n(2)	Percentage slope change
Snake River above Warren, MN	mobilizing	0.44	0.22	<0.01	0.12	78	0.21	<0.01	0.11	77	-5.76
Snake River near Big Woods, MN220	chemostatic	0.26	0.12	<0.01	0.13	327	0.12	<0.01	0.13	325	0.48
Snake River near Pine City, MN	mobilizing	0.57	0.23	<0.01	0.11	213	0.22	<0.01	0.10	206	-4.32
South Branch Buffalo River near Glyndon, 28th Ave S	chemostatic	0.28	0.20	<0.01	0.17	105	0.29	<0.01	0.24	98	49.53
South Branch Middle Fork Zumbro River near Oronoco, 5th St	mobilizing	0.59	0.49	<0.01	0.39	103	0.52	<0.01	0.40	100	6.68
South Branch Root River at Lanesboro, Rochelle Ave N	mobilizing	1.05	0.79	<0.01	0.47	127	0.80	<0.01	0.45	120	1.00
South Branch Two Rivers at Hallock, MN175	mobilizing	0.46	0.21	<0.01	0.11	104	0.28	<0.01	0.14	100	33.96
South Branch Two Rivers at Lake Bronson, MN	mobilizing	0.46	0.17	0.01	0.07	89	0.17	0.02	0.06	86	1.82
South Fork Crow River at Delano, Bridge Ave	mobilizing	0.53	0.10	0.05	0.02	212	0.12	0.03	0.02	206	16.77
South Fork Watonwan River near Madelia, CSAH13	mobilizing	0.94	0.21	<0.01	0.08	123	0.31	<0.01	0.13	117	46.6
South Fork Zumbro River near Oronoco, CR121	mobilizing	0.86	0.18	<0.01	0.06	126	0.23	<0.01	0.09	120	31.70
Split Rock Creek near Jasper, 201st St.	mobilizing	0.52	0.60	<0.01	0.50	171	0.59	<0.01	0.47	165	-2.05
Spring Creek near Hanley Falls, 480th St.	chemodynamic	0.49	-0.07	0.26	0.01	106	0.02	0.77	0.00	99	-133.05
St Francis River near Big Lake, 164th St.	chemodynamic	0.78	-0.17	0.27	0.02	61	-0.16	0.32	0.02	56	-2.19
St Louis River at Floodwood, CSAH8	mobilizing	0.99	0.24	<0.01	0.09	87	0.30	<0.01	0.12	82	21.11
St Louis River at Scanlon, MN	mobilizing	1.08	0.24	<0.01	0.11	138	0.20	<0.01	0.06	127	-16.9
St Louis River near Forbes, US53	mobilizing	0.58	0.15	0.01	0.06	120	0.13	0.05	0.03	111	-13.42
Stony River near Babbitt, Tomahawk Rd	chemodynamic	0.9	0.04	0.70	0.00	76	-0.13	0.33	0.01	70	-419.25
Straight River near Faribault, MN	mobilizing	0.50	0.34	<0.01	0.28	111	0.35	<0.01	0.28	109	2.89
Sunrise River at Sunrise, CR88	chemodynamic	0.51	-0.04	0.53	0.00	90	-0.02	0.81	0.00	86	-57.9
Swan River near Jacobson, CR438	chemodynamic	0.94	-0.19	0.20	0.03	55	-0.22	0.24	0.03	51	14.27
Swan River near Sobieski, MN238	mobilizing	1.06	0.52	<0.01	0.26	62	0.57	<0.01	0.27	59	9.49
Tamarac River near Florian, CSAH1	mobilizing	0.73	0.18	<0.01	0.14	111	0.26	<0.01	0.17	101	41.22
Tamarac River near Stephen, CSAH22	mobilizing	0.38	0.25	<0.01	0.29	289	0.24	<0.01	0.27	287	-2.40
Thief River downstream of CSAH 7, 6 mi E of Holt	mobilizing	1.53	0.11	0.05	0.02	161	0.06	0.34	0.01	155	-45.73
Thief River near Thief River Falls, MN	mobilizing	0.83	0.14	<0.01	0.05	421	0.13	<0.01	0.04	410	-1.92
Turtle Creek at Austin, 43rd St.	mobilizing	0.92	0.58	<0.01	0.21	103	0.72	<0.01	0.24	94	23.05
Twelve Mile Creek near Wheaton, CSAH14	mobilizing	0.32	0.15	0.02	0.07	84	0.33	<0.01	0.20	79	117.23
Two Rivers near Bowlus, 40th St.	chemodynamic	0.88	-0.16	0.47	0.03	21	-0.16	0.47	0.03	21	0
Two Rivers near Hallock, CSAH16	mobilizing	0.46	0.29	<0.01	0.35	303	0.27	<0.01	0.30	294	-5.38
Watonwan River near Garden City, CSAH13	mobilizing	0.66	0.45	<0.01	0.38	360	0.42	<0.01	0.32	345	-6.66
Watonwan River near La Salle, CSAH3	mobilizing	0.44	0.22	<0.01	0.12	140	0.30	<0.01	0.18	134	38
Wells Creek near Frontenac, US61	mobilizing	1.57	1.26	<0.01	0.59	56	1.26	<0.01	0.58	54	-0.52
West Branch Lac qui Parle River at Dawson, Diagonal St.	mobilizing	0.47	0.25	<0.01	0.12	64	0.42	<0.01	0.22	60	67.62
West Branch Rum River near Princeton, CR102	chemodynamic	0.33	0.15	0.12	0.10	25	0.15	0.12	0.10	25	0
West Fork Des Moines River at Jackson, River St.	chemodynamic	1.57	-0.04	0.59	0.00	165	-0.05	0.56	0.00	160	16.04
West Fork Des Moines River near Avoca, CSAH6	mobilizing	0.69	0.60	<0.01	0.33	77	0.80	<0.01	0.41	72	34.59
Whitewater River near Beaver, CSAH30	mobilizing	1.28	0.82	<0.01	0.53	206	0.83	<0.01	0.53	201	0.52
Wild Rice River at Hendrum, MN	mobilizing	0.48	0.43	<0.01	0.36	402	0.46	<0.01	0.36	388	7.08
Wild Rice River at Twin Valley, MN	mobilizing	0.75	0.58	<0.01	0.49	57	0.55	<0.01	0.39	53	-3.98
Wild Rice River near Mahnomens, CSAH25	mobilizing	0.73	0.22	0.04	0.10	43	0.36	0.03	0.13	38	60.21
Yellow Bank River near Odessa, CSAH40	mobilizing	0.52	0.55	<0.01	0.45	177	0.56	<0.01	0.44	173	1.26
Yellow Medicine River near Granite Falls, MN	mobilizing	0.7	0.35	<0.01	0.25	257	0.34	<0.01	0.23	249	-2.22
Yellow Medicine River near Hanley Falls, CR18	mobilizing	0.7	0.46	<0.01	0.34	119	0.48	<0.01	0.30	112	3.82
Zumbro River at Kellogg, US61	mobilizing	1.03	0.59	<0.01	0.38	229	0.60	<0.01	0.37	220	2.57

Table A6. Conditional permutation importance value for predictor variables used in the random forest model. Note that AOI refers to the area of interest and defines whether variables were summarized at the watershed (Ws) or catchment (Cat) scale as well as whether they were limited to the 100 m riparian areas in the watershed or catchment (Rp100).

Predictor	Importance	Description
PctCrop2019CatRp100	0.009498	Percentage of the AOI classified as crop land use (NLCD class 82)
PctCrop2019WsRp100	0.009437	Percentage of the AOI area classified as crop land use (NLCD class 82)
KffactCat	0.009059	Mean of STATSGO Kffactor raster within the AOI – the Universal Soil Loss Equation (USLE) represents a relative index of the susceptibility of bare, cultivated soil to particle detachment and transport by rainfall
PermCat	0.005716	Mean permeability (cm h ⁻¹) of soils (STATSGO) within the AOI
AgKffactWs	0.005292	Mean of STATSGO Kffactor raster on agricultural land (NLCD 2006) within the AOI – the Universal Soil Loss Equation (USLE) represents a relative index of the susceptibility of bare, cultivated soil to particle detachment and transport by rainfall
PctMxFst2019WsRp100	0.005098	Percentage of the AOI area classified as mixed deciduous- and/or evergreen-forest land cover (NLCD class 43)

Table A6. Continued.

Predictor	Importance	Description
PctUrbOp2019CatRp100	0.004543	Percentage of the AOI area classified as developed, open-space land use (NLCD class 21)
Precip_Minus_EVTWs	0.004364	This dataset represents surplus precipitation (mm) (precipitation minus potential evaporation) as described in https://doi.org/10.1016/j.scitotenv.2020.137661 (Pennino et al., 2020) within individual, local NHDPlusV2 catchments and upstream, contributing watersheds
ClayWs	0.004223	Mean percentage of clay content of soils (STATSGO) within the AOI
PctWdWet2019WsRp100	0.004041	Percentage of the AOI area classified as woody-wetland land cover (NLCD class 90)
PctGrS2019Ws	0.003979	Percentage of the AOI area classified as grassland and/or herbaceous land cover (NLCD class 71)
Pestic97Cat	0.003880	Mean pesticide use (kg km^{-2}) in 1997 within the AOI
MAST_2013	0.003805	Predicted mean annual stream temperature (January–December) for 2008, 2009, 2013, and 2014
Phos_Crop_UptakeWs	0.003715	Phosphorus uptake by crops in the watershed
FertWs	0.003536	Mean rate of synthetic nitrogen fertilizer application to agricultural land (in $\text{kg N ha}^{-1} \text{yr}^{-1}$) within the AOI
WWTPAllDensWs	0.003328	Density (number km^{-2}) of all wastewater treatment plants per AOI
SiO2Cat	0.003151	Mean percentage of lithological silicon dioxide (SiO_2) content in surface or near-surface geology within the AOI
PctHay2019Cat	0.003151	Percentage of the AOI area classified as hay land use (NLCD class 81)
RdCrSslpWtdCat	0.003115	Density of road–stream intersections (2010 Census Tiger Lines–NHD stream lines) multiplied by NHDPlusV21 slope within the AOI (crossings \times slope km^{-2})
PctImp2013CatRp100	0.003096	Mean imperviousness of anthropogenic surfaces within the AOI (NLCD)
Al2O3Cat	0.003007	Mean percentage of lithological aluminum oxide (Al_2O_3) content in surface or near-surface geology within the AOI
PctGlacLakeFineWs	0.002988	Percentage of the AOI area classified as lithology type glacial lake sediment, fine-textured
PctCrop2019Ws	0.002930	Percentage of the AOI area classified as crop land use (NLCD class 82)
CompStrgthCat	0.002860	Mean lithological uniaxial compressive strength (megapascals) content in surface or near-surface geology within the AOI
NsurpCat	0.002853	Nitrogen surplus (kg N yr^{-1}) per AOI – excluding biological N fixation
K2OCat	0.002668	Mean percentage of lithological potassium oxide (K_2O) content in surface or near-surface geology within the AOI
AgKffactCat	0.002657	Mean of STATSGO Kffactor raster on agricultural land (NLCD 2006) within the AOI – the Universal Soil Loss Equation (USLE) represents a relative index of the susceptibility of bare, cultivated soil to particle detachment and transport by rainfall
NABD_NIDStorWs	0.002568	Volume all reservoirs (NID_STORA in NID) per unit area of the AOI ($\text{m}^3 \text{km}^{-2}$)
PctMxFst2019Ws	0.002464	Percentage of the AOI area classified as mixed deciduous- and/or evergreen-forest land cover (NLCD class 43)
ElevWs	0.002449	Mean AOI elevation (m)
PctOw2019Cat	0.002403	Percentage of the AOI area classified as open-water land cover (NLCD class 11)
PctDecid2019CatRp100	0.002028	Percentage of the AOI area classified as deciduous-forest land cover (NLCD class 41)
OmCat	0.002027	Mean organic matter content (percentage by weight) of soils (STATSGO) within the AOI

Table A6. Continued.

Predictor	Importance	Description
PctCrop2019Cat	0.001864	Percentage of the AOI area classified as crop land use (NLCD class 82)
WaterInputCat	0.001863	Water input ($\text{km}^2 \text{cm}^{-1}$): ratio of the total area of irrigated land to precipitation within the AOI
FertCat	0.001784	Mean rate of synthetic nitrogen fertilizer application to agricultural land (in $\text{kg N ha}^{-1} \text{yr}^{-1}$) within the AOI
PctDecid2019Cat	0.001709	Percentage of the AOI area classified as deciduous-forest land cover (NLCD class 41)
NO3_2008Ws	0.001689	Annual gradient map of precipitation-weighted mean deposition for nitrate ion concentration wet deposition for 2008 (in $\text{kg of NO}_3 \text{ ha}^{-1} \text{yr}^{-1}$) within the AOI
Phos_FertCat	0.001659	Mean rate of synthetic nitrogen fertilizer application to agricultural land (in $\text{kg N ha}^{-1} \text{yr}^{-1}$) within the AOI
MAST_2014	0.001589	Predicted mean annual stream temperature (January–December) for 2008, 2009, 2013, 2014
Na2OCat	0.001586	Mean percentage of lithological sodium oxide (Na_2O) content in surface or near-surface geology within the AOI
WaterInputWs	0.001507	Water input ($\text{km}^2 \text{cm}^{-1}$): ratio of the total area of irrigated land to precipitation within the AOI
RockNWs	0.001481	N from rock weathering (kg km^{-2}) within the AOI
Pestic97Ws	0.001459	Mean pesticide use (kg km^{-2}) in 1997 within the AOI
PctUrbMd2019CatRp100	0.001402	Percentage of the AOI area classified as developed, medium-intensity land use (NLCD class 23)
MSST_2014	0.001387	Predicted mean summer stream temperature (July–August) for 2008, 2009, 2013, 2014
MgOCat	0.001343	Mean percentage of lithological magnesium oxide (MgO) content in surface or near-surface geology within the AOI
MWST_2013	0.001315	Predicted mean winter stream temperature (January–February) for 2008, 2009, 2013, 2014
PctHbWet2019Cat	0.001298	Percentage of the AOI area classified as herbaceous-wetland land cover (NLCD class 95)
Fe2O3Cat	0.001270	Mean percentage of lithological ferric oxide (Fe_2O_3) content in surface or near-surface geology within the AOI
PctShrb2019Ws	0.001265	Percentage of the AOI area classified as shrub or scrub land cover (NLCD class 52)
HydrlCondCat	0.001220	Mean lithological hydraulic conductivity ($\mu\text{m s}^{-1}$) content in surface or near-surface geology within the AOI
RdDensWs	0.001211	Density of roads (2010 Census Tiger Lines) within the AOI (km km^{-2})
Phos_ManureCat	0.001210	Mean rate of manure application to agricultural land from confined animal feeding operations (in $\text{kg N ha}^{-1} \text{yr}^{-1}$) within the AOI
PctWdWet2019Ws	0.001191	Percentage of the AOI area classified as woody-wetland land cover (NLCD class 90)
RdCrsws	0.001175	Density of road–stream intersections (2010 Census Tiger Lines–NHD stream lines) within the AOI (crossings km^{-2})
NPDES DensWs	0.001156	Density of permitted NPDES (National Pollutant Discharge Elimination System) sites within the AOI (sites km^{-2})
PctImp2008Ws	0.001152	Mean imperviousness of anthropogenic surfaces within the AOI (NLCD)
PctHbWet2019CatRp100	0.001149	Percentage of the AOI area classified as herbaceous-wetland land cover (NLCD class 95)

Table A6. Continued.

Predictor	Importance	Description
MSST_2013	0.001115	Predicted mean summer stream temperature (July–August) for 2008, 2009, 2013, 2014
NANIWs	0.001108	Net anthropogenic nitrogen within the AOI: farm fertilizer + urban fertilizer + NO _x deposition + C-based N fixation + human and livestock food – crop N content – livestock N content
Precip8110Ws	0.001107	PRISM climate data – 30-year normal mean precipitation (mm) (annual period – 1981–2010) within the AOI
MAST_2009	0.001104	Predicted mean annual stream temperature (January–December) for 2008, 2009, 2013, 2014
SepticWs	0.000991	Density of septic systems per AOI – based on 1990 Census
Tmean8110Cat	0.000952	PRISM climate data – 30-year normal mean temperature (C°) (annual period – 1981–2010) within the AOI
RunoffCat	0.000932	Mean runoff (mm) within the AOI
PctHbWet2019Ws	0.000893	Percentage of the AOI area classified as herbaceous-wetland land cover (NLCD class 95)
SandCat	0.000878	Mean percentage sand content of soils (STATSGO) within the AOI
SuperfundDensWs	0.000855	Density of Superfund sites within the AOI (sites km ⁻²)
PctGlacTilLoamCat	0.000825	Percentage of the AOI area classified as lithology type glacial till, loamy
PctImp2013Cat	0.000805	Mean imperviousness of anthropogenic surfaces within the AOI (NLCD)
NCat	0.000726	Mean percentage of lithological nitrogen (N) content in surface or near-surface geology within the AOI
BFIWs	0.000721	Base flow is the component of streamflow that can be attributed to groundwater discharge into streams – the BFI is the ratio of base flow to total flow, expressed as a percentage, within the AOI
PctImp2006WsRp100	0.000699	Mean imperviousness of anthropogenic surfaces within the AOI (NLCD)
ManureWs	0.000695	Mean rate of manure application to agricultural land from confined animal feeding operations (in kg N ha ⁻¹ yr ⁻¹) within the AOI
TRIDensWs	0.000673	Density of TRI (Toxic Release Inventory) sites within the AOI (sites km ⁻²)
PctAlluvCoastWs	0.000662	Percentage of the AOI area classified as lithology type alluvium and fine-textured coastal zone sediment
CaOCat	0.000651	Mean percentage of lithological calcium oxide (CaO) content in surface or near-surface geology within the AOI
SandWs	0.000650	Mean percentage sand content of soils (STATSGO) within the AOI
PctImp2019Cat	0.000636	Mean imperviousness of anthropogenic surfaces within the AOI (NLCD)
PctHbWet2019WsRp100	0.000595	Percentage of the AOI area classified as herbaceous-wetland land cover (NLCD class 95)
PctColluvSedWs	0.000576	Percentage of the AOI area classified as lithology type colluvial sediment
PctBl2019Cat	0.000569	Percentage of the AOI area classified as barren land cover (NLCD class 31)
NH4_2008Ws	0.000547	Annual gradient map of precipitation-weighted mean deposition for ammonium ion concentration wet deposition for 2008 (in kg NH ₄ ha ⁻¹ yr ⁻¹) within the AOI
PctGrs2019Cat	0.000543	Percentage of the AOI area classified as grassland and/or herbaceous land cover (NLCD class 71)
PctImp2016Ws	0.000522	Mean imperviousness of anthropogenic surfaces within the AOI (NLCD)

Table A6. Continued.

Predictor	Importance	Description
PctUrbHi2019WsRp100	0.000522	Percentage of the AOI area classified as developed, high-intensity land use (NLCD class 24)
PctImp2004CatRp100	0.000521	Mean imperviousness of anthropogenic surfaces within the AOI (NLCD)
Tmax8110Ws	0.000520	PRISM climate data – 30-year normal maximum temperature ($C\hat{A}^\circ$) (annual period – 1981–2010) within the AOI
PctOw2019Ws	0.000495	Percentage of the AOI area classified as open-water land cover (NLCD class 11)
KffactWs	0.000492	Mean of STATSGO Kffactor raster within the AOI – the Universal Soil Loss Equation (USLE) represents a relative index of the susceptibility of bare, cultivated soil to particle detachment and transport by rainfall
RdDensCat	0.000450	Density of roads (2010 Census Tiger Lines) within the AOI (km km^{-2})
PctImp2016WsRp100	0.000447	Mean imperviousness of anthropogenic surfaces within the AOI (NLCD)
MSST_2009	0.000422	Predicted mean summer stream temperature (July–August) for 2008, 2009, 2013, 2014
CBNFCat	0.000417	Mean rate of biological nitrogen fixation from the cultivation of crops (in $\text{kg N ha}^{-1} \text{yr}^{-1}$) within the AOI
WtDepWs	0.000408	Mean seasonal water table depth (cm) of soils (STATSGO) within the AOI
PctImp2008Cat	0.000407	Mean imperviousness of anthropogenic surfaces within the AOI (NLCD)
Phos_Crop_UptakeCat	0.000385	Phosphorus uptake by crops in the catchment
WWTPMinorDensWs	0.000353	Density (number km^{-2}) of minor wastewater treatment plants per AOI
RockNCat	0.000350	N from rock weathering (kg km^{-2}) within the AOI
PctImp2013Ws	0.000327	Mean imperviousness of anthropogenic surfaces within the AOI (NLCD)
Tmean8110Ws	0.000292	PRISM climate data – 30-year normal mean temperature ($C\hat{A}^\circ$) (annual period – 1981–2010) within the AOI
NO3_2008Cat	0.000290	Annual gradient map of precipitation-weighted mean deposition for nitrate ion concentration wet deposition for 2008 (in $\text{kg NO}_3 \text{ha}^{-1} \text{yr}^{-1}$) within the AOI
PctUrbOp2019WsRp100	0.000271	Percentage of the AOI area classified as developed, open-space land use (NLCD class 21)
PctImp2008WsRp100	0.000255	Mean imperviousness of anthropogenic surfaces within the AOI (NLCD)
SWs	0.000224	Mean percentage of lithological sulfur (S) content in surface or near-surface geology within the AOI
PctShrb2019CatRp100	0.000215	Percentage of the AOI area classified as shrub and/or scrub land cover (NLCD class 52)
Tmax8110Cat	0.000193	PRISM climate data – 30-year normal maximum temperature ($C\hat{A}^\circ$) (annual period – 1981–2010) within the AOI
Phos_ManureWs	0.000193	Mean rate of manure application to agricultural land from confined animal feeding operations (in $\text{kg N ha}^{-1} \text{yr}^{-1}$) within the AOI
PctAg2006Slp10Cat	0.000163	Mean percentage of lithological sulfur (S) content in surface or near-surface geology within the AOI
Fe2O3Ws	0.000162	Mean percentage of lithological ferric oxide (Fe_2O_3) content in surface or near-surface geology within the AOI
WsAreaSqKm	0.000155	Mean percentage of lithological sulfur (S) content in surface or near-surface geology within the AOI
PctUrbHi2019CatRp100	0.000138	Percentage of the AOI area classified as developed, high-intensity land use (NLCD class 24)
PctUrbOp2019Cat	0.000138	Percentage of the AOI area classified as developed, open-space land use (NLCD class 21)

Table A6. Continued.

Predictor	Importance	Description
NPDESdensWsRp100	0.000119	Density of permitted NPDES (National Pollutant Discharge Elimination System) sites within the AOI (sites km ⁻²)
DamNrmStorWs	0.000118	Volume of all reservoirs (NORM_STORA in NID) per unit area of the AOI (m ³ km ⁻²)
SiO2Ws	0.000107	Mean percentage of lithological silicon dioxide (SiO ₂) content in surface or near-surface geology within the AOI
SuperfundDensWsRp100	0.000097	Density of Superfund sites within the AOI (sites km ⁻²)
SCat	0.000096	Mean percentage of lithological sulfur (S) content in surface or near-surface geology within the AOI
CBNFWs	0.000092	Mean rate of biological nitrogen fixation from the cultivation of crops (in kg N ha ⁻¹ yr ⁻¹) within the AOI
PctAlluvCoastCat	0.000091	Percentage of the AOI area classified as lithology type alluvium and fine-textured coastal zone sediment
PctImp2001WsRp100	0.000074	Mean imperviousness of anthropogenic surfaces within the AOI (NLCD)
PctGlacLakeCrsCat	0.000069	Percentage of the AOI area classified as lithology type glacial outwash and glacial lake sediment, coarse-textured
PctImp2001Ws	0.000058	Mean imperviousness of anthropogenic surfaces within the AOI (NLCD)
PctWdWet2019CatRp100	0.000049	Percentage of the AOI area classified as woody-wetland land cover (NLCD class 90)
PctColluvSedCat	0.000046	Percentage of the AOI area classified as lithology type colluvial sediment
PctHydricWs	0.000042	Percentage of the AOI area classified as lithology type hydric, peat, and muck
PctConif2019CatRp100	0.000038	Percentage of the AOI area classified as evergreen-forest land cover (NLCD class 42)
PctGlacLakeCrsWs	0.000014	Percentage of the AOI area classified as lithology type glacial outwash and glacial lake sediment, coarse-textured
PctGlacTilClayCat	0.000000	Percentage of the AOI area classified as lithology type glacial till, clayey
DamNIDStorCat	0.000000	Volume of all reservoirs (NID_STORA in NID) per unit area of the AOI (m ³ km ⁻²)
MineDensCat	0.000000	Density of mine sites within the AOI (mines km ⁻²)
NABD_NrmStorCat	0.000000	Volume of all reservoirs (NORM_STORA in NID) per unit area of the AOI (m ³ km ⁻²)
PctGlacTilCrsCat	0.000000	Percentage of the AOI area classified as lithology type glacial till, coarse-textured
PctGlacTilCrsWs	0.000000	Percentage of the AOI area classified as lithology type glacial till, coarse-textured
PctHydricCat	0.000000	Percentage of the AOI area classified as lithology type hydric, peat, and muck
SuperfundDensCat	0.000000	Density of Superfund sites within the AOI (sites km ⁻²)
TRIDensCat	0.000000	Density of TRI (Toxic Release Inventory) sites within the AOI (sites km ⁻²)
WWTPMajDensCat	0.000000	Density (number km ⁻²) of major wastewater treatment plants per AOI
DamDensCat	-0.000001	Density of georeferenced dams within the AOI (dams km ⁻²)
ElevCat	-0.000003	Mean AOI elevation (m)
RckDepCat	-0.000010	Mean depth (cm) to bedrock of soils (STATSGO) within the AOI
NABD_DensCat	-0.000011	Density of georeferenced dams within the AOI (dams km ⁻²)
DamNrmStorCat	-0.000043	Volume of all reservoirs (NORM_STORA in NID) per unit area of the AOI (m ³ km ⁻²)
PctWaterWs	-0.000051	Percentage of the AOI area classified as lithology type water

Table A6. Continued.

Predictor	Importance	Description
NPDESDensCat	−0.000064	Density of permitted NPDES (National Pollutant Discharge Elimination System) sites within the AOI (sites km ^{−2})
PctImp2011WsRp100	−0.000079	Mean imperviousness of anthropogenic surfaces within the AOI (NLCD)
PctUrbLo2019Ws	−0.000088	Percentage of the AOI area classified as developed, low-intensity land use (NLCD class 22)
ClayCat	−0.000090	Mean percentage clay content of soils (STATSGO) within the AOI
PctHay2019WsRp100	−0.000098	Percentage of the AOI area classified as hay land use (NLCD class 81)
CatAreaSqKm	−0.000113	Mean percentage of lithological sulfur (S) content in surface or near-surface geology within the AOI
NABD_NIDStorCat	−0.000113	Volume of all reservoirs (NID_STORA in NID) per unit area of the AOI (m ³ km ^{−2})
PctUrbLo2019CatRp100	−0.000115	Percentage of the AOI area classified as developed, low-intensity land use (NLCD class 22)
PctAg2006Slp20Ws	−0.000120	Mean percentage of lithological sulfur (S) content in surface or near-surface geology within the AOI
WWTPMajorDensWs	−0.000130	Density (number km ^{−2}) of major wastewater treatment plants per AOI
P2O5Cat	−0.000134	Mean percentage of lithological phosphorous oxide (P ₂ O ₅) content in surface or near-surface geology within the AOI
PctShrb2019WsRp100	−0.000136	Percentage of the AOI area classified as shrub and/or scrub land cover (NLCD class 52)
PctOw2019WsRp100	−0.000158	Percentage of the AOI area classified as open-water land cover (NLCD class 11)
RdCrSslpWtdWs	−0.000164	Density of road–stream intersections (2010 Census Tiger Lines–NHD stream lines) multiplied by NHDPlusV21 slope within the AOI (crossings × slope km ^{−2})
SepticCat	−0.000164	Density of septic systems per AOI – based on 1990 Census
PctBl2019CatRp100	−0.000189	Percentage of the AOI area classified as barren land cover (NLCD class 31)
PctHay2019CatRp100	−0.000195	Percentage of the AOI area classified as hay land use (NLCD class 81)
PctImp2006CatRp100	−0.000210	Mean imperviousness of anthropogenic surfaces within the AOI (NLCD)
CompStrgthWs	−0.000219	Mean lithological uniaxial compressive strength (megapascals) content in surface or near-surface geology within the AOI
PctUrbMd2019Ws	−0.000224	Percentage of the AOI area classified as developed, medium-intensity land use (NLCD class 23)
MgOWs	−0.000235	Mean percentage of lithological magnesium oxide (MgO) content in surface or near-surface geology within the AOI
PctConif2019Ws	−0.000236	Percentage of the AOI area classified as evergreen-forest land cover (NLCD class 42)
SN_2008Cat	−0.000237	Annual gradient map of precipitation-weighted mean deposition for average sulfur and nitrogen wet deposition for 2008 (in kg S + N ha ^{−1} yr ^{−1}) within the AOI
PctAg2006Slp20Cat	−0.000257	Mean percentage of lithological sulfur (S) content in surface or near-surface geology within the AOI
PctUrbLo2019WsRp100	−0.000281	Percentage of the AOI area classified as developed, low-intensity land use (NLCD class 22)
PctGlacLakeFineCat	−0.000284	Percentage of the AOI area classified as lithology type glacial lake sediment, fine-textured
RdDensCatRp100	−0.000293	Density of roads (2010 Census Tiger Lines) within the AOI (km km ^{−2})
PctImp2013WsRp100	−0.000297	Mean imperviousness of anthropogenic surfaces within the AOI (NLCD)
TRIDensWsRp100	−0.000311	Density of TRI (Toxic Release Inventory) sites within the AOI (sites km ^{−2})
MineDensWs	−0.000323	Density of mines sites within the AOI (mines km ^{−2})

Table A6. Continued.

Predictor	Importance	Description
PctImp2019CatRp100	−0.000369	Mean imperviousness of anthropogenic surfaces within the AOI (NLCD)
CaOWs	−0.000370	Mean percentage of lithological calcium oxide (CaO) content in surface or near-surface geology within the AOI
WWTPMinorDensCat	−0.000371	Density (number km ^{−2}) of minor wastewater treatment plants per AOI
Al2O3Ws	−0.000384	Mean percentage of lithological aluminum oxide (Al ₂ O ₃) content in surface or near-surface geology within the AOI
NANICat	−0.000387	Net anthropogenic nitrogen within the AOI: farm fertilizer + urban fertilizer + NO _x deposition + CBNF + human and livestock food – crop N content – livestock N content
PctImp2011Cat	−0.000388	Mean imperviousness of anthropogenic surfaces within the AOI (NLCD)
PctUrbHi2019Ws	−0.000391	Percentage of the AOI area classified as developed, high-intensity land use (NLCD class 24)
PctGrs2019WsRp100	−0.000395	Percentage of the AOI area classified as grassland and/or herbaceous land cover (NLCD class 71)
PctShrb2019Cat	−0.000403	Percentage of the AOI area classified as shrub and/or scrub land cover (NLCD class 52)
NH4_2008Cat	−0.000420	Annual gradient map of precipitation-weighted mean deposition for ammonium ion concentration wet deposition for 2008 (in kg NH ₄ ha ^{−1} yr ^{−1}) within the AOI
PctGlacTilClayWs	−0.000429	Percentage of the AOI area classified as lithology type glacial till, clayey
PctImp2001Cat	−0.000448	Mean imperviousness of anthropogenic surfaces within the AOI (NLCD)
RckDepWs	−0.000461	Mean depth (cm) to bedrock of soils (STATSGO) within the AOI
HydrlCondWs	−0.000479	Mean lithological hydraulic conductivity (micrometers per second) content in surface or near-surface geology within the AOI
Na2OWs	−0.000487	Mean percentage of lithological sodium oxide (Na ₂ O) content in surface or near-surface geology within the AOI
NABD_NrmStorWs	−0.000488	Volume of all reservoirs (NORM_STORA in NID) per unit area of the AOI (m ³ km ^{−2})
PctImp2004Ws	−0.000492	Mean imperviousness of anthropogenic surfaces within the AOI (NLCD)
WWTPAllDensCat	−0.000542	Density (number km ^{−2}) of all wastewater treatment plants per AOI
PermWs	−0.000550	Mean permeability (cm h ^{−1}) of soils (STATSGO) within the AOI
PctMxFst2019CatRp100	−0.000556	Percentage of the AOI area classified as mixed deciduous- and/or evergreen-forest land cover (NLCD class 43)
BFICat	−0.000560	Base flow is the component of streamflow that can be attributed to groundwater discharge into streams – the BFI is the ratio of base flow to total flow, expressed as a percentage, within the AOI
PctImp2019WsRp100	−0.000576	Mean imperviousness of anthropogenic surfaces within the AOI (NLCD)
NsurpWs	−0.000592	Nitrogen surplus (kg N yr ^{−1}) per AOI – excluding biological N fixation
MineDensWsRp100	−0.000632	Density of mines sites within the AOI (mines km ^{−2})
P2O5Ws	−0.000647	Mean percentage of lithological phosphorous oxide (P ₂ O ₅) content in surface or near-surface geology within the AOI
PctDecid2019WsRp100	−0.000675	Percentage of the AOI area classified as deciduous-forest land cover (NLCD class 41)
PctImp2004Cat	−0.000691	Mean imperviousness of anthropogenic surfaces within the AOI (NLCD)
PctImp2011Ws	−0.000768	Mean imperviousness of anthropogenic surfaces within the AOI (NLCD)
PctConif2019Cat	−0.000774	Percentage of the AOI area classified as evergreen-forest land cover (NLCD class 42)
PctImp2011CatRp100	−0.000784	Mean imperviousness of anthropogenic surfaces within the AOI (NLCD)

Table A6. Continued.

Predictor	Importance	Description
NWs	−0.000812	Mean percentage of lithological nitrogen (N) content in surface or near-surface geology within the AOI
PctGlacTilLoamWs	−0.000859	Percentage of the AOI area classified as lithology type glacial till, loamy
PctImp2008CatRp100	−0.000863	Mean imperviousness of anthropogenic surfaces within the AOI (NLCD)
PctBl2019Ws	−0.000940	Percentage of the AOI area classified as barren land cover (NLCD class 31)
InorgNWetDep_2008Ws	−0.000977	Annual gradient map of precipitation-weighted mean deposition for inorganic nitrogen wet deposition from nitrate and ammonium for 2008 (in kg N ha ^{−1} yr ^{−1}) within the AOI
Tile_density	−0.000989	Tile density in the watershed (in m ² km ^{−2})
PctMxFst2019Cat	−0.000993	Percentage of the AOI area classified as mixed deciduous- and/or evergreen-forest land cover (NLCD class 43)
PctImp2004WsRp100	−0.000997	Mean imperviousness of anthropogenic surfaces within the AOI (NLCD)
Tmin8110Ws	−0.001004	PRISM climate data – 30-year normal minimum temperature (CÂ°) (annual period – 1981–2010) within the AOI
MAST_2008	−0.001057	Predicted mean annual stream temperature (January–December) for 2008, 2009, 2013, 2014
DamNIDStorWs	−0.001058	Volume of all reservoirs (NID_STORA in NID) per unit area of the AOI (m ³ km ^{−2})
Phos_FertWs	−0.001065	Mean rate of synthetic nitrogen fertilizer application to agricultural land (in kg N ha ^{−1} yr ^{−1}) within the AOI
PctConif2019WsRp100	−0.001095	Percentage of the AOI area classified as evergreen-forest land cover (NLCD class 42)
PctImp2001CatRp100	−0.001121	Mean imperviousness of anthropogenic surfaces within the AOI (NLCD)
RdDensWsRp100	−0.001130	Density of roads (2010 Census Tiger Lines) within the AOI (km km ^{−2})
PctUrbOp2019Ws	−0.001147	Percentage of the AOI area classified as developed, open-space land use (NLCD class 21)
WtDepCat	−0.001155	Mean seasonal water table depth (cm) of soils (STATSGO) within the AOI
Tmin8110Cat	−0.001190	PRISM climate data – 30-year normal minimum temperature (CÂ°) (annual period – 1981–2010) within the AOI
RunoffWs	−0.001264	Mean runoff (mm) within the AOI
PctDecid2019Ws	−0.001384	Percentage of the AOI area classified as deciduous-forest land cover (NLCD class 41)
PctWdWet2019Cat	−0.001398	Percentage of the AOI area classified as woody-wetland land cover (NLCD class 90)
PctImp2016CatRp100	−0.001416	Mean imperviousness of anthropogenic surfaces within the AOI (NLCD)
SN_2008Ws	−0.001443	Annual gradient map of precipitation-weighted mean deposition for average sulfur and nitrogen wet deposition for 2008 (in kg S + N ha ^{−1} yr ^{−1}) within the AOI
RdCrscat	−0.001469	Density of roads-stream intersections (2010 Census Tiger Lines-NHD stream lines) within the AOI (crossings km ^{−2})
PctOw2019CatRp100	−0.001521	Percentage of the AOI area classified as open-water land cover (NLCD class 11)
Precip8110Cat	−0.001556	PRISM climate data – 30-year normal mean precipitation (mm) (annual period – 1981–2010) within the AOI
PctImp2006Ws	−0.001586	Mean imperviousness of anthropogenic surfaces within the AOI (NLCD)
ManureCat	−0.001594	Mean rate of manure application to agricultural land from confined animal feeding operations (in kg N ha ^{−1} yr ^{−1}) within the AOI
PctUrbHi2019Cat	−0.001652	Percentage of the AOI area classified as developed, high-intensity land use (NLCD class 24)

Table A6. Continued.

Predictor	Importance	Description
NABD_DensWs	−0.001661	Density of georeferenced dams within the AOI (dams km ^{−2})
PctImp2019Ws	−0.001693	Mean imperviousness of anthropogenic surfaces within the AOI (NLCD)
PctUrbLo2019Cat	−0.001734	Percentage of the AOI area classified as developed, low-intensity land use (NLCD class 22)
Precip_Minus_EVTCat	−0.001799	This dataset represents surplus precipitation (mm) (precipitation minus potential evaporation) as described in https://doi.org/10.1016/j.scitotenv.2020.137661 (Pennino et al., 2020) within individual, local NHDPlusV2 catchments and upstream, contributing watersheds.
OmWs	−0.001820	Mean organic matter content (percentage by weight) of soils (STATSGO) within the AOI
PctAg2006Slp10Ws	−0.001835	Mean percentage of lithological sulfur (S) content in surface or near-surface geology within the AOI
K2OWs	−0.001836	Mean percentage of lithological potassium oxide (K ₂ O) content in surface or near-surface geology within the AOI
PctUrbMd2019Cat	−0.001852	Percentage of the AOI area classified as developed, medium-intensity land use (NLCD class 23)
PctImp2006Cat	−0.001861	Mean imperviousness of anthropogenic surfaces within the AOI (NLCD)
PctImp2016Cat	−0.001956	Mean imperviousness of anthropogenic surfaces within the AOI (NLCD)
CanalDensWs	−0.001980	Density of NHDPlus line features classified as canal, ditch, or pipeline within the AOI (km km ^{−2})
InorgNWetDep_2008Cat	−0.002086	Annual gradient map of precipitation-weighted mean deposition for inorganic nitrogen wet deposition from nitrate and ammonium for 2008 (in kg N ha ^{−1} yr ^{−1}) within the AOI
PctUrbMd2019WsRp100	−0.002287	Percentage of the AOI area classified as developed, medium-intensity land use (NLCD class 23)
PctGrs2019CatRp100	−0.002320	Percentage of the AOI area classified as grassland and/or herbaceous land cover (NLCD class 71)
DamDensWs	−0.002323	Density of georeferenced dams within the AOI (dams km ^{−2})
PctBl2019WsRp100	−0.002483	Percentage of the AOI area classified as barren land cover (NLCD class 31)
CanalDensCat	−0.002813	Density of NHDPlus line features classified as canal, ditch, or pipeline within the AOI (km km ^{−2})
MSST_2008	−0.003001	Predicted mean summer stream temperature (July–August) for 2008, 2009, 2013, 2014
PctHay2019Ws	−0.003454	Percentage of the AOI area classified as hay land use (NLCD class 81)

Code availability. All R scripts used for data analysis are available in a permanent data repository at <https://doi.org/10.5281/zenodo.13936951> (Dolph, 2024).

Data availability. All input data used in this paper are available in a permanent data repository at <https://doi.org/10.5281/zenodo.13936951> (Dolph, 2024).

Author contributions. CLD, BD, GWF, and JCF conceived the study design, identified the available datasets, and identified the research questions. CLD performed the data analysis and developed the R scripts. CLD prepared paper with contributions from all the co-authors.

Competing interests. The contact author has declared that none of the authors has any competing interests.

Disclaimer. Publisher's note: Copernicus Publications remains neutral with regard to jurisdictional claims made in the text, published maps, institutional affiliations, or any other geographical representation in this paper. While Copernicus Publications makes every effort to include appropriate place names, the final responsibility lies with the authors.

Acknowledgements. This project was supported through the US Department of Agriculture's Conservation Effects Assessment Project (CEAP) National Legacy Phosphorus Assessment, with funding provided by USDA Natural Resources Conservation Service (NRCS) through an Interagency Agreement (grant no. NRC21IRA0010879). CEAP (<https://www.nrcs.usda.gov/ceap>, last access: 26 November 2024) is a multi-agency effort led by the Natural Resources Conservation Service and the Agricultural Research Service to quantify the effects of voluntary conservation and to strengthen data-driven management decisions across the nation's private lands.

Financial support. This research has been supported by the US Department of Agriculture (grant no. NRC21IRA0010879).

Review statement. This paper was edited by Nadia Ursino and reviewed by two anonymous referees.

References

- Basu, N. B., Destouni, G., Jawitz, J. W., Thompson, S. E., Loukinova, N. V., Darracq, A., Zanardo, S., Yaeger, M., Sivapalan, M., Rinaldo, A., and Rao, P. S. C.: Nutrient loads exported from managed catchments reveal emergent biogeochemical stationarity, *Geophys. Res. Lett.*, 37, L23404, <https://doi.org/10.1029/2010gl045168>, 2010.
- Bennett, E. M., Carpenter, S. R., and Caraco, N. F.: Human Impact on Erodable Phosphorus and Eutrophication: A Global Perspective, *BioScience*, 51, 227, [https://doi.org/10.1641/0006-3568\(2001\)051\[0227:hioepa\]2.0.co;2](https://doi.org/10.1641/0006-3568(2001)051[0227:hioepa]2.0.co;2), 2001.
- Berhe, A. A., Barnes, R. T., Six, J., and Marín-Spiotta, E.: Role of Soil Erosion in Biogeochemical Cycling of Essential Elements: Carbon, Nitrogen, and Phosphorus, *Annu. Rev. Earth Pl. Sc.*, 46, 521–548, <https://doi.org/10.1146/annurev-earth-082517-010018>, 2018.
- Bieroza, M. Z. and Heathwaite, A. L.: Seasonal variation in phosphorus concentration–discharge hysteresis inferred from high-frequency in situ monitoring, *J. Hydrol.*, 524, 333–347, <https://doi.org/10.1016/j.jhydrol.2015.02.036>, 2015.
- Boardman, E., Danesh-Yazdi, M., Foufoula-Georgiou, E., Dolph, C. L., and Finlay, J. C.: Fertilizer, landscape features and climate regulate phosphorus retention and river export in diverse Midwestern watersheds, *Biogeochemistry*, 146, 293–309, <https://doi.org/10.1007/s10533-019-00623-z>, 2019.
- Casquin, A., Gu, S., Dupas, R., Petitjean, P., Gruau, G., and Durand, P.: River network alteration of C-N-P dynamics in a mesoscale agricultural catchment, *Sci. Total Environ.*, 749, 141551, <https://doi.org/10.1016/j.scitotenv.2020.141551>, 2020.
- Debeer, D., Hothorn, T., and Strobl, C.: `permimp: Conditional Permutation Importance`, R package version 1.0-2, <https://CRAN.R-project.org/package=permimp> (last access: 14 February 2024), 2021.
- Dewitz, J.: National Land Cover Database (NLCD) 2019 Products, U.S. Geological Survey [data set], <https://doi.org/10.5066/P9KZCM54>, 2021.
- Diamond, J. S., Moatar, F., Recoura-Massaquant, R., Chaumot, A., Zarnetske, J., Valette, L., and Pinay, G.: Hypoxia is common in temperate headwaters and driven by hydrological extremes, *Ecol. Indic.*, 147, 109987, <https://doi.org/10.1016/j.ecolind.2023.109987>, 2023.
- Dolph, C. L.: `cldolph/instream_legacyP`: Data repository for Dolph et al., “Phosphorus transport in a hotter and drier climate: in-channel release of legacy phosphorus during summer low flow conditions”, Zenodo [code and data set], <https://doi.org/10.5281/zenodo.13936951>, 2024.
- Dolph, C. L., Hansen, A. T., Kemmitt, K. L., Janke, B., Rorer, M., Winikoff, S., Baker, A., Boardman, E., and Finlay, J.: Characterization of streams and rivers in the Minnesota River Basin Critical Observatory: Water chemistry and biological field collections, 2013–2016, Data Repository for the University of Minnesota [data set], <https://doi.org/10.13020/D6FH44>, 2017a.
- Dolph, C. L., Hansen, A. T., and Finlay, J. C.: Flow-related dynamics in suspended algal biomass and its contribution to suspended particulate matter in an agricultural river network of the Minnesota River Basin, USA, *Hydrobiologia*, 785, 127–147, <https://doi.org/10.1007/s10750-016-2911-7>, 2017b.
- Dolph, C. L., Boardman, E., Danesh-Yazdi, M., Finlay, J. C., Hansen, A. T., Baker, A. C., and Dalzell, B.: Phosphorus Transport in Intensively Managed Watersheds, *Water Resour. Res.*, 55, 9148–9172, <https://doi.org/10.1029/2018wr024009>, 2019.
- Dolph, C. L., Cho, S. J., Finlay, J. C., Hansen, A. T., and Dalzell, B.: Predicting high resolution total phosphorus concentrations for soils of the Upper Mississippi River Basin using machine learning, *Biogeochemistry*, 163, 289–310, <https://doi.org/10.1007/s10533-023-01029-8>, 2023.
- Dupas, R., Casquin, A., Durand, P., and Viaud, V.: Landscape spatial configuration influences phosphorus but not nitrate concentrations in agricultural headwater catchments, *Hydrol. Process.*, 37, e14816, <https://doi.org/10.1002/hyp.14816>, 2023.
- ESRI: ArcGIS Pro version 3.0.3. Redlands, CA: Environmental Systems Research Institute, <https://www.esri.com/en-us/arcgis/products/arcgis-pro/overview> (last access: 26 November 2024), 2022.
- Felton, R., Dalzell, B. J., Baker, J., Flynn, K. D., and Porter, S. A.: Novel, Ultralight Platform for Mapping Water Quality Parameters in Low-Order Streams, *ACS ES&T Water*, 3, 3305–3314, <https://doi.org/10.1021/acsestwater.3c00280>, 2023.
- Feyereisen, G. W., Francesconi, W., Smith, D. R., Papiernik, S. K., Krueger, E. S., and Wentz, C. D.: Effect of Replacing Surface Inlets with Blind or Gravel Inlets on Sediment and Phosphorus Subsurface Drainage Losses, *J. Environ. Qual.*, 44, 594–604, <https://doi.org/10.2134/jeq2014.05.0219>, 2015.
- Godsey, S. E., Kirchner, J. W., and Clow, D. W.: Concentration–discharge relationships reflect chemostatic characteristics of US catchments, *Hydrol. Process.*, 23, 1844–1864, <https://doi.org/10.1002/hyp.7315>, 2009.

- Goyette, J.-O., Bennett, E. M., and Maranger, R.: Low buffering capacity and slow recovery of anthropogenic phosphorus pollution in watersheds, *Nat. Geosci.*, 11, 921–925, <https://doi.org/10.1038/s41561-018-0238-x>, 2018.
- Greenwell, B. M.: pdp: An R Package for Constructing Partial Dependence Plots, *The R Journal*, 9, 421, <https://doi.org/10.32614/rj-2017-016>, 2017.
- Hagenauer, J., Omrani, H., and Helbich, M.: Assessing the performance of 38 machine learning models: the case of land consumption rates in Bavaria, Germany, *Int. J. Geogr. Inf. Sci.*, 33, 1399–1419, <https://doi.org/10.1080/13658816.2019.1579333>, 2019.
- Haque, S. E.: How Effective Are Existing Phosphorus Management Strategies in Mitigating Surface Water Quality Problems in the U.S.?, *Sustainability*, 13, 6565, <https://doi.org/10.3390/su13126565>, 2021.
- Hill, R. A., Hawkins, C. P., and Carlisle, D. M.: Predicting thermal reference conditions for USA streams and rivers, *Freshw. Sci.*, 32, 39–55, <https://doi.org/10.1899/12-009.1>, 2013.
- Hill, R. A., Weber, M. H., Leibowitz, S. G., Olsen, A. R., and Thornbrugh, D. J.: The Stream-Catchment (StreamCat) Dataset: A Database of Watershed Metrics for the Conterminous United States, *J. Am. Water Resour. As.*, 52, 120–128, <https://doi.org/10.1111/1752-1688.12372>, 2016.
- Inamdar, S., Sienkiewicz, N., Lutgen, A., Jiang, G., and Kan, J.: Streambank Legacy Sediments in Surface Waters: Phosphorus Sources or Sinks?, *Soil Systems*, 4, 30, <https://doi.org/10.3390/soilsystems4020030>, 2020.
- Jarvie, H. P., Pallett, D. W., Schäfer, S. M., Macrae, M. L., Bowes, M. J., Farrand, P., Warwick, A. C., King, S. M., Williams, R. J., Armstrong, L., Nicholls, D. J. E., Lord, W. D., Rylett, D., Roberts, C., and Fisher, N.: Biogeochemical and climate drivers of wetland phosphorus and nitrogen release: Implications for nutrient legacies and eutrophication risk, *J. Environ. Qual.*, 49, 1703–1716, <https://doi.org/10.1002/jeq2.20155>, 2020.
- Johnson, L., Bartsch, W., Hudak, G., Davenport, M., Johnson, K., Nixon, K., Reed, J., and Atlas Team: Minnesota Natural Resource Atlas: Online mapping tools and data for natural resource planning, management, and research in Minnesota, Natural Resources Research Institute, University of Minnesota Duluth, <https://mnatlas.org/> (last access: 7 March 2024), 2022.
- Keiser, D. and Shapiro, J.: Consequences of the Clean Water Act and the Demand for Water Quality, *Q. J. Econ.*, 134, 349–396, <https://doi.org/10.1093/qje/qjy019>, 2019.
- King, K. W., Williams, M. R., and Fausey, N. R.: Contributions of Systematic Tile Drainage to Watershed-Scale Phosphorus Transport, *J. Environ. Qual.*, 44, 486–494, <https://doi.org/10.2134/jeq2014.04.0149>, 2015.
- Kreiling, R. M., Perner, P. M., Breckner, K. J., Williamson, T. N., Bartsch, L. A., Hood, J. M., Manning, N. F., and Johnson, L. T.: Watershed- and reach-scale drivers of phosphorus retention and release by streambed sediment in a western Lake Erie watershed during summer, *Sci. Total Environ.*, 863, 160804, <https://doi.org/10.1016/j.scitotenv.2022.160804>, 2023.
- Kuhn, M. and Wickham, H.: Tidymodels: a collection of packages for modeling and machine learning using tidyverse principles, <https://www.tidymodels.org> (last access: 25 September 2024), 2020.
- Liaw, A. and Wiener, M.: Classification and Regression by random-Forest, *R News* 2, 18–22, 2002.
- Margenot, A. J., Zhou, S., McDowell, R., Hebert, T., Fox, G., Schilling, K., Richmond, S., Kovar, J. L., Wickramarathne, N., Lemke, D., Boomer, K., and Golovay, S.: Stream-bank erosion and phosphorus loading to surface waters: Knowns, unknowns, and implications for nutrient loss reduction research and policy, *J. Environ. Qual.*, 52, 1063–1079, <https://doi.org/10.1002/jeq2.20514>, 2023.
- Mayer, M.: `_missRanger`: Fast Imputation of Missing Values, R package version 2.2.1, <https://CRAN.R-project.org/package=missRanger> (last access: 14 February 2024), 2023.
- MDA: MDA Discovery Farms Program field data and sample collection SOP, Minnesota Department of Agriculture, St. Paul, Minnesota, https://discoveryfarmsmn.org/wp-content/uploads/2021/07/DFM_Monitoring-SOP_v5_signed_Final.pdf (last access: 17 March 2023), 2021.
- Mendoza-Lera, C. and Detry, T.: Relating hydraulic conductivity and hyporheic zone biogeochemical processing to conserve and restore river ecosystem services, *Sci. Total Environ.*, 579, 1815–1821, <https://doi.org/10.1016/j.scitotenv.2016.11.166>, 2017.
- Meybeck, M. and Moatar, F.: Daily variability of river concentrations and fluxes: indicators based on the segmentation of the rating curve, *Hydrol. Process.*, 26, 1188–1207, <https://doi.org/10.1002/hyp.8211>, 2012.
- Minnesota Department of Natural Resources and Minnesota Pollution Control Agency: DNR/MPCA Cooperative Stream Gaging Locations, <https://gisdata.mn.gov/dataset/env-wiski-coop-stream-gaging> (last access: 30 January 2023), 2023.
- MPCA: Watershed Pollutant Load Monitoring Network (WPLMN) standard operating procedures and guidance: Surface water evaluate SRP transport behavior quality sampling, Minnesota Pollution Control Agency, St. Paul, Minnesota, <https://www.pca.state.mn.us/sites/default/files/wq-cm1-02.pdf> (last access: 4 October 2023), 2015.
- MPCA: Proposed impaired waters list. Minnesota Pollution Control Agency, St. Paul, Minnesota, <https://www.pca.state.mn.us/air-water-land-climate/minnesotas-impaired-waters-list> (last access: 7 March 2024), 2022.
- Musolff, A., Schmidt, C., Selle, B., and Fleckenstein, J.H.: Catchment controls on solute export, *Adv. Water Resour.*, 86, 133–146, <https://doi.org/10.1016/j.advwatres.2015.09.026>, 2015.
- Osterholz, W. R., Hanrahan, B. R., and King, K. W.: Legacy phosphorus concentration–discharge relationships in surface runoff and tile drainage from Ohio crop fields, *J. Environ. Qual.*, 49, 675–687, <https://doi.org/10.1002/jeq2.20070>, 2020.
- Paerl, H. W. and Huisman, J.: Blooms Like It Hot, *Science*, 320, 57–58, <https://doi.org/10.1126/science.1155398>, 2008.
- Pennino, M. J., Leibowitz, S. G., Compton, J. E., Hill, R. A., and Sabo, R. D.: Patterns and predictions of drinking water nitrate violations across the conterminous United States, *Sci. Total Environ.*, 722, 137661, <https://doi.org/10.1016/j.scitotenv.2020.137661>, 2020.
- Pentáková, L., Su, K., Penták, M., and Stucki, J. W.: A review of microbial redox interactions with structural Fe in clay minerals, *Clay Miner.*, 48, 543–560, <https://doi.org/10.1180/claymin.2013.048.3.10>, 2013.
- Poikane, S., Várbró, G., Kelly, M. G., Birk, S., and Phillips, G.: Estimating river nutrient concentrations consistent with good ecological condition: More stringent

- nutrient thresholds needed, *Ecol. Indic.*, 121, 107017, <https://doi.org/10.1016/j.ecolind.2020.107017>, 2021.
- R Core Team *_R: A Language and Environment for Statistical Computing_*, R Foundation for Statistical Computing, Vienna, Austria, <https://www.R-project.org/> (last access: 26 November 2024), 2023.
- Records, R. M., Wohl, E., and Arabi, M.: Phosphorus in the river corridor, *Earth-Sci. Rev.*, 158, 65–88, <https://doi.org/10.1016/j.earscirev.2016.04.010>, 2016.
- Ren, X. W. and Santamarina, J. C.: The hydraulic conductivity of sediments: A pore size perspective, *Eng. Geol.*, 233, 48–54, <https://doi.org/10.1016/j.enggeo.2017.11.022>, 2018.
- Rode, M., Tittel, J., Reinstorf, F., Schubert, M., Knöller, K., Gilfedder, B., Merensky-Pöhlein, F., and Musolff, A.: Seasonal variation and release of soluble reactive phosphorus in an agricultural upland headwater in central Germany, *Hydrol. Earth Syst. Sci.*, 27, 1261–1277, <https://doi.org/10.5194/hess-27-1261-2023>, 2023.
- Schilling, K. E., Streeter, M. T., Vogelgesang, J., Jones, C. S., and Seeman, A.: Subsurface nutrient export from a cropped field to an agricultural stream: Implications for targeting edge-of-field practices, *Agr. Water Manage.*, 241, 106339, <https://doi.org/10.1016/j.agwat.2020.106339>, 2020.
- Siebers, N., Kruse, J., Jia, Y., Lennartz, B., and Koch, S.: Loss of subsurface particulate and truly dissolved phosphorus during various flow conditions along a tile drain–ditch–brook continuum, *Sci. Total Environ.*, 866, 161439, <https://doi.org/10.1016/j.scitotenv.2023.161439>, 2023.
- Simpson, Z. P., McDowell, R. W., Condrón, L. M., McDaniel, M. D., Jarvie, H. P., and Abell, J. M.: Sediment phosphorus buffering in streams at baseflow: A meta-analysis, *J. Environ. Qual.*, 50, 287–311, <https://doi.org/10.1002/jeq2.20202>, 2021.
- Søndergaard, M., Jensen, P. J., and Jeppesen, E.: Retention and Internal Loading of Phosphorus in Shallow, Eutrophic Lakes, *Sci. World J.*, 1, 427–442, <https://doi.org/10.1100/tsw.2001.72>, 2001.
- Smith, D. R., King, K. W., Johnson, L., Francesconi, W., Richards, P., Baker, D., and Sharpley, A. N.: Surface Runoff and Tile Drainage Transport of Phosphorus in the Midwestern United States, *J. Environ. Qual.*, 44, 495–502, <https://doi.org/10.2134/jeq2014.04.0176>, 2015.
- Smolders, E., Baetens, E., Verbeeck, M., Nawara, S., Diels, J., Verdriev, M., Peeters, B., De Cooman, W., and Baken, S.: Internal Loading and Redox Cycling of Sediment Iron Explain Reactive Phosphorus Concentrations in Lowland Rivers, *Environ. Sci. Technol.*, 51, 2584–2592, <https://doi.org/10.1021/acs.est.6b04337>, 2017.
- Thompson, S. E., Basu, N. B., Lascrain Jr., J., Aubeneau, A., and Rao, P. S. C.: Relative dominance of hydrologic versus biogeochemical factors on solute export across impact gradients, *Water Resour. Res.*, 47, W00J05, <https://doi.org/10.1029/2010wr009605>, 2011.
- Ury, E. A., Arrumugam, P., Herbert, E. R., Badiou, P., Page, B., and Basu, N. B.: Source or sink? Meta-analysis reveals diverging controls of phosphorus retention and release in restored and constructed wetlands, *Environ. Res. Lett.*, 18, 083002, <https://doi.org/10.1088/1748-9326/ace6bf>, 2023.
- USEPA: National Hydrography Dataset Plus Version 2, U.S. Environmental Protection Agency, <https://www.epa.gov/waterdata/get-nhdplus-national-hydrography-dataset-plus-data> (last access: 23 May 2023), 2019.
- USGS: USGS Streamgage NHDPlus Version 1 Basins 2011, U.S. Geological Survey, <https://water.usgs.gov/GIS/metadata/usgswrd/XML/streamgagebasins.xml#stdorder> (last access: 22 February 2023), 2012.
- Valayamkunnath, P., Barlage, M., Chen, F., Gochis, D. J., and Franz, K. J.: Mapping of 30-meter resolution tile-drained croplands using a geospatial modeling approach, *Scientific Data*, 7, 257, <https://doi.org/10.1038/s41597-020-00596-x>, 2020.
- van Dael, T., De Cooman, T., and Smolders, E.: In-stream oxygenation to mitigate internal loading of phosphorus in lowland streams, *J. Hydrol.*, 590, 125536, <https://doi.org/10.1016/j.jhydrol.2020.125536>, 2020.
- Vilmin, L., Bouwman, A. F., Beusen, A. H. W., van Hoek, W. J., and Mogollón, J. M.: Past anthropogenic activities offset dissolved inorganic phosphorus retention in the Mississippi River basin, *Biogeochemistry*, 161, 157–169, <https://doi.org/10.1007/s10533-022-00973-1>, 2022.
- Vissers, M. A., Roy, J. W., Yates, A. G., Robinson, K., Rakhimbekova, S., and Robinson, C. E.: Spatio-temporal variability of porewater phosphorus concentrations in streambed sediments of an agricultural stream, *J. Hydrol.*, 617, 129133, <https://doi.org/10.1016/j.jhydrol.2023.129133>, 2023.
- Wanner, O., Egli, T., Fleischmann, T., Lanz, K., Reichert, P., and Schwarzenbach, R. P.: Behavior of the insecticides disulfoton and thiometon in the Rhine River: a chemodynamic study, *Environ. Sci. Technol.*, 23, 1232–1242, <https://doi.org/10.1021/es00068a007>, 1989.
- Warrick, J. A.: Trend analyses with river sediment rating curves, *Hydrol. Process.*, 29, 936–949, <https://doi.org/10.1002/hyp.10198>, 2015.
- Wilson, A. B., Baker, J. M., Ainsworth, E. A., Andresen, J., Austin, J. A., Dukes, J. S., Gibbons, E., Hoppe, B. O., LeDee, O. E., Noel, J., Roop, H. A., Smith, S. A., Todey, D. P., Wolf, R., and Wood, J. D.: Ch. 24. Midwest, in: Fifth National Climate Assessment, edited by: Crimmins, A. R., Avery, C. W., Easterling, D. R., Kunkel, K. E., Stewart, B. C., and Maycock, T. K., U.S. Global Change Research Program, Washington, DC, USA, <https://doi.org/10.7930/NCA5.2023.CH24>, 2023.
- Wright, M. N. and Ziegler, A.: ranger: A Fast Implementation of Random Forests for High Dimensional Data in C++ and R, *J. Stat. Softw.*, 77, 1–17, <https://doi.org/10.18637/jss.v077.i01>, 2017.
- Zeng, Q., Qin, L., Bao, L., Li, Y., and Li, X.: Critical nutrient thresholds needed to control eutrophication and synergistic interactions between phosphorus and different nitrogen sources, *Environ. Sci. Pollut. R.*, 23, 21008–21019, <https://doi.org/10.1007/s11356-016-7321-x>, 2016.